University of Guanajuato
Engineering Division
Campus Irapuato - Salamanca
Department of Mechanical Engineering

Evaluation of Microchannel Networks for Efficient Cooling of IC Chips using Single-Phase Cooling

THESIS

Submitted to the Department of Mechanical Engineering
in partial fulfillment to the requirements for the degree of
Doctor of Mechanical Engineering

by

Carlos Alberto Rubio-Jimenez, M.S.

Co-Advisors

Satish G. Kandlikar, Ph.D.
Abel Hernandez-Guerrero, Ph.D.

Salamanca, Gto, Mex. August 2012

To Mama and Lupe...

You are always behind me

To Erika...

We are walking together

To Valeria...

You have changed my world

Acknowledgment

At this point of my life I have not more to thank everyone who supported me to achieve this goal. Mainly, I have to thank my Mamá and Lupe for their unconditional support. Similarly, I have to say thank Erika and Valeria for allowing me to get this dream. Furthermore, I have to recognize the important support that my family has gave me. I hope you will be always proud of me.

I am very grateful to my adviser, Professor Satish G. Kandlikar for his support, education and talks upon this research, and more important, upon life. Similarly I want to thank to Dr. Abel Hernandez for his support and teaching. Besides, I have not more to thank to all my teachers and professors who have been part of my education along my life.

I would also like to express my grateful to all my friends that I have made along these years such in Mexico as in US. I have specially to say thank you to Valentina, Preethi, Jeet, Ankit and Yao for their help and comprehension in my abroad adventure. Thanks everyone.

Carlos Alberto Rubio Jimenez

Abstract

This era is called information age. Computational equipment make possible to generate, transfer and process data each second worldwide. IC chips are the bases of these electronic devices. Thus, there is a deep interest in these high-tech electronic technologies. Since the development of the transistor in the *Bell Laboratories*, the IC chips have grown strongly, mainly in the slenderness and its number of transistors. For example, the *Intel® Core® i7* is currently a part of the newest computational processor generation manufactured by *Intel® Corporations*. Its architecture is formed by 774 million of 64 nm-transistor (compared on its predecessor, this device has an increase of fourteen times the number of these vital components.) By 2016, it is projected that the next computation processor generation will have 10-30 nm architecture with an increase of 1.3 times in the number of transistors. Although the panorama looks pretty good, there is an important drawback of this tendency. The transfer of electrons into the IC chip generates an important amount of thermal energy, which is affected directly by the increase of the number of transistors, and inversely by the decrease of the computational processor size. Thus, several researchers have been focused to enhance current cooling IC chip technology as well as generate novel cooling systems.

Since the beginning of this century, liquid cooling technologies have received a deep attention for the next cooling electronic device generation. Large part of the researchers developed in this area has been addressed to study microchannel heat sinks. The large heat transfer coefficient that the cooling fluid can achieve when is flowing through these tiny devices as well as the heat sink slenderness, make them a true alternative for dissipating the high heat fluxes to be generated in the next computational processors generation. Good knowledge of the phenomena and generation of novel configurations have been the main result of these studies. However, a couple of problem remains present: non-uniform junction temperature and high fluid pressure drop. Studies focused to analyze the thermo-mechanical effects generated on the IC chip have shown that the hotspots produce several damages into the chip. Thus, it is highly desirable to generate homogeneous temperature in the cooling system. Moreover, the system energy requirements increase directly with the pressure drop. Thus, reduction of this energy losses is desirable in order to do more reliable the cooling system (appropriate pumping power).

This work is a contribution in the microchannel heat sink area aimed to obtain a micro cooling system capable to generate uniform junction temperature with the lowest pressure drop penalty. Analytical and numerical studies are carried out in order to achieve this goal.

Index

List of Figures

Chapter I
Micro Cooling Systems – Literature Review

Chapter II
Evaluation of Enhancement Techniques in Microchannels - Formulation

List of Tables

Chapter I
Micro Cooling Systems - Literature Review

INTRODUCTION

A large part of the industrial processes, services, researches and entertainment is based on high-tech electronic devices. Integrated circuit chips are the keystones of these devices. Since their development in *The Bell Laboratories* (1947) [A,1,2], the IC chips have evolved, increasing strongly their processing capacity and decrease their size. The industry´s ability to exponentially decrease the minimal feature sizes used to fabricate the integrated circuits leads to this tendency (*Moore`s law* (1965) *"The number of components per chip doubles roughly every 24 months"* [3]). Thereby, each new electronic system is improved in its performance and size. Currently, the electronic industries have a strong competition. Their major goal is to generate novel devices (e.g. desktop PCs, system servers, etc.) with remarkable improvements on their features (size, performance, weight, etc.) than the previous generation.

A major portion of the semiconductor device production is devoted to digital logic systems, which are classified in *High-Performance Logic* (HPL) and *Low-Power Logic* (LPL). HPL refers to chips of high complexity, high performance, and high power dissipation, such as microprocessor unit (MPU) chips for desktop PCs, servers, etc. LPL refers to chips for mobile systems where the allowable power dissipation and hence the allowable leakage currents are limited by battery life [4]. In 2001, the *International Technology Roadmap for Semiconductors* (ITRS) projected that the 2016 HPL *Complementary Metal-Oxide Semiconductor* (CMOS) will have power leakage around 288 W based on 9-nm technology [5]. In 2010, the ITRS made updates, indicating that the heat leakage expected by the 2016 HPL *Metal-Oxide Semiconductors Field-Effect Transistor* (MOSFET) would have values around 320 W based on 16-nm technology [4].

Important engineering challenges emerge with this panorama such as the improvement of manufacturing techniques, characterization of materials, efficient and faster designs of devices capable to be easily integrated, etc. Furthermore, the time for testing is very short. In the field of thermal management, the major challenge is the design of reliable, smaller and easy-integration cooling systems. Based on the ITRS projections, the 2016`s HPL chips are going to request cooling systems capable to reach thermal resistance values ranging from 0.10 to 0.30 K/W [4-6], considering the maximum IC chip temperature below 85°C.

The cooling systems have evolved with each new generation of IC chips, from natural convection systems (flat-plate or passive pin fin heat sinks) to forced convection packages (air moved through pin fin heat sinks using fans). Although the last one is currently used for cooling HPL chips, its application is going to be limited in the near future due to the direct dependency that the cooling package size has with the amount of heat to be dissipated [B-D] (e.g. the Intel® i7-900® Processor generated <100 W of thermal energy; and its cooling system has a volume ~300 cm^3 [E]). Thereby, in the last years, alternatives for cooling these electronic devices considering the size and thermal dissipation as constrains have been proposed and studied.

Liquid cooling technologies are proposed as reliable alternatives for solving the thermal management challenges. Microchannel heat sinks using water in single or two phase flow, enclosed systems using refrigerants as cooling medium, inject cooling systems, boiling using micro gaps at subatmospheric pressures, spray cooling systems, etc. are the main proposal worldwide [7-12]. Overall, important thermal advantages are reached with these novel-cooling systems. However, each alternative present drawbacks that should be considered for their integration in future IC chips.

MICROCHANNEL HEAT SINKS

In early 1980's, Tuckerman and Pease [13] proposed a novel alternative for transferring high heat fluxes in a system. Their proposal was based on the Nusselt number definition for internal flow. Since the heat transfer coefficient is inversely affected by the channel hydraulic diameter, a large amount of thermal energy can be transferred from the channel walls to the fluid when the hydraulic diameter is of the order of micrometers. Their hypothesis was validated experimentally using some heat sink configurations formed by rectangular microchannels manufactured parallel on a silicon substrate. Their results showed that it is possible to transfer up to 790 W/cm^2 with a fluid temperature rise of 71°C. Thereby, the thermal resistance of their system is 0.09 K/W. According to these terrific results, the cooling systems to be required by 2016 have already been designed in the early 1980's. Although the panorama looks pretty good, there are important drawbacks that affect their reliability. One of those is the large pressure drop in the system. Tuckerman and Pease reported that the thermal performance of their best heat sink had a pressure drop slightly larger than 200 kPa with a volumetric flow of 8.6 cm^3/s. Therefore, the pumping power required for moving the fluid through the cooling system is 1.8 W (~5% of the total power input in a current computational equipment that consumes 20 W of electrical energy). Moreover, important temperature variations are generated when microchannel heat sinks are used. The increase of the fluid temperature along the flow length and its direct relationship on the junction wall temperature (IC chip temperature) are the major generators of these temperature gradients and hotspots. Thermo-mechanical stresses, accumulative of failure and fatigue per cycle, intermetallic growth, void formation, temperature-induced, acceleration on chemical reactions, skew of the clock signal network, corrosion and cracking on the die and IC chip package are generated with these temperature variations [F, 13-15].

Based on this panorama, cooling systems for future applications must have thermal resistance performance ranging from 0.1 K/W to 0.3 K/W, with the minimal pumping power requirements, easy integration, and capable to generate the most uniform temperature distribution on the IC chips, improving significantly their performance and lifetime.

Several studies upon heat sink based on microchannels for dissipating large heat fluxes have been carried out in order to understand the micro-phenomena, and geometrical effects, to generate parameterization curves and optimal configuration, etc. [16-73]. From these studies, it is known that:

1. Channels with hydraulic diameter ranging from 10 μm to 200 μm can be considered as microchannels.
2. Water in single-phase and laminar regime flowing through microchannels presents similar thermal performance that water in turbulent regime flowing through macroscale systems.
3. Experimental results present slightly variations with analytical and numerical studies because of the channel roughness, bias, complexity of measuring, etc.
4. Rectangular microchannel heat sinks present the best thermal performance.
5. Pin fin and porous media techniques are good approaches for analytical analyses.
6. Thermal and hydrodynamic entrance effects are important in this kind of cooling systems due to the relatively small channel length.
7. Transition from laminar to turbulent regimes is achieved at lower Reynolds number than conventional channel size.
8. The thermal resistance in the heat sink increases when the channel height is increased.
9. Analytical and numerical studies should consider the dependency that the fluid properties have with temperature.
10. H2 boundary conditions (constant wall heat flux such circumferentially as axially) should be considered in these microanalyses.
11. Channel roughness affects strongly the thermal and hydrodynamic performance.
12. This kind of micro cooling systems has to be easily embedded with the IC chip.
13. Overall pressure drop increases strongly when the heat sink thermal resistance is slightly decreased.
14. Comparisons of the Nusselt number and friction factor correlations for microchannels and macrochannels with rectangular and trapezoidal cross section are exposed by [40,52,55,66].

Overall, the conclusion reached by Tuckerman and Pease [13] on the thermal and hydrodynamic performance of heat sinks based on parallel microchannels manufactured on silicon subtracted and placed on the back-side of IC chips, using water in single-phase and laminar regime, are ratified on these studies: *"The reduction of heat sink thermal resistance has an important pressure drop penalty and temperature variations on the IC chip."*

ALTERNATIVE MICRO COOLING SYSTEMS

Recently, some researches have been aimed to generate alternative micro cooling systems for electronic applications. The majority of these studies have proposed geometrical configurations in order to achieve this goal reducing the pumping power requirements. The most outstanding proposals are shown in this section.

Bejan's Constructal theory exposed has been considered in the field of micro cooling systems. This theory is based on the fact that *"the device shape requested in engineering field is developed*

since the specific engineering necessity." Bejan [H,74] and West *et al.* [75] proposed some geometrical ratios which describe the growing, distribution and bifurcation of channels in order to cover the major amount of system volume with the minimal pressure drop penalty. Pence [76] and Wechsatol *et al.* [77,78] proposed disk-shaped fractal-like configurations as alternative for dissipating high heat fluxes. Figure 1.1 shows a sketch of these heat sink configurations. Their conclusions emphasized the robustness of these fractal-like arrangements compared on parallel microchannel heat sinks. Furthermore, their results showed that *i*) the thermal resistance is reduce when the number of branching channels is increased and *ii*) the fluid friction is reduced when non-branching channels are used. Lorente *et al.* [79] carried out an analytical analysis in order to observe the effects of channel length in this kind of configurations. Their results showed a decrease of the flow resistance when the channel lengths per bifurcation are reduced.

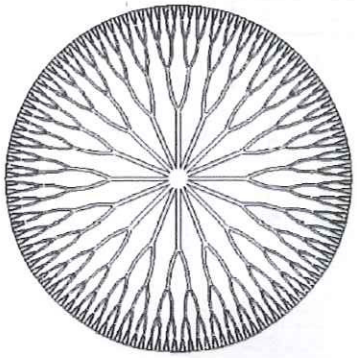

Figure 1.1 Disk-shaped fractal-like heat sink proposed by [76-78].

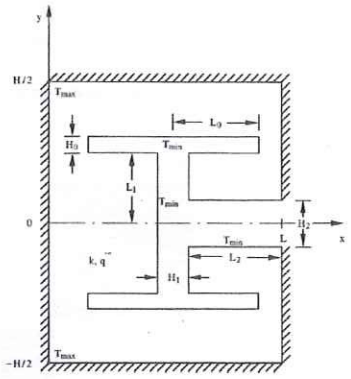

Figure 1.2 H-shape branching channels [82].

Zimparov *et al.* [80,81] optimized the thermal performance of T- and Y-shaped flow systems for constant temperature as boundary condition. They indicated that their methodology is applicable to more complex channel configurations. Following this work, Biserni *et al.* [82] optimized H-shaped channel configurations similar to the sketch shown in Figure 1.2. Their conclusion indicated that the arrangement configuration and complexity should evolve gradually with the performance of the global system. Wechsatol *et al.* [83] and Wang *et al.* [84] evaluated the attributes of using constructal networks as micro loops. Their major conclusion indicated that these loops are effective design for remaining the network performance when the system suffers local blockage. These loops assure the continuity of the flow along the working period. Wang *et al.* [85] took into account this observation and analyzed numerically the performance of vascular composites, which are cooled with grids and radial channels. Figure 1.3 shows a sketch of these channel configurations. Their results shown that the systems with outlet in the center offer shorter response of removing heat. Although these analytical optimizations and numerical analyses show that these systems work efficiently with coolant in single phase, the heat flux ratio considered in the analyzes is very low compared on the heat expected to be generated by near future IC chips. Furthermore, the assumptions of these models reduce significantly their approach with reality.

One alternative for improving these constructal cooling systems is the use of coolant in two-phase flow. Revillen *et al.* [86] carried out an analytical work aimed to maximize the saturated critical heat flux in a disk-shaped fractal-like heat sink. Their results showed that this system can dissipate up

to 50 W/cm^2 with a pumping power of 0.8 W. Following this thematic, Daguenet-Frick *et al.* [87] analyzed numerically a 3-D disk-shape fractal-like heat sink using refrigerant R-134a as coolant. Their results showed a pretty good temperature distribution on the bottom wall of the heat sink (e.g. Figure 1.4). Although the system reached a thermal resistance of 0.13 K/W with a pumping power of 0.03 W, the maximum heat removed was only 2.5 W/cm^2. These results clearly limit their use in future IC chip cooling applications.

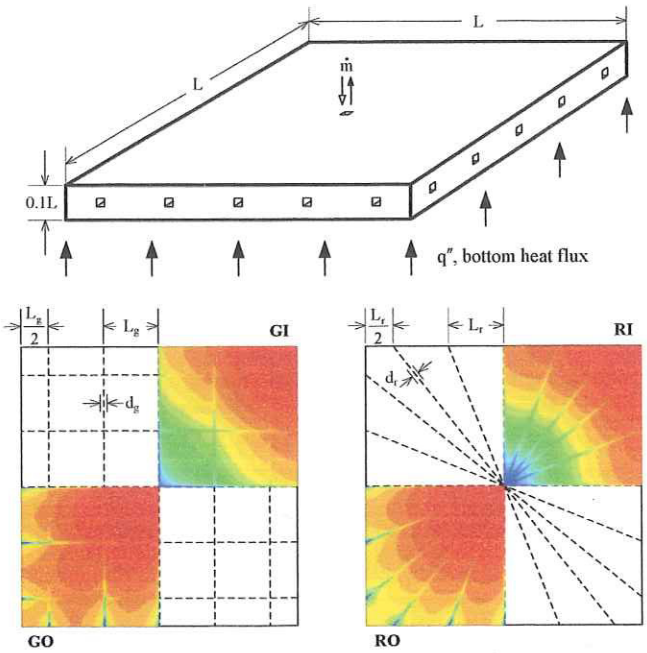

Figure 1.3 Vascular composites cooled with grids and radial channels [85]

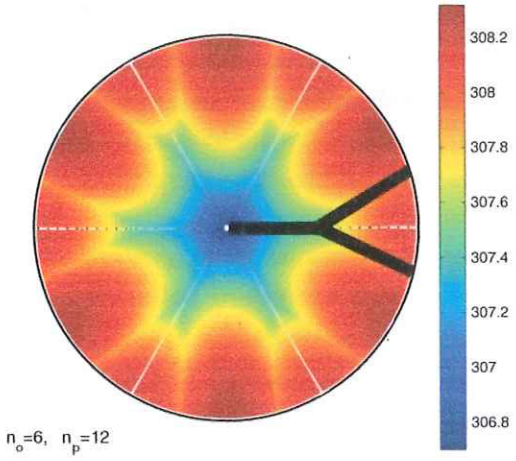

Figure 1.4 Temperature distribution in disk-shape heat sink [87].

Some other works focused on improving the flow distribution in a 3D system have been proposed as well. These studies are based on the fact that *"the shape of the systems requested in engineering fields should be developed since natural structures."* Pence [88] proposed a 1D model for fractal-like branching network. Pressure and temperature distributions were computed, showing

robustness compared to conventional parallel straight channels. Chen and Cheng [89,90] proposed other fractal-like configurations based on rectangular-branching channels. Figure 1.5 presents sketches of them. Their results showed that these configurations increase the average heat transfer coefficient and reduce the pressure drop penalty compared on parallel microchannel heat sinks. Wang *et al.* [91,92] developed 3D numerical analyses of branching microchannel networks. The results showed that the increase in the network complexity does not necessarily provide a better thermal performance, however, the manufacturing costs rises directly with the system complexity.

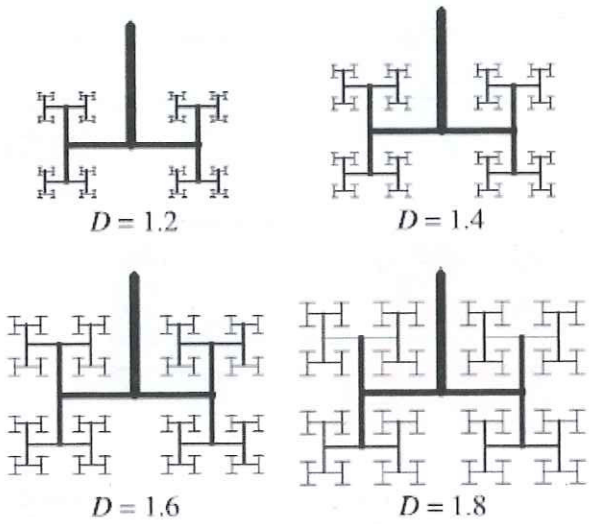

Figure 1.5 Fractal-like branching microchannel heat sinks [89].

Wang *et al.* [93] and Luo *et al.* [94] analyzed flow and thermal behavior of offset left-like and branching microchannels heat sinks and asymmetric two bifurcation networks (Figure 1.6). Their results showed that the pressure drop in the offset leaf–like branching arrangements decreases significantly compared to symmetry left-like branching configurations. Xu *et al.* [95] demonstrated that the heat conduction in a channel network configuration is rather different from Murray´s law [96]. Pence [97] developed an experimental work of fractal-like flow networks using disk-shaped. Their results showed the difference between fractal-like and constructal approaches applied to these devices, and the importance of including geometric and manufacturing constraints.

Overall, fractal-like cooling systems show an important improvement in the pressure drop penalty, but the thermal performance is limited. In some cases, the temperature profile on the die has a pretty good homogeneous distribution, however, the heat flux supplied into the systems is lower than the values expected in future applications (e.g. Wang *et al.* [93] analyzed their system considering a heat flux of only 10 W/cm^2). Therefore, heat sinks based on branching channel configuration could be appropriate cooling systems for LPL applications, considering single-, two-phase flow or boiling as cooling mechanism. For HPL applications, these configurations are not appropriate due to the robustness of the system and manufacturing complexity.

On the other hand, alternative micro cooling systems based on random geometries have been proposed. Zhang *et al.* [98] and Miao *et al.* [99] proposed rectangular channels embedded on rectangular dies, which are extruded along spiral and serpentine paths, as micro cooling systems.

Figure 1.7 shows sketches of these configurations. Their results showed a pretty good temperature distribution when the heat flux supplied into the system was ranging from 2 to 4 W/cm^2. However, the pressure drop penalty was larger compared on the values obtained in branching channel configurations.

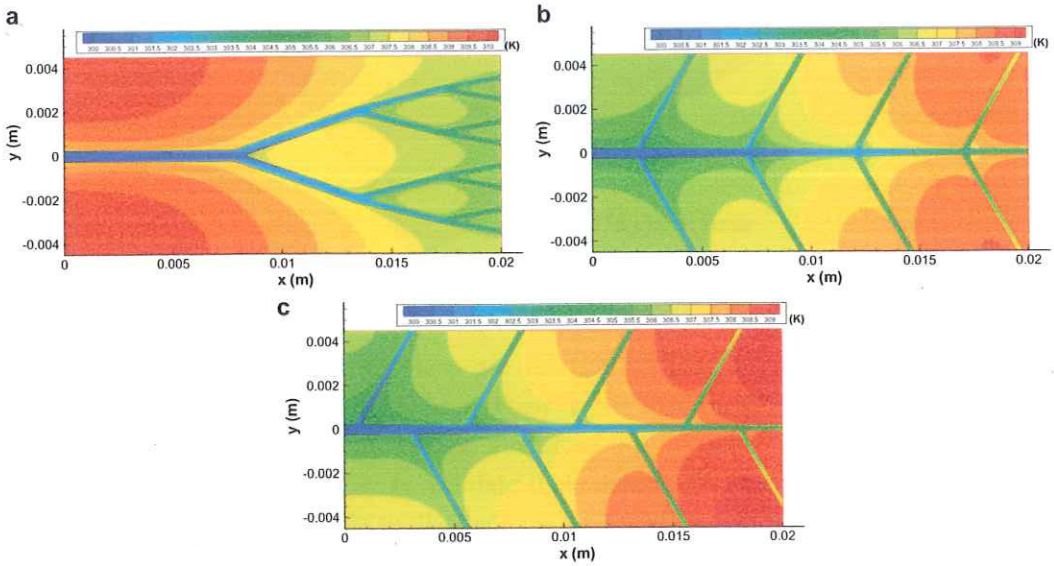

Figure 1.6 Temperature distribution in offset and inline left- and tree-shaped branching networks proposed by [93].

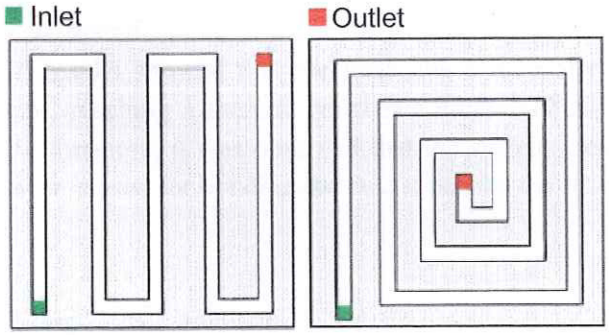

Figure 1.7 Serpentine and spiral networks configurations studied by [98].

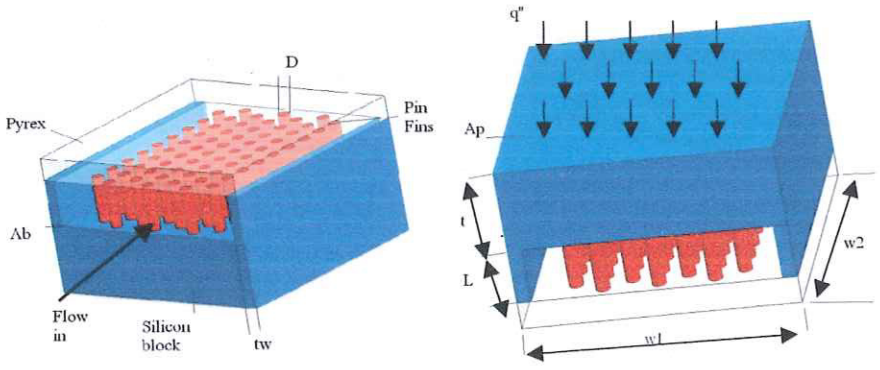

Figure 1.8 Micro pin fin heat sink proposed by [100].

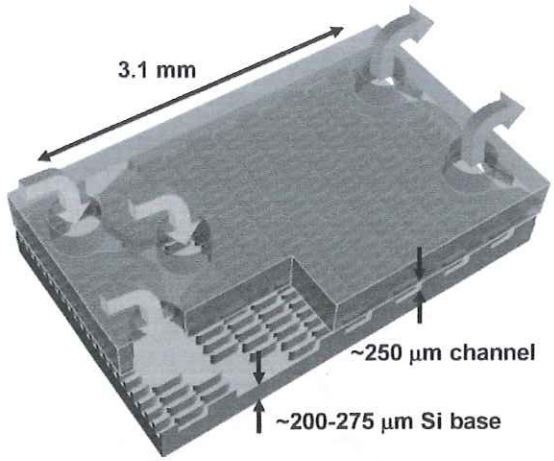

Figure 1.9 Alternative micro cooling system proposed by [101,102].

Peles *et al.* [100] proposed a micro pin fin heat sink as alternative micro cooling system. Figure 1.8 shows a sketch of this device. Their analytical model was based on thermal and hydrodynamic correlations provided in the literature for systems of conventional size. Then, experiments were carried out in order to validate their model. The results showed a good approach. Also, the cooling system was capable to dissipate up to 790 W/cm^2 with a temperature rise of 30.7°C. Although the overall thermal resistance of the system was 0.039 K/W, the pressure drop penalty was considerably large (>200 kPa). Colgan *et al.* [101,102] offered non-conventional heat sinks using water and fluorinated fluids as coolants. Two manufactured layers placed face-to-face make up the heat sink. A specific number of staggered fins are manufactured in the first layer. Several zigzagged fluid inlets/outlet channels are manufactured in the second layer. Figure 1.9 shows this micro cooling system. Their experimental results showed that the heat sink with water as coolant is capable of dissipating up to 500 W/cm^2, reaching a thermal resistance around 12 K-mm^2/W, and a maximum pressure drop of 65 kPa. Furthermore, it was observed that the system thermal resistance is reduced when Indium solder TIM layer is used for bonding the heat sink with the IC chip.

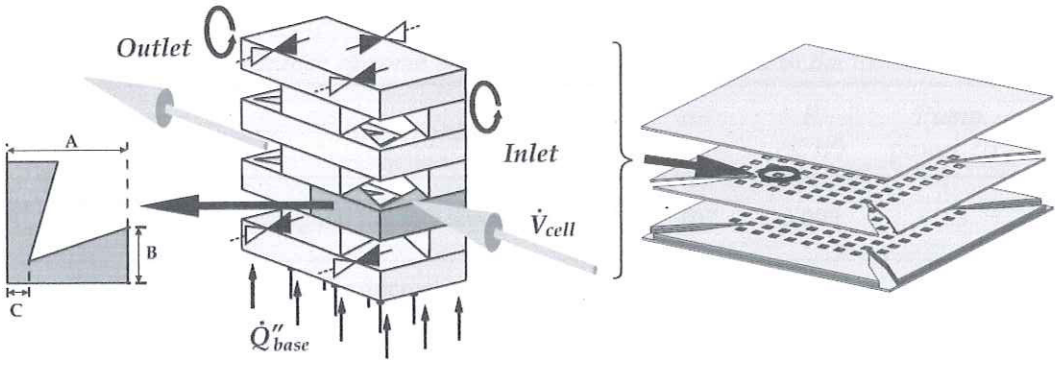

Figure 1.10 Mesh-like heat exchanger configuration proposed by [103].

More recently, Wälchli *et al.* [103] proposed a mesh-like heat exchanger configuration as an alternative for dissipating high heat fluxes. Figure 1.10 presents a sketch of this arrangement. The

device was formed by three interconnected layers, which are bonded using a *Direct Cooper Bounding Process* (DCB). Water is entering to the system from one port and leaves from the opposed port, suffering several change of direction in the system. Thereby, the heat transfer coefficient is increased, reducing the overall thermal resistance. Their numerical results showed that this system reaches thermal resistance values down 0.08 K/W with a pumping power near 0.33 W.

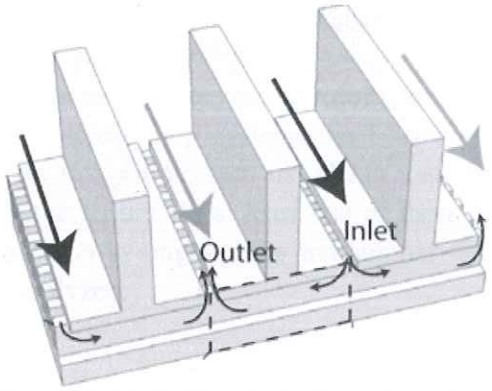

Figure 1.11 Manifold microchannel heat sink proposed by [104].

Escher *et al.* [104] followed this tendency and proposed a heat sink configuration based on several manifolds. Figure 1.11 shows a sketch of this arrangement. The system configuration is based on two layers. Several parallel channels are found in the first layer similar to a conventional microchannel heat sink. Then, some larger channels cross perpendicularly the first layer. A significant increase of the heat transfer area is achieved with these crossed channels. The numerical results provided by [104] indicated that this configuration dissipates up to 750 W/cm^2 with a temperature rise around 65 K. Thus, the system has a thermal resistance of 0.087 cm^2-K/W with a pressure drop penalty lower than 10 kPa (~20 times lower pressure drop than conventional microchannel heat sinks [13]). These results clearly show the evolution that micro heat sinks for electronic applications have endured over the last three decades. Table 1.1 shows a summary of the overall performance of some micro cooling systems found in the thecnical literature.

Table 1.1 Overall performance of some micro cooling systems found in the technical literature.

Author	*Description*	*ΔP (kPa)*	*R (K/W)*	*Pump. power (W)*	*q''_{max}* (W/cm^2)*
Tuckerman and Pease (1981) [13]	Rectangular microchannel heat sink	207	0.090	2.3	>650
Knight *et al.* (1992) [22]	Rectangular microchannel heat sink using turbulent flow	207	0.056	>10.0	>1000
Gillot *et al.* (2000) [37]	Rectangular microchannel heat sink for multichips modules	180	0.092	~47.0	>650
Peles *et al.* (2005) [100]	Micro heat sink with circular staggered pin fins	203	0.039	--	>1500

Colgan *et al.* (2007) [101]	Micro heat sink with "semi-elliptical" staggered pin fins	<35	0.105	<0.9	>500
Husain and Kim (2008) [64]	Optimized microchannel heat sink	--	0.081	--	>700
Escher *et al.* (2010) [104]	Heat sink formed by manifold channels	<10	0.087	~0.15	>680

*Considering 1 cm x 1 cm IC chip with maximum design temperature of 85°C and ambient temperature of 25°C.

Despite these great thermal and hydrodynamic results, some important aspects have not been considered in these alternative microcooling systems, such as uniformity of the die temperature, feasibility of the cooling system integration, fast and cheap manufacturing processes, etc. Clearly, these proposals of heat sinks have failures in at least one of these points. Thus, novel proposals of micro heat sinks, working with water in single-phase and laminar regime, and capable to cover these points should be proposed and analyzed.

ENHANCEMENT TECHNIQUES FOR MICROCHANNEL HEAT SINKS

Although single-phase heat transfer techniques for conventional channel and compact heat exchangers are well established, there are not several researches considering microchannel heat sinks. Steinke and Kandlikar [105] evaluated the feasibility of using the conventional enhancement techniques in microchannel and minichannels. They indicated that some passive techniques, such as flow disruptions, are good possibilities for thermal enhancement. Furthermore, there is not additional power costs for using these techniques since the system does not have moving parts or activation of components. The authors suggested the experimental and numerical evaluation of the pressure drop penalties and heat transfer performance when these passive techniques are used. Based upon this evaluation, Steinke and Kandlikar [106] carried out experiments with enhanced microchannel heat sinks formed by offset strip fins with lengths ranging from 250-500 μm and 50 μm width. Figure 1.12 shows SEM micrographs of the arrangement. The results showed that the system reaches a thermal resistance of 0.1 K/W and dissipated up to 1000 W/cm^2. The pressure drop penalty was ranging from 150 to 180 kPa.

On the other hand, Gong *et al.* [107] developed numerical analysis of microchannel formed by wavy walls along the flow length as a passive scheme for improving the heat transfer performance at low Reynolds number. Figure 1.13 shows sketches of this configuration. Their results showed that these configurations provide an overall thermal performance improvement of up to 26% compared on conventional microchannel. The increase of the pressure drop was ~30% compared to smooth channels. Wei *et al.* [108] analyzed numerically microchannels with one dimple at the bottom surface. Interesting thermal enhancements were observed at the vicinity of the downstream of the dimple (~30%) compared on smooth channels. The results indicated that this passive enhancement technique is a good alternative for enhancing the heat transfer coefficient inside microchannels. The pressure drop penalty was equivalent to smooth channels.

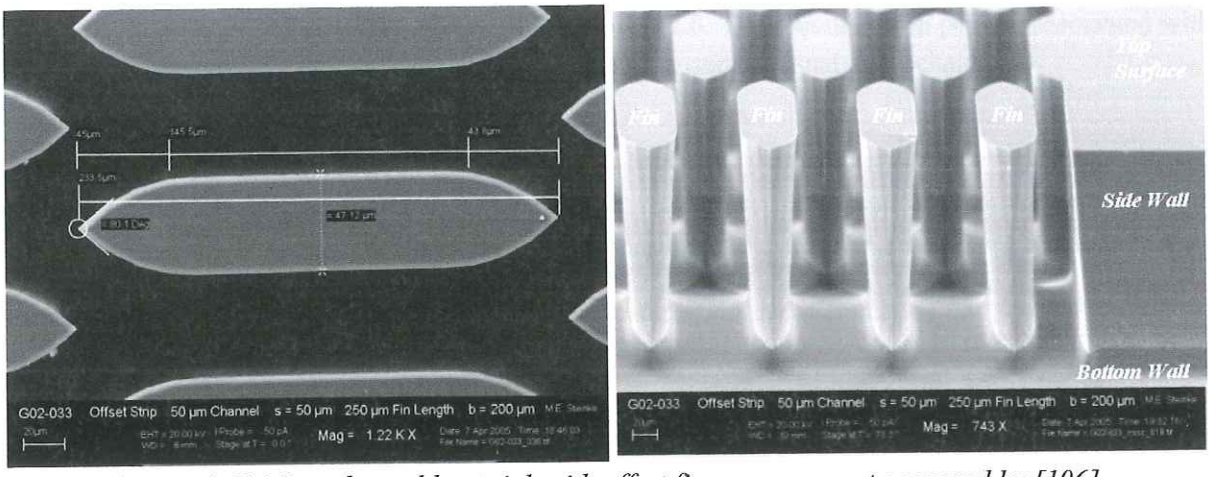

Figure 1.12 Microchannel heat sink with offset fins arrangement proposed by [106].

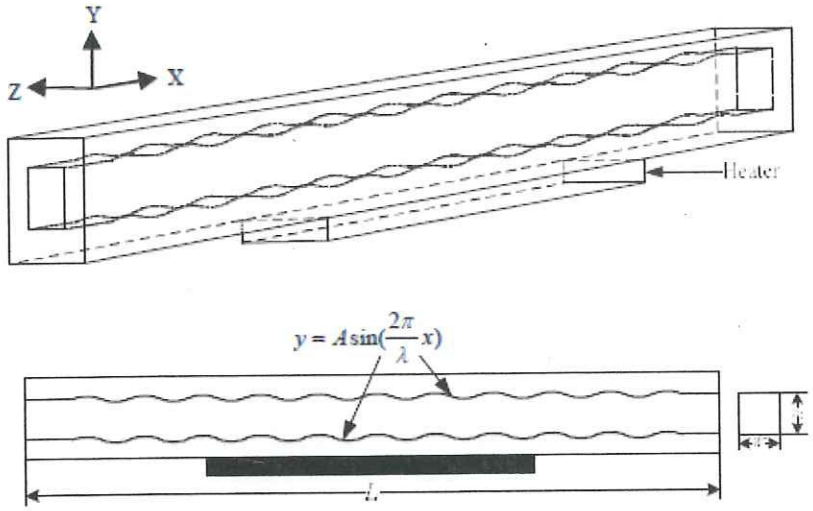

Figure 1.13 Microchannel heat sink with wavy channel walls proposed by [107].

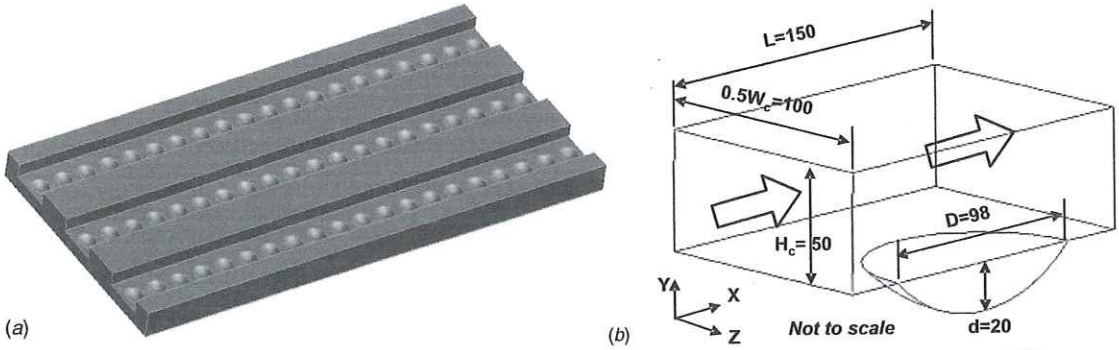

Figure 1.14 Microchannel heat sink with dimpled surfaces proposed by [108].

Xia *et al.* [109] introduced the concept of triangular reentrant cavities as a passive technique for enhancing microchannel heat sinks. Figure 1.15 shows a sketch of this arrangement. Their results showed that the thermal performance is importantly increased when these cavities are used, majorly

when the ration between H_t and Le (Figure 1.15) is near 2.0. The pressure drop penalty associated with this enhancement technique is relatively low compared to conventional microchannels.

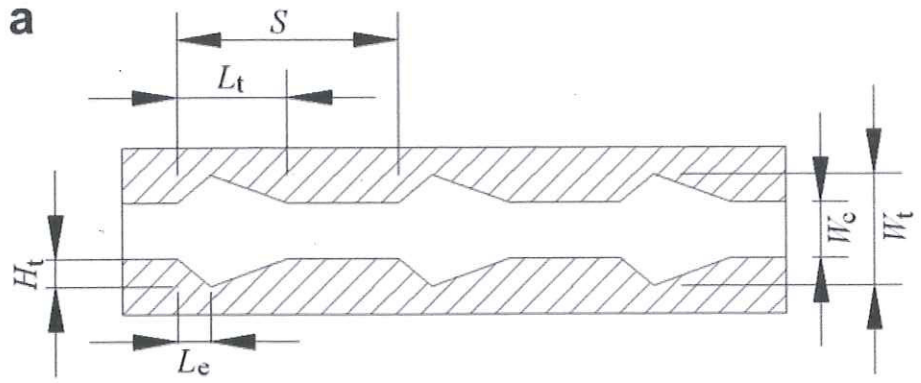

Figure 1.15 Microchannel heat sink with triangular reentrant cavities proposed by [109].

Conceptually, the variations of the channel cross-section along the flow length and sectioned channel with change of hydraulic diameter at each section are a couple of passive technique to increase the heat transfer in microchannels. Works aimed to analyze the thermal and hydrodynamic effects on these enhanced techniques for microchannels have not been reported in the technical literature. Table 1.2 summarizes the passive thermal enhancement techniques discussed above. The abbreviation *ETM-n* is used for indicating the number enhancement thermal model that is analyzing.

Table 1.2 Summary of passive thermal enhancement techniques to be analyzed in this work.

Enhancement Technique	*Main features*	*Ref.*
Channels with variable cross section area along the flow length (ETM-1)	- There are not studies in the technical literature.	N/A
Sectioned channels along the flow length with change of hydraulic diameter (ETM-2)	- There are not studies in the technical literature.	N/A
Channels with pin fins (ETM-3)	- The heat transfer area is significantly increased. - The pressure drop penalty is similar to straight channels	[106]
Channels with wavy walls (ETM-4)	- Thermal effects are important at low Reynolds numbers. - Overall, the thermal performance increases ~26%. - The pressure drop penalty is relatively large ~30%.	[107]
Channels with dimpled surface (ETM-5)	- The local heat transfer is increased at the vicinity of the downstream of the dimple. - Pressure drop penalty is not clearly reported.	[108]
Channels with reentrant triangular cavities (ETM-6)	- The heat transfer is significantly increased when the systems have $\alpha \sim 2.0$. - Pressure drop penalty associated with the thermal enhancement in not clearly provided.	[109]

Since the major goal of this work is to design a reliable microcooling system for cooling near-future IC chips considering passive enhancement techniques, with the feature of generating homogenous temperature profiles, the work is divided in two stages mentioned below.

1. The first stage focuses on evaluating the overall performance of each enhancement technique listed in Table 1.2. A dimensionless parameter ϕ is proposed for these purposes. Chapter 2 presents its formulation and definition. Results reported in the technical literature and/or numerical results for each enhancement technique are used for the evaluation of their overall performance.
2. Based upon the previous results and the goal of generating homogeneous temperature profiles on the IC chip, a micro cooling system is designed using numerical tools. Its performance with different operating conditions is evaluated.

A better performance of the near future IC chips and a significant increase in their lifetime is expected with this non-conventional microcooling system.

Chapter II
Evaluation of Enhancement Techniques in Microchannels –Formulation

DIMENSIONLESS OVERALL PERFORMANCE, ϕ

In Chapter I, some thermal performance enhancement techniques in microchannel, which have been recently analyzed, are presented (Tables 1.1 and 1.2). The current technical literature shows that the overall pressure drop increases strongly when the microchannel thermal resistance is slightly decreased (i.e. $\uparrow\Delta P >> \downarrow\Delta R$). Thus, although each technique improves, in different degree, the heat transfer coefficient in the microchannel, there is an important increase in the pressure drop penalty associated with this thermal improvement.

Thereby, this work proposes the use of the dimensionless parameter ϕ in order to evaluate quantitatively the real performance that each enhancement technique has in the cooling system. Thus, ϕ is defined as the ratio between thermal improvement and the rise of the pressure drop penalty (Equation (2.1)).

$$\phi = \frac{Thermal\ improvement}{Increase\ of\ pressure\ drop\ penalty} \tag{2.1}$$

By definition, the Nusselt number is a dimensionless parameter that involves the ratio of energy transferred from the channel walls to the fluid under specific boundary conditions. Based on this definition, the thermal improvement can be quantified as the ratio given by the Nusselt number in enhanced microchannels, Nu_i, divided by the Nusselt number in straight microchannels, Nu_0. Equation (2.2) shows this ratio.

$$Thermal\ improvement = \frac{Nu_i}{Nu_0} \tag{2.2}$$

$$Increase\ of\ pressure\ drop\ penalty = \frac{f_i}{f_0} \tag{2.3}$$

Moreover, the pressure drop penalty is directly affected by the operating conditions and the friction factor associated to the geometry and regime of the fluid. By definition, the Fanning friction factor, f, has the ability to represent the momentum transfer process of the fluid flow in a manner consistent with the heat and mass transfer representation. Thus, the increase of the pressure drop

penalty can be quantified by the ratio between Fanning friction factor in the improved channels, f_i, and the friction factor in straight microchannels, f_0. Equation (2.3) shows this ratio.

Substituting Equations (2.2) and (2.3) in Equation (2.1), the dimensionless overall performance, ϕ, is defined by Equation (2.4). Since this work is aimed to generate uniform temperature profiles on the IC chip considering the development of the fluid boundary layers, the local performance of the thermal enhanced microchannel heat sinks is needed to evaluate, i.e. $\phi=f(z^*)$, where z^* is the dimensionless channel length. Equation (2.5) is used for this purpose.

$$\phi = \frac{Nu_i}{Nu_0} \Big/ \frac{f_i}{f_0} \tag{2.4}$$

$$\phi(z^*) = \left(\frac{Nu_i}{Nu_0}(z^*)\right) \Big/ \left(\frac{f_i}{f_0}(z^*)\right) \tag{2.5}$$

From these equations, it is possible to conclude the following:

1. When $\phi>1.0$, the decrease of the microchannel thermal resistance is larger than the increase of the friction resistance associated to the enhancement technique.
2. When $\phi=1.0$, the increase in the thermal and fluid resistances remains in similar proportion. Thus, the enhancement technique does not have important effects on the microchannel.
3. When $\phi<1.0$, the decrease on the microchannel thermal resistance is lower than the increase in the friction resistance associated to the enhancement technique.

Thus, enhancement techniques that generates ϕ values larger than 1.0 are good alternatives in the design of the next generation of IC chip cooling systems.

Local and overall Nu_0 and f_0 are already found in the technical literature, as well as some overall Nu_i and f_i. However, only a few local Nu_i and f_i have been determined in the technical literature. Thus, numerical analyses are carried out in order to generate these local values. The formulation for each enhancement technique is presented in this chapter. The most up to date correlations for Nu_0 and f_0 are discussed in the next section.

STRAIGHT MICROCHANNEL HEAT SINKS

As it was mentioned in Chapter I, conventional microchannel heat sinks have been widely studied along the years. The manufacturing of these cooling systems is based typically on removing material from a silicon substrate until the channel height (channel depth) is achieved. Then, a thin plate of Pyrex is placed onto the substrate in order to cover the grooves. Thus, several straight and parallel channels with rectangular cross sections are formed. Figure 2.1 shows a sketch of these conventional configurations. A heat flux is supplied on the bottom wall of the cell and transferred to the channel walls by conduction. The coolant moves through these channels, removing the heat from the three-heating walls and taken out of the system. Technical literature presents correlations for their thermal and hydrodynamic performances considering fully as non-developed boundary conditions [C].

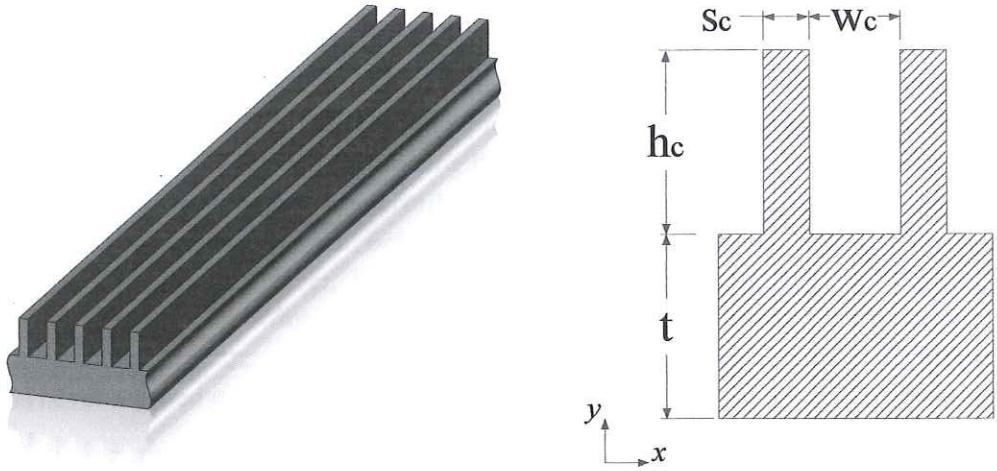

Figure 2.1 Sketch of straight microchannel heat sinks with width w_c, height h_c, silicon thickness t, and space between channels s_c.

The dimensionless parameter ϕ was defined in the previous section. ϕ is based on the thermal and hydrodynamic performance that straight microchannels have for specific operating conditions. Since the pressure and temperature gradients found in small diameter channels are quite high, the length of the channel in the developing region forms a major portion of the total channel length. Therefore, the system performance becomes a function of the dimensionless channel length. Equations (2.6) and (2.7) are used for computing them, respectively. Numerical values of these parameters for different channel aspect ratios, α_c, are available in the technical literature [C].

$$Nu_o(z^*) = Nu_{3,x}(z^*) = Nu_{4,x}(z^*)\frac{Nu_{3,fd}}{Nu_{4,fd}} \tag{2.6}$$

$$f_0(z^*) = f_{app} = \frac{\Delta P D_h^2}{2\mu u_m L z^*}\frac{1}{\mathrm{Re}} \tag{2.7}$$

Figures 2.2 and 2.3 present plots of $Nu_0(z^*)$ and $f_{app}\mathrm{Re}(z^*)$ for different values of α_c. This dimensionless parameter involves the relationship between the channel height and channel width. The largest variation of both parameters is clearly observed at the fluid inlet section. Although the curves present a quasi-constant Nu_o and $f_{app}\mathrm{Re}$ values after $z^* \geq 0.2$, the velocity and temperature profiles have not reached the fully developed conditions, affecting the heat dissipation and the pressure drop variation. Figures 2.4 and 2.5 show velocity and temperature profiles along the axial direction at the x^* and y^* dimensionless directions computed numerically. Four z^* positions are plotted (z^*~0, z^*=0.01, z^*=0.4 and z^*=0.95). The coolant is entering the channel with a constant velocity of 1 m/s and a temperature of 300 K.

The development of the velocity profiles along the flow length is observed in Figure 2.4 for both dimensionless planes (x^* and y^*). Comparing the velocity profiles at z^*=0.4 and z^*=0.95 (40% and 95% of the total flow length, respectively), a slight variation is observed. This means that the

coolant does not reach the fully developed condition in the channel, and, thereby the assumption of considering the apparent friction factor in the analyses is appropriate for this work. On the other hand, Figure 2.5 shows the dimensionless temperature profiles along the flow length for the same dimensionless planes. A symmetric temperature profile is clearly observed in the left figure (T^* vs x^*) since both parallel channel walls are transferring heat to the coolant. Moreover, the temperature profile along the y^*-plane shows an asymmetric profile caused by the insulated wall (right figure). The energy transferred to the fluid through the bottom wall of the channel increases gradually the fluid temperature on this plane; however, the thermal boundary layer is uniquely "developing" on this bottom wall of the channel. After z^*=0.4, the thermal energy supplied on this plane increases the temperature gradient near the upper wall of the channel; nevertheless, a fully developed thermal condition is never reached with these operating conditions.

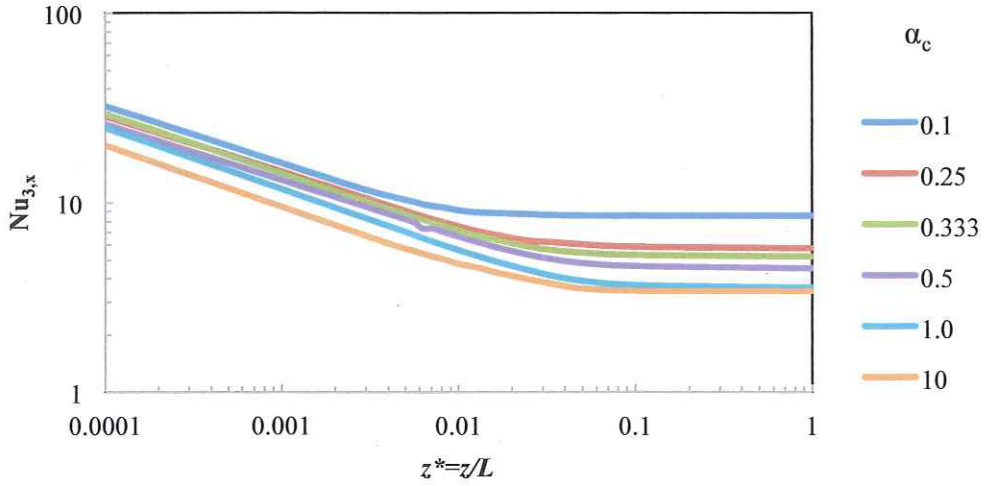

Figure 2.2 Nusselt number variations for rectangular channels subject to three-side heating walls and non-developed boundary conditions along the dimensionless channel length for different α_c.

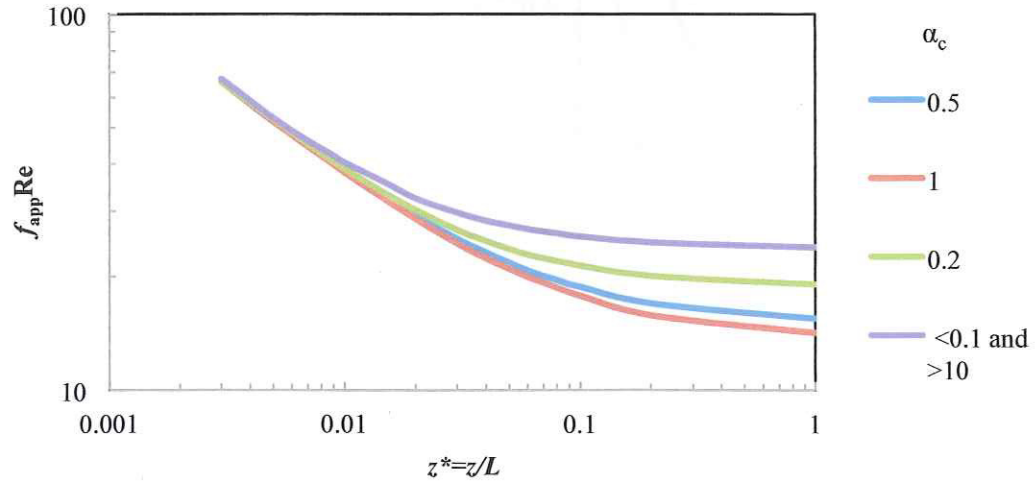

Figure 2.3 $f_{app}Re$ variations for rectangular channels subject to non-developed boundary conditions along the dimensionless channel length for different α_c.

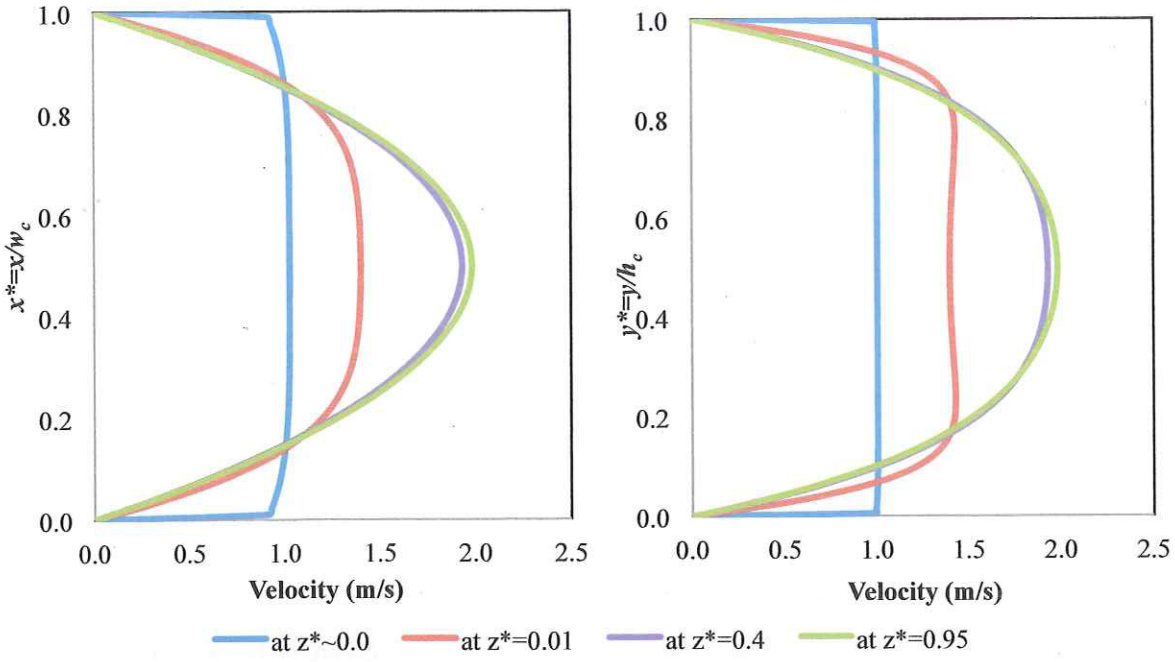

Figure 2.4 Fluid velocity profiles along the x (left) and y* (right) directions at different z* positions. Numerical simulation considering an inlet velocity of 1 m/s.*

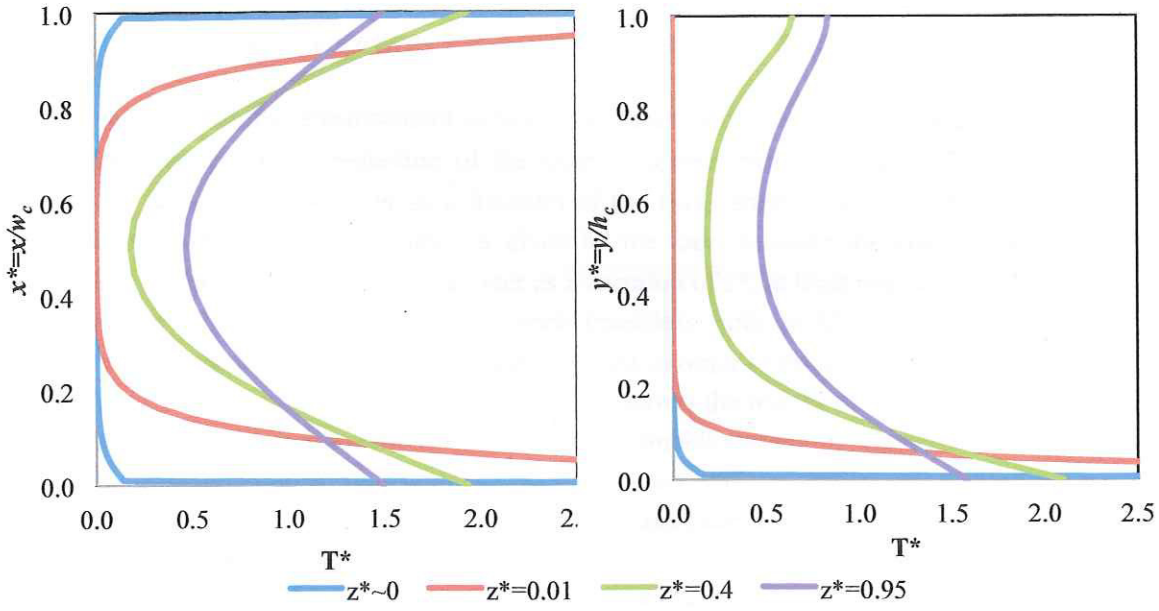

Figure 2.5 Fluid temperature profiles along the x (left) and y* (right) directions at different z* positions. Numerical simulation considering an inlet temperature of 1 m/s.*

According to these observations, the assumption of non-developed boundary condition at the fluid inlet section for both thermal and hydrodynamic performance has to be considered in the

analyses. Since the current micro-manufacturing processes are limited to microchannels larger than 50 μm width (due to the fact that the cost and complexity increase when the channel width is reduced), the following correlations are appropriated for this study. Equations (2.8) and (2.9) show the apparent friction factor and Nusselt number for rectangular channels subject to three-side heating, respectively. These correlations are based on the results given by Phillips [110].

$$f_0(z^*) = \frac{4196(z^*)^2 + 292.5(z^*) + 1.721}{(z^*)^3 + 275.8(z^*)^2 + 6.841(z^*) + 0.007316} \tag{2.8}$$

$$\mathrm{Nu}_3(z^*) = \frac{3.655x10^4(z^*)^2 + 3233(z^*) - 12.36}{(z^*)^3 + 8498(z^*)^2 + 165.1(z^*) - 0.5272} \tag{2.9}$$

PASSIVE ENHANCEMENT TECHNIQUES FOR MICROCHANNEL HEAT SINKS

In Chapter 1, a review of several passive enhancement techniques was presented. Based on this review, six outstanding techniques are considered for deeper studies. Table 1.2 shows these techniques. Numerical analyses are conducted in order to generate curves of their dimensionless overall performance, ϕ. Thereby, a pretty good comparison between them can be developed, considering both the thermal enhancement and the pressure drop penalty associated to the geometrical configuration. A description of the six enhancement techniques is presented below.

3.1 CHANNELS WITH VARIABLE CROSS SECTION (ETM-1)

The first thermal enhancement technique is based on the fact that the heat transfer coefficient is directly affected by the reduction of the channel aspect ratio α_c (Figure 2.6). Thus, this work proposes to define this parameter as a function of the flow length, (i.e. $\alpha_c=f(z^*)$). It is found in the technical literature that this parameter is given by the ratio between the channel width and height ($\alpha_c=wc/hc$). In order to obtain this parameter as a function of z^*, at least one of these dimensions must be a function of the flow length. This work considers both width and height variations. Two dimensionless parameters (β_{ETM-1}, γ_{ETM-1}) are proposed in order to obtain parametric results. Equations (2.10) and (2.11) define these parameters. Table 2.1 shows the matrix of cases to analyze considering the maximum channel hydraulic diameter for microchannels (hydraulic diameter of 200 μm) and the current minimal manufacturing channel capability (50 μm channel width). Five cases are considered in the analysis. Table 2.2 shows the dimensions of each case. In order to keep similarities with the straight channel, the thickness silicon substrate is 500 μm. The heat flux is supplied at the same bottom wall of the cell. The coolant is entering at the largest channel aspect ratio section (i.e. at $z^*=0$).

$$\beta_{ETM-1} = \frac{w_{c,o}}{w_c} \tag{2.10}$$

$$\gamma_{ETM-1} = \frac{h_{c,o}}{h_c} \tag{2.11}$$

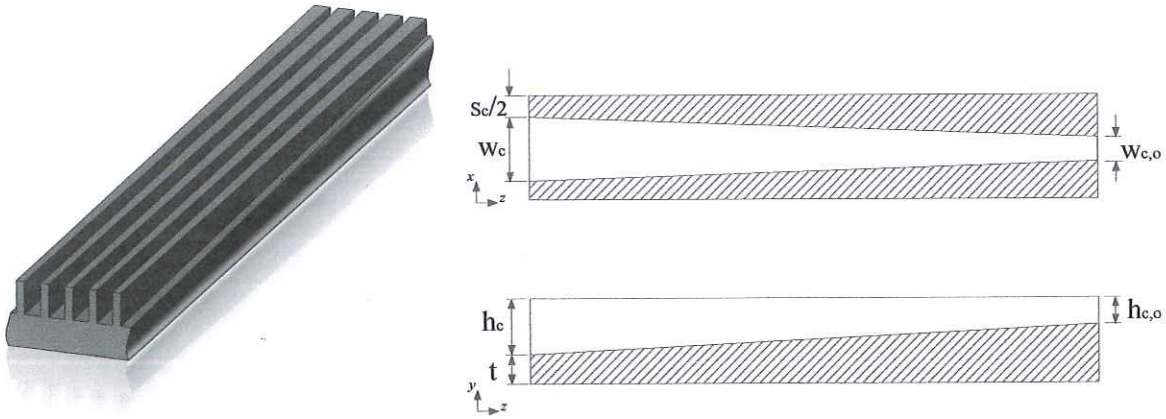

Figure 2.6 Channel with variable cross section (ETM-1). 3D sketch (left), sketch from the top and lateral planes (right).

Table 2.1 Matrix of cases for ETM-1.

		γ_{ETM-1}		
		0.25	**0.5**	**1.0**
β_{ETM-1}	**0.5**	ETM-1-I	ETM-1-II	ETM-1-III
	1.0	ETM-1-IV	ETM-1-V	

Table 2.2 Dimensions of cases for ETM-1.

ETM-1	*I*	*II*	*III*	*IV*	*V*
wc,i (μm)	100	100	100	100	100
wc,o (μm)	50	50	50	100	100
hc,i (μm)	200	200	200	200	200
hc,o (μm)	50	100	200	50	100

3.2 Sectioned Channels with Change of Hydraulic Diameter (ETM-2)

This second enhancement technique is following the idea exposed in ETM-1. According with the theory, the channel hydraulic diameter is defined by the channel aspect ratio and the channel height (Equation (2.12)). Thus, there is a direct relationship between the heat transfer coefficient and the channel height at constant channel aspect ratio. Furthermore, drastic changes of section improve the heat dissipation due to the destruction of the thermal boundary layer. Thereby, this technique considers the use of sectioned channels with specific channel hydraulic diameters, at constant channel aspect ratio, connected in straight line. Figure 2.7 shows sketches of this passive thermal enhancement technique. Six dimensionless parameters ($\beta_{ETM-2}, \beta'_{ETM-2}, \gamma_{ETM-2}$, γ'_{ETM-2}, ξ_{ETM-2} and ξ'_{ETM-2}) are introduced for generating a parametric analysis of this configuration. Equations (2.13) - (2.15) define these parameters. Table 2.3 presents the matrix of cases for ETM-2. Eight cases are considered in the analysis. Table 2.4 shows the channel dimensions for each case. Only three sections are considered in the analysis in order to reduce the manufacturing complexity. The dimensions of channel width and height are within the range of 50 μm to 200 μm. The heat flux is supplied on the bottom wall of the cell. The coolant is entering at the largest channel hydraulic diameter (i.e. at $z^*=0$)

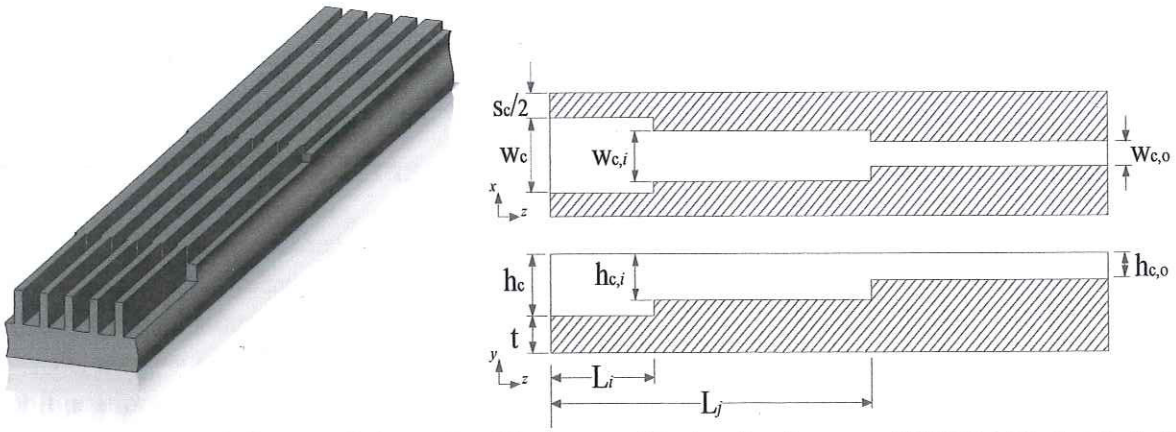

Figure 2.7 Sectioned channels with change of hydraulic diameter (ETM-2). 3D sketch (left), sketch from the top and lateral planes (right).

$$D_h = 2\frac{\alpha}{\alpha+1}h_c\Big|_{at\ \alpha_c=ctte} \tag{2.12}$$

$$\beta_{ETM-2} = \frac{w_{ci}}{w_c},\quad \beta'_{ETM-2} = \frac{w_{co}}{w_{ci}} \tag{2.13}$$

$$\gamma_{ETM-2} = \frac{h_{ci}}{h_c},\quad \gamma'_{ETM-2} = \frac{h_{co}}{h_{ci}} \tag{2.14}$$

$$\xi_{ETM-2} = \frac{L_i}{L},\quad \xi'_{ETM-2} = \frac{L_j}{L} \tag{2.15}$$

Table 2.3 Matrix of cases for ETM-2.

		β'_{ETM-2}	
		0.5	**1.0**
β_{ETM-2}	**0.5**		ETM-2-I
	1.0	ETM-2-VIII	
		γ'_{ETM-2}	
		0.5	**1.0**
γ_{ETM-2}	**0.5**	ETM-2-II	ETM-2-V
	1.0	ETM-2-VI	ETM-2-VII
		ξ'_{ETM-2}	
		0.5	**0.75**
ξ_{ETM-2}	**0.25**	ETM-2-II	ETM-2-III
	0.5		ETM-2-IV

Table 2.4 Channel dimensions for ETM-2.

ETM-2	*I*	*II*	*III*	*IV*	*V*	*VI*	*VII*	*VIII*
w_c (μm)	100	100	100	100	100	100	100	100
w_{ci} (μm)	50	75	75	75	75	75	75	100
w_{co} (μm)	50	50	50	50	50	50	50	50
h_c (μm)	200	200	200	200	200	200	200	200
h_{ci} (μm)	100	100	100	100	100	200	200	100

h_{co} (μm)	50	50	50	50	100	100	200	50
L_i (mm)	2.5	2.5	2.5	5.0	2.5	2.5	2.5	2.5
L_j (mm)	5.0	5.0	7.5	7.5	5.0	5.0	5.0	5.0

3.3 Channel with Pin Fins (ETM-3)

Knowing the thermal advantages that pin fins generate in systems aimed to transfer thermal energy due to the increase of the heat transfer area and effects on the fluid motion, the third enhancement technique is based on these configurations. In the technical literature, several studies of systems using conventional size fins are found. However, there is not enough information of these fin configurations working at microscale. Thus, an analysis of the effects that four fin shapes in specific configurations cause on the heat transfer and pressure drop in microcooling systems is studied. These fin shapes are: circular, square, ellipse and flat with rounded sides. Figure 2.8 shows sketches of each shape. On-line fin configurations are analyzed for each fin shape (Figure 2.9).

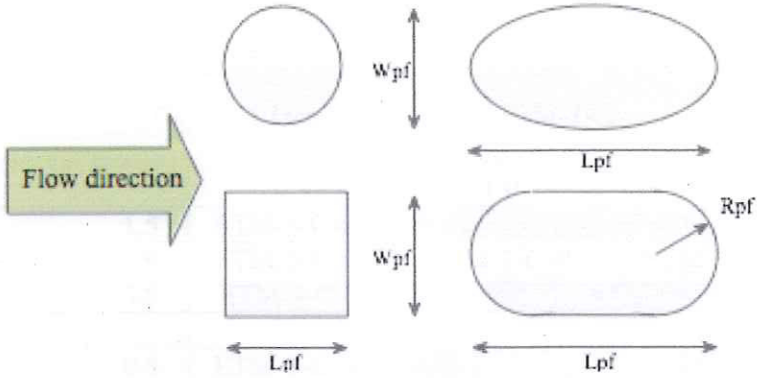

Figure 2.8 Pin fin shapes considered in the analysis: circle (top-left), square (bottom-left), ellipse (top-right), and flat with rounded sides (bottom-right).

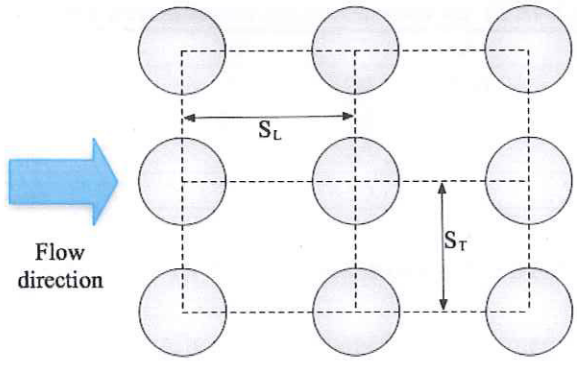

Figure 2.9 On-line fin configurations considered in the analysis.

In order to generate a dimensionless analysis, some parameters are proposed according to the fin shape to be studied. Based on these dimensionless numbers, a matrix of cases for each fin shape is proposed. The definition of these parameters and the matrix of cases for each configuration are presented in the subsequent subsections. As in the previous cases, the dimension of fin height, width and length (radius, length of side, large and short sides, etc.) are within the range of 50 μm to 200 μm.

3.3.1 Circle-shaped Micro Pin Fin Heat Sink (ETM-3-C)

Based on Figure 2.8, three dimensionless ratios are proposed in order to analyze this circle-shaped fin configuration. These ratios relate the longitudinal and transversal pitches (S_L and S_T, respectively) with the fin width, w_{pf} (radius of the circle), as well as the fin width with the fin height, h_{pf}.. These dimensionless parameters are called $\beta_{T\text{-}ETM\text{-}3\text{-}C}$ (Equation (2.16)), $\beta_{L\text{-}ETM\text{-}3\text{-}C}$ (Equation (2.17)), and $\gamma_{T\text{-}ETM\text{-}3\text{-}C}$ (Equation (2.18)). The matrix of cases to analyze is shown in Table 2.5. The dimensions of each case are shown in Table 2.6.

$$\beta_{T-ETM-3-C} = \frac{S_T}{W_{pf}} \tag{2.16}$$

$$\beta_{L-ETM-3-C} = \frac{S_L}{W_{pf}} \tag{2.17}$$

$$\gamma_{ETM-3-C} = \frac{w_{pf}}{h_{pf}} \tag{2.18}$$

Table 2.5 Matrix of cases for ETM-3-C.

		$\gamma_{ETM\text{-}3\text{-}C}$		
		0.5	**1.0**	**2.0**
$\beta_{L\text{-}ETM\text{-}3\text{-}C}$	**1.5**	ETM-3-C-IV		
	2.0	ETM-3-C-III	ETM-3-C-II	ETM-3-C-I
	3.0	ETM-3-C-V		
$\beta_{T\text{-}ETM\text{-}3\text{-}C}$	**0.5**	ETM-3-C-VI		
	1.0	ETM-3-C-III	ETM-3-C-II	ETM-3-C-I
	1.5	ETM-3-C-VII		

Table 2.6 Circle-shaped fin dimensions for ETM-3-C.

ETM-3-C	*I*	*II*	*III*	*IV*	*V*	*VI*	*VII*
w_{pf} (μm)	100	100	100	100	100	100	100
h_{pf} (μm)	50	100	200	200	200	200	200
S_T (μm)	200	200	200	200	200	150	300
S_L (μm)	200	200	200	150	300	200	200

3.3.2 Square-shaped Micro Pin Fin Heat Sink (ETM-3-S)

The analysis of this fin shape configuration is based on the dimensionless parameter shown in the previous section for circle-shaped fins. Only the names of these parameters are rewritten as: $\beta_{T\text{-}ETM\text{-}3\text{-}S}$ (Equation (2.16)), $\beta_{L\text{-}ETM\text{-}3\text{-}S}$ (Equation (2.17)), and $\gamma_{T\text{-}ETM\text{-}3\text{-}S}$ (Equation (2.18)). The matrix of cases to analyze is the same that for the circle-shaped fin case (Table 2.7). The dimensions for each case are presented in Table 2.8.

Table 2.7 Matrix of cases for ETM-3-S.

		$\gamma_{ETM\text{-}3\text{-}S}$		
		0.5	**1.0**	**2.0**
$\beta_{L\text{-}ETM\text{-}3\text{-}S}$	**1.5**	ETM-3-S-IV		
	2.0	ETM-3-S-III	ETM-3-S-II	ETM-3-S-I
	3.0	ETM-3-S-V		
$\beta_{T\text{-}ETM\text{-}3\text{-}S}$	**0.5**	ETM-3-S-VI		
	1.0	ETM-3-S-III	ETM-3-S-II	ETM-3-S-I
	1.5	ETM-3-S-VII		

Table 2.8 Circle-shaped fin dimensions for ETM-3-S.

ETM-3-S	*I*	*II*	*III*	*IV*	*V*	*VI*	*VII*
w_{pf} (μm)	100	100	100	100	100	100	100
h_{pf} (μm)	50	100	200	200	200	200	200
S_T (μm)	200	200	200	200	200	150	300
S_L (μm)	200	200	200	150	300	200	200

3.3.3 Ellipse-shaped Micro Pin Fin Heat Sink (ETM-3-E)

Following the same methodology of analysis, three dimensionless parameters are proposed to evaluate this fin shaped configuration based on the relationship between the longitudinal and transversal pitch with fin length and width, and the relationship between fin length and height. These parameters are called $\beta_{T\text{-}ETM\text{-}3\text{-}E}$, $\beta_{L\text{-}ETM\text{-}3\text{-}E}$, and $\gamma_{T\text{-}ETM\text{-}3\text{-}E}$, and are given by Equations (2.19) to (2.21), respectively. Table 2.9 presents the matrix of cases to analyze and Table 2.10 the dimensions for each case. The ratio between the short and large sides of the ellipse is kept constant (w_{pf}/L_{pf}=0.5).

$$\beta_{T-ETM-3-E} = \frac{S_T}{W_{pf}} \tag{2.19}$$

$$\beta_{L-ETM-3-E} = \frac{S_L}{L_{pf}} \tag{2.20}$$

$$\gamma_{ETM-3-E} = \frac{L_{pf}}{h_{pf}} \tag{2.21}$$

Table 2.9 Matrix of cases for ETM-3-E.

		$\gamma_{ETM\text{-}3\text{-}E}$		
		0.5	**1.0**	**2.0**
$\beta_{L\text{-}ETM\text{-}3\text{-}E}$	**1.5**	ETM-3-E-IV		
	2.0	ETM-3-E-III	ETM-3-E-II	ETM-3-E-I
	3.0	ETM-3-E-V		
$\beta_{T\text{-}ETM\text{-}3\text{-}E}$	**0.5**	ETM-3-E-VI		
	1.0	ETM-3-E-III	ETM-3-E-II	ETM-3-E-I
	1.5	ETM-3-E-VII		

Table 2.10 Ellipse-shaped fin dimensions for ETM-3-E.

ETM-2	I	II	III	IV	V	VI	VII
w_{pf} (μm)	100	100	100	100	100	100	100
L_{pf} (μm)	200	200	200	200	200	200	200
h_{pf} (μm)	50	100	200	200	200	200	200
S_T (μm)	200	200	200	200	200	150	300
S_L (μm)	400	400	400	300	600	400	400

3.3.4 Flat-shaped with Rounded Sides Micro Pin Fin Heat Sink (ETM-3-F)

The analysis of this fin shape is based on four dimensionless parameters: $\beta_{T\text{-}ETM\text{-}3\text{-}F}$, $\beta_{L\text{-}ETM\text{-}3\text{-}F}$, $\gamma_{T\text{-}ETM\text{-}3\text{-}F}$, and $\xi_{T\text{-}ETM\text{-}3\text{-}F}$. The first three parameters are ratios similar to the previous sections. The fourth parameter is based on the relationship between the fin width and the radius of curvature of the fin, R_{pf} (Figure 2.8). The definitions of these parameters are expressed in Equations (2.22) to (2.25), respectively. Tables 2.11 and 2.12 present the matrix of cases for this fin shape and the dimensions of each case, respectively. A constant ratio of 0.5 between the fin length and width is used in the cases. The silicon substrate thickness for all these pin fin configurations remains as 500 μm.

$$\beta_{T-ETM-3-F} = \frac{S_T}{W_{pf}} \tag{2.22}$$

$$\beta_{L-ETM-3-F} = \frac{S_L}{L_{pf}} \tag{2.23}$$

$$\gamma_{ETM-3-F} = \frac{L_{pf}}{h_{pf}} \tag{2.24}$$

$$\zeta_{ETM-3-F} = \frac{w_{pf}}{R_{pf}} \tag{2.25}$$

Table 2.11 Matrix of cases for ETM-3-F.

		$\gamma_{ETM\text{-}3\text{-}F}$		
		0.5	**1.0**	**2.0**
$\beta_{L\text{-}ETM\text{-}3\text{-}F}$	**1.5**	ETM-3-F-VI		
	2.0	ETM-3-F-III	ETM-3-F-II	ETM-3-F-I
	3.0	ETM-3-F-VII		
$\beta_{T\text{-}ETM\text{-}3\text{-}F}$	**0.5**	ETM-3-F-VIII		
	1.0	ETM-3-F-III	ETM-3-F-II	ETM-3-F-I
	1.5	ETM-3-F-IX		
μ	**0.25**	ETM-3-F-IV		
	0.50	ETM-3-F-III	ETM-3-F-II	ETM-3-F-I
	0.75	ETM-3-F-V		

Table 2.12 Flat-shaped fin dimensions for ETM-3-F.

ETM-2	I	II	III	IV	V	VI	VII	VIII	IX
w_{pf} (μm)	100	100	100	100	100	100	100	100	100
L_{pf} (μm)	200	200	200	200	200	200	200	200	200
h_{pf} (μm)	50	100	200	200	200	200	200	200	200
S_T (μm)	200	200	200	200	200	200	200	150	300
S_L (μm)	400	400	400	400	400	300	600	400	400
R_{pf}(μm)	50	50	50	25	75	50	50	50	50

3.4 Channel with Wavy Walls (ETM-4)

The fourth thermal enhancement technique proposed is the use of channel with wavy walls. The increase in the heat transfer area does interesting the use of these configurations. Furthermore, the fluid does not suffer drastic flow variations, having just a slight increase in the pressure drop penalty. The channel shape is based on a sinusoidal shape, with α_{wave} and λ_{wave} as the amplitude and half-cycle, respectively. Figure 2.10 shows sketches of this thermal enhancement technique. Two dimensionless parameters (β_{ETM-4}, γ_{ETM-4}) are used in the analysis. Equations (2.26) and (2.27) define these parameters. Table 2.13 shows the matrix of cases to analyze. Nine configurations are obtained from this matrix. Table 2.14 shows the dimensions for each case. The channel width and height are $w_{c,i}$=100 μm and $h_{c,i}$=200 μm. The silicon substrate thickness remains as 500 μm. The heat flux is supplied on the bottom wall of the heat sink.

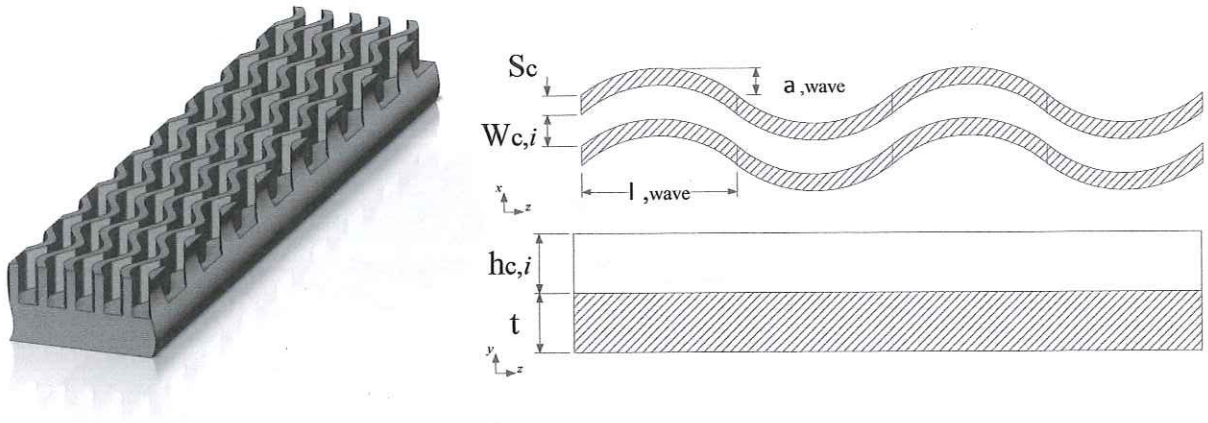

Figure 2.10 Channel with wavy walls (ETM-4). 3D sketch (left), sketch from the top and lateral planes (right).

$$\beta_{ETM-4} = \frac{\alpha_{wave}}{w_{ci}} \tag{2.26}$$

$$\gamma_{ETM-4} = \frac{\lambda_{wave}}{L} \tag{2.27}$$

Table 2.13 Matrix of cases for ETM-4.

		β_{ETM-4}		
		0.25	**0.5**	**1.0**
γ_{ETM-4}	**0.05**	ETM-4-I	ETM-4-IV	ETM-4-VII
	0.1	ETM-4-II	ETM-4-V	ETM-4-VIII
	0.2	ETM-4-III	ETM-4-VI	ETM-4-IX

Table 2.14 Channel dimensions for ETM-4.

ETM-4	*I*	*II*	*III*	*IV*	*V*	*VI*	*VII*	*VIII*	*IX*
α_{wave} (μm)	25	25	25	50	50	50	100	100	100
λ_{wave} (mm)	0.5	1.0	2.0	0.5	1.0	2.0	0.5	1.0	2.0

3.5 Channel with Dimpled Surface (ETM-5)

Channels with dimpled surface are also proposed as thermal enhancement techniques due to the destruction of the developed thermal boundary layers that the dimples do in the fluid along the flow length. Also, a slight increase in the heat transfer area is reached. Figure 2.11 shows sketches of the geometry used for this enhancement technique. Four dimensionless parameters (α_{ETM-5}, β_{ETM-5}, γ_{ETM-5}, and ξ_{ETM-5}) are used for the analysis. Equations (2.28) – (2.31) show the definition of each parameter. Table 2.15 shows the matrix of cases to analyze. The channel width and height are the same that for ETM-4. Table 2.16 presents the dimensions of the dimple width, length and height for each case. The longitudinal pitch is also shown in this table. These cases are selected in order to observe the effects that each dimensionless parameter has in the channel considering the other parameters as constants.

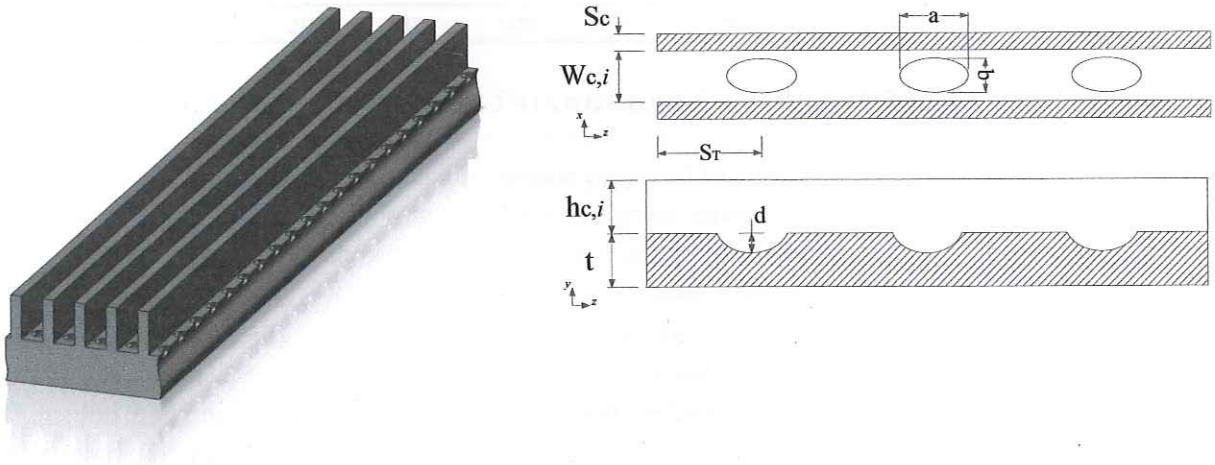

Figure 2.11 Channel with dimpled surface (ETM-5). 3D sketch (left), sketch from the top and lateral planes (right).

$$\alpha_{ETM-5} = \frac{a}{b} \tag{2.28}$$

$$\beta_{ETM-5} = \frac{d}{h_{ci}} \tag{2.29}$$

$$\gamma_{ETM-5} = \frac{b}{w_{ci}} \tag{2.30}$$

$$\xi_{ETM-5} = \frac{a}{S_l} \tag{2.31}$$

Table 2.15 Matrix of cases for ETM-5.

		β_{ETM-5}		
		0.025	**0.05**	**0.1**
α_{ETM-5}	**0.75**	ETM-5-VI	ETM-5-VII	ETM-5-VIII
	1.0	ETM-5-IX		
	1.5	ETM-5-X		
γ_{ETM-5}	**0.7**	ETM-5-IV		
	0.85	ETM-5-V		
	1.0	ETM-5-VI		
ξ_{ETM-5}	**0.125**	ETM-5-I		
	0.25	ETM-5-II		
	0.5	ETM-5-III		

Table 2.16 Channel dimensions for ETM-5.

ETM-5	*I*	*II*	*III*	*IV*	*V*	*VI*	*VII*	*VIII*	*IX*	*X*
a (μm)	50	50	50	52.5	63.75	75	75	75	100	150
b (μm)	66.67	66.67	66.67	70	85	100	100	100	100	100
d (μm)	5	5	5	5	5	5	10	20	5	5
S_l (μm)	400	200	100	105	127.5	150	150	150	200	300

3.6 Channel with Reentrant Triangular Cavities (ETM-6)

The last thermal enhancement technique proposed to analyze is based on the work developed by Xia *et al.* [109]. Channels with reentrant triangular cavities have shown an important thermal improvement. Figure 2.12 shows a sketch of this configuration. Four ratios are proposed to analyze this configuration: α_{ETM-6}, β_{ETM-6}, γ_{ETM-6} and ξ_{ETM-6}. These parameters relate the channel width and height (Equation (2.32), the inlet channel width and the maximum channel width at the triangular cavity (Equation 2.33), the small triangular cavity length with the large triangular cavity length (Equation 2.34), and the pitch between cavities with the large triangular cavity length (Equation 2.35). The matrix of cases to analyze is shown in Table 2.17. These cases are enough to describe the geometrical effects on the overall performance of the heat sink. The dimensions of each case are listed in Table 2.18. These dimensions are within the range of 50 μm to 200 μm in order to cover the restrictions specified previously.

$$\alpha_{ETM-6} = \frac{w_c}{h_c} \tag{2.32}$$

$$\beta_{ETM-6} = \frac{w_c}{w_{c,max}} \tag{2.33}$$

$$\gamma_{ETM-6} = \frac{L_{out}}{L_{in}} \tag{2.34}$$

$$\zeta_{ETM-6} = \frac{S_T}{L_{in}} \tag{2.35}$$

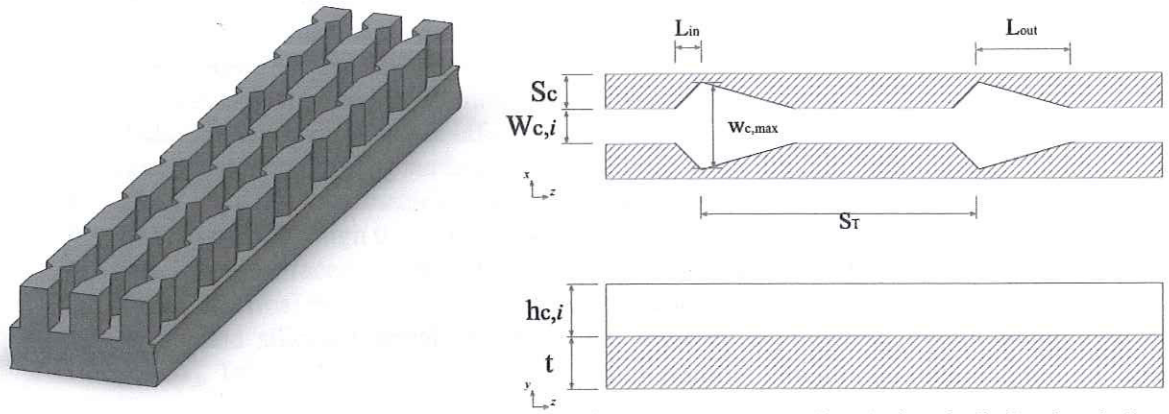

Figure 2.12 Channel with reentrant triangular cavities (ETM-6). 3D sketch (left), sketch from the top and lateral planes (right).

Table 2.17 Matrix of cases for ETM-6.

		α_{ETM-6}		
		0.25	**0.5**	**1.0**
β_{ETM-6}	**0.25**		ETM-6-IV	
	0.50	ETM-6-I	ETM-6-II	ETM-6-III
	0.75		ETM-6-V	
γ_{ETM-6}	**1.0**		ETM-6-VI	
	1.5	ETM-6-I	ETM-6-II	ETM-6-III
	2.0		ETM-6-VII	
ξ_{ETM-6}	**1.5**		ETM-6-VIII	
	2.0		ETM-6-IX	
	4.0	ETM-6-I	ETM-6-II	ETM-6-III

Table 2.18 Channel dimensions for ETM-6.

ETM-6	*I*	*II*	*III*	*IV*	*V*	*VI*	*VII*	*VIII*	*IX*
w_c (μm)	50	100	200	100	100	100	100	100	100
h_c (μm)	200	200	200	200	200	200	200	200	200
$w_{c,max}$ (μm)	100	200	400	400	133.3	200	200	200	200
L_{in} (μm)	50	50	50	50	50	50	50	50	50
L_{out} (μm)	75	75	75	75	75	50	100	75	75
S_t (μm)	200	200	200	200	200	200	200	75	100

ASSUMPTIONS, GOVERNING EQUATIONS AND BOUNDARY CONDITIONS

4.1 ASSUMPTIONS

Temperature, velocity and pressure distributions need to be computed for each single model in order to determine their overall performance. The assumptions to be considered in this work are the following:

1. Analyses in steady state,
2. Water is the coolant,
3. Silicon is the material used for building the different heat sinks,
4. Single phase and laminar regime,
5. Non-developed boundary conditions at the fluid inlet section,
6. Radiation and electrokinetic effects are negligible,
7. Smooth and non-sliding surfaces are considered in the fluid-solid interface,
8. Thick plate of Pyrex material is covering each heat sink configuration,
9. Heat transfer through the Pyrex plate is negligible,
10. The silicon surfaces do not suffer erosion caused by the fluid motion,
11. Wasted thermal energy through to the environment is negligible, and
12. Water and silicon thermal properties are assumed as constant, except water viscosity [43,64]. Table 2.19 shows the values for each property and the function for fluid viscosity.

Table 2.19 Thermophysical properties for water and silicon substrate.

Properties	*Value/Function*	*Units*
	Water	
Viscosity, μ	$2.414x10^{-5}\left(10^{247.8/(T-140)}\right)$	N-s/m^2
Thermal conductivity, k_f	0.6	W/m-K
Density, ρ_f	998.3	kg/m^3
Specific heat, cp_f	4.183	kJ/kg-K
	Silicon	
Thermal conductivity, k_s	148	W/m-K
Density, ρ_s	2330	kg/m^3
Specific heat, cp_s	0.712	kJ/kg-K

The governing equation are the continuity, Navier-Stokes and energy equations for solid and fluid domains. According with the assumption, these equations are given by:

4.2 GOVERNING EQUATIONS

Continuity equation:

$$\nabla \cdot \mathrm{U} = 0 \tag{2.36}$$

Navier-Stokes equation:

$$\mathrm{U}(\nabla \cdot \mathrm{U}) = -\frac{1}{\rho_f}\nabla \cdot \mathrm{P} + \lambda_{x,y,z} \tag{2.37}$$

Energy equation for solid domain:

$$\nabla \cdot (k_s \nabla \cdot \mathrm{T}) = 0 \tag{2.38}$$

Energy equation for fluid domain:

$$\mathrm{U} \cdot (\nabla \cdot \mathrm{T}) = \alpha \, \nabla^2 \cdot \mathrm{T} + \mu \psi \tag{2.39}$$

Where:

$$\lambda_x = \frac{1}{\rho_f}\left[\frac{\partial}{\partial x}\left(2\mu\frac{\partial u}{\partial x}\right)+\frac{\partial}{\partial y}\left(\mu\left(\frac{\partial v}{\partial x}+\frac{\partial u}{\partial y}\right)\right)+\frac{\partial}{\partial z}\left(\mu\left(\frac{\partial w}{\partial x}+\frac{\partial u}{\partial z}\right)\right)\right]$$

$$\lambda_y = \frac{1}{\rho_f}\left[\frac{\partial}{\partial y}\left(2\mu\frac{\partial v}{\partial y}\right)+\frac{\partial}{\partial x}\left(\mu\left(\frac{\partial v}{\partial x}+\frac{\partial u}{\partial y}\right)\right)+\frac{\partial}{\partial z}\left(\mu\left(\frac{\partial w}{\partial y}+\frac{\partial v}{\partial z}\right)\right)\right]$$

$$\lambda_x = \frac{1}{\rho_f}\left[\frac{\partial}{\partial z}\left(2\mu\frac{\partial w}{\partial z}\right)+\frac{\partial}{\partial x}\left(\mu\left(\frac{\partial w}{\partial x}+\frac{\partial u}{\partial z}\right)\right)+\frac{\partial}{\partial y}\left(\mu\left(\frac{\partial w}{\partial y}+\frac{\partial v}{\partial z}\right)\right)\right]$$

$$\psi = \frac{1}{\rho_f c p_f}\left[2\left(\left(\frac{\partial u}{\partial x}\right)^2+\left(\frac{\partial v}{\partial y}\right)^2+\left(\frac{\partial w}{\partial z}\right)^2\right)+\left(\left(\frac{\partial u}{\partial y}+\frac{\partial v}{\partial x}\right)^2+\left(\frac{\partial u}{\partial z}+\frac{\partial w}{\partial x}\right)^2+\left(\frac{\partial v}{\partial z}+\frac{\partial w}{\partial y}\right)^2\right)\right]$$

4.3 Boundary Conditions

Finally, the boundary conditions to be considered in the analyses are the following:

1. Water at T_{in}=300 K and constant velocity is entering to the system at the inlet section (pressure is computed by the numerical model),
2. Outlet boundary condition is set at the outlet section at zero static pressure (temperature and velocity are computed by the numerical model),
3. A constant heat flux value is supplied on the bottom wall of the heat sink,
4. Solid walls adjacent to the Pyrex plate are considered as adiabatic,
5. Fluid and solid symmetry conditions are set at the cut walls of the cell,
6. Interface condition is set at the walls which have interaction between solid and fluid domain, and
7. Remaining walls are considered as insulated walls.

Chapter III shows a description of the numerical analysis used for solving the models and getting the dimensionless overall performance ϕ. Chapter IV presents the results and comparisons of each enhancement technique.

Chapter III
Numerical Analysis

NUMERICAL ANALYSIS

1.1 BUILDING THE COMPUTATIONAL MODEL

Chapter II exposes the different enhancement techniques to be analyzed in order to determine their dimensionless overall performance, ϕ, and the effects of varying their geometrical parameters. Commercial *Computational Fluid Dynamic* (CFD) tools are required for computing the temperature, velocity and pressure in each model subject to the system operating conditions. According to this, a conjugate heat transfer model is built, considering the boundary conditions discussed in the previous chapter. Thus, 3D computational models based on the different cases to analyze are built using *Computational Aided Design* (CAD) tools. Both fluid and solid domains are considered in these computational models. Since most of the configurations present symmetry conditions, the models are built considering only one part of the whole system. This helps to strongly reduce computation time. Figure 3.1 presents a 3D sketch of a straight microchannel heat sink in order to clarify the symmetric characteristics of the problem. The fluid inlet and outlet, heat flux and symmetry conditions are indicated in the figure.

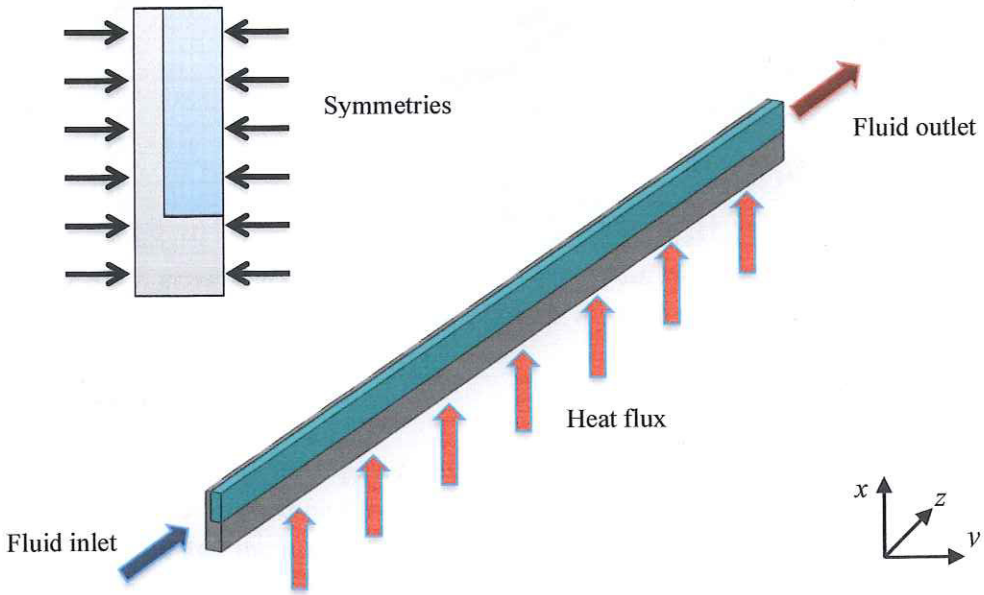

Figure 3.1 3D sketch of the straight channel. Both solid (gray) and fluid (blue) domains are indicated. Flow direction, heat flux and symmetry are shown.

1.2 Mesh Generation

The *Computational Fluid Dynamic* tools to be used in these analyses are based on the *Finite Volume Method* (FVM), this means, that the whole model is divided in a specific number of finite control volumes which are solved separately and then, the results are compiled to determine the overall temperature, velocity and pressure variations in the system. The "partition" of the whole system is based on a 3D mesh generation. A commercial powerful tool specialized in mesh bulding for this kind of systems is used for generating the whole mesh in each thermal enhancement technique model. Figure 3.2 shows the mesh generated in a straight microchannel heat sink (e.g. Figure 3.1). Tetrahedral elements are used in the mesh considering both solid and fluid domains. In order to compute the effects near the channel walls, a bi-exponential mesh distribution is used, decreasing the space between elements on these zones at a ratio of 1.5. Figure 3.2 presents details of these distributions. Moreover, although a normal distribution along the flow length is used, the number of elements is large enough for computing the flow variation along this direction (at least 200 elements are used along the z-axis). Similar mesh processes are carried out in the other models.

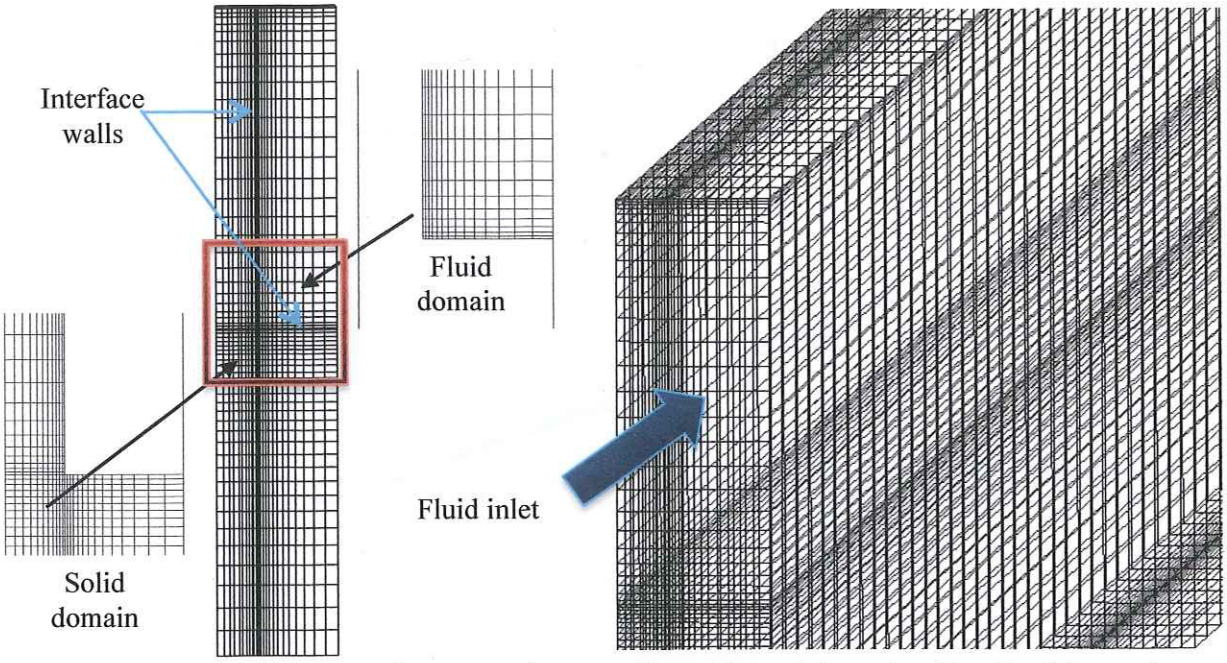

Figure 3.2 Mesh generated in a straight microchannel heat sink section. Details of the mesh distributions near the channel walls are shown. Flow direction is indicated as well.

1.3 Mesh Sensibility Analysis

In order to reduce the error generated by the mesh density, a *Mesh Sensibility Analysis* is carried out. This analysis is based on the fact of generating an "initial" mesh in the model and getting the numerical solution for the specific boundary and operating conditions. Once the solution is computed, the number of elements of the mesh is increased (e.g. the number of elements may be increased twice the number of elements used in the "initial" mesh), generating a "second" mesh. Then, the model is solved using this improved mesh considering the same boundary and operating

conditions. The results for each solution are then compared and the difference is evaluated. This process is repeated until the difference can be assumed as negligible. This work carries out this analysis considering a straight microchannel model.

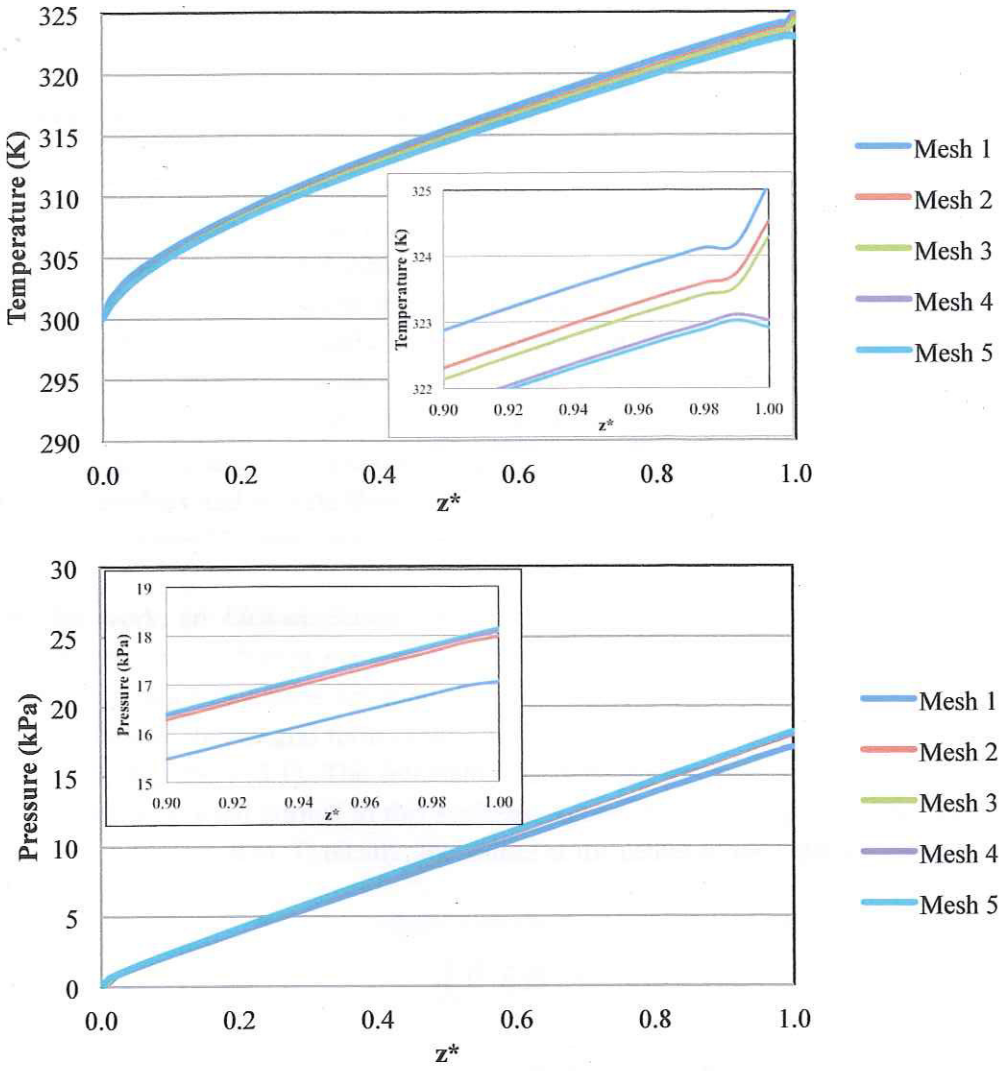

Figure 3.3 Mesh Sensibility Analysis for the fluid temperature variation (top) and pressure variation (bottom) along the flow length.

In this work, the "initial" mesh was formed by 26,800 tetrahedral elements (Mesh 1). An increase of two times is done in the mesh along each axial direction (x-, y- and z-axis), generating a second mesh of 53,600 elements (Mesh 2). Once the solutions were computed and compared according to the iterative process, is taken the decision of generating three subsequent meshes (Mesh 3, Mesh 4 and Mesh 5), having 145,000, 290,000 and 514,800 elements, respectively. Figure 3.3 presents the fluid temperature and pressure variations along the flow length for the five meshes. The results show that the difference generated by "meshing" is negligible when Mesh 3 is used (the difference between this mesh and Mesh 4 is ~10 Pa); however, the difference in the temperature variation is significantly large (~1.2 K). Analyzing the curves, it is observed that the fluid temperature

and pressure variations between Mesh 4 and Mesh 5 are negligible (~0.1 K and 5 Pa, respectively). Thus, this work considers the number of elements and mesh density used in Mesh 4 for generating the mesh in the different thermal enhancement technique models to be analyzed (i.e. number of elements > 300,000 tetrahedral elements). Since some models have important variations in the geometry configuration (e.g. pin fins), the number of elements is going to be larger due to the mesh distribution used near walls.

1.4 Overview of the Numerical Solution of the System

Previously, it was mentioned that commercial CFD tools are used for solving each model, determining their temperature, fluid velocity and pressure distributions. These tools are based on replacing the continuous problem domain with discrete domains using the grid distribution described in the previous section. In the discrete domain, each variable is defined only at the grid points. Thus, the relevant variable solutions are only known at these grid points. The values at other locations are determined by interpolating the values at the grid points. The governing partial differential equations and boundary conditions are defined in terms of the continuous variable (e.g. u, v, w, p, T). Thereby, the discrete system is a large set of coupled algebraic equations in the discrete variables. Setting up these discrete variables and solving them involves a very large number of repetitive calculations or iterations. Thus, a powerful computational equipment is required for this purpose.

In this work, an *Element-Based Finite Volume* code is used in this discretization process considering the mesh distribution generated in the previous stage. Under this approach, the integral form of the conservation equations are applied to the control volume defined by a cell generated with the mesh distribution. The integral form of the continuity equation for steady state and incompressible flow is given by Equation (3.1). The integration is done on the surface of the differential control volume and n is the outward normal to this surfaces. According to this equation, the net volume flow into the control volume is zero. Typically, the values at the center of the cells are computed when this approach is used.

$$\int_S \vec{V} \cdot \hat{n} \, dS = 0 \tag{3.1}$$

Similarly, momentum and energy conservations are satisfied in order to determine velocity vectors and temperature in the cell-centers of the mesh. The velocity and temperature at the faces is determined by interpolating the cell-center values at the adjacent cells. Thus, the partial differential governing equations become a linear algebraic approach, generating a system of n-equation and m-variables. Then, the boundary condition values fix the system. Once the system is discretized, a numerical method is applied for computing the value of each variable (e.g. Gauss-Jordan method). As a result, each finite volume has relevant quantities of mass, momentum and energy. Each of these volumes is then coupled in a general equation-system. Segregated solvers employ a solution strategy where the momentum equations are initially solved, considering a "guessed" pressure. Then, the temperature distribution is computed using these parameters. Because of the "guess and correct" nature of the linear system, a large number of iterations are typically required in addition to the need for judiciously selecting relaxation parameters for each variable.

In order to obtain a good approach, it is necessary to define the iterative convergence to be used in the iterative process. In this numerical tool, the iteration process is carried out until some selected measure of the difference between u_{i+1} and u_i, referred to as a residual is "small enough", this means, that the residual R is defined as the value of the difference between u_{i+1} and u_i in the grid. Equation (3.2) shows the above.

$$R = \sqrt{\frac{\sum_{i=1}^{N} (u_i - u_{i+1})^2}{N}} \tag{3.2}$$

Commonly, the residual is scaled with the average value of u in the domain in order to avoid error generated by low velocities in the domain. Thus, the residuals are re-defined as:

$$R = \frac{\sqrt{N \sum_{i=1}^{N} (u_i - u_{i+1})^2}}{\sum_{i=1}^{N} u_i} \tag{3.3}$$

The commercial software requires a residual value for each conservation equation. Thus, the iterative convergences for continuity, energy and momentum equations have to be defined, where each convergence value selected for each governing equation is problem- and code-dependent.

1.5 Model Validation

In order to validate the numerical model shown previously, a couple of cases found in the technical literature are considered. The five cases analyzed experimentally by Tuckerman in his Ph.D. thesis [I] are good candidates for doing the thermal validation. These geometries are similar to the system shown in Figure 3.1. Table 3.1 presents the characteristics of these cases.

Table 3.1 Feature of the five cases studied by Tuckerman [I].

	Case				
	0	*1*	*2*	*3*	*4*
w_c *(μm)*	64	64	56	55	50
h_c *(μm)*	280	280	320	287	302
q'' *(W/cm²)*	34.6	34.6	181	277	790
Q *(cm³/s)*	1.277	1.86	4.7	6.5	8.6
Number of channels	150	150	200	200	200

In his work, Tuckerman presents the local thermal resistance at different positions of the channel length. For Case 0, these values are presented in Figure 3.4. This figure shows that the maximum thermal resistance is located at 90% of the total channel length (i.e. R=0.227 cm²K/W at x=0.9 mm). Also, it is observed that the thermal resistance increases almost lineally before this maximum point, except near the entrance region. By using the numerical model discussed in this

chapter, the same case was solved (Case 0) and the local thermal resistance along the flow length was determined. Figure 3.4 shows the path of this local thermal resistance. The results show a very good agreement with the experimental result for positions of the channel length less than x= 0.85. After this point, a larger variation is observed. In 2002, Toh *et al.* [43] developed a numerical code for solving Tuckerman's cases [I]. Their results show the local thermal resistance variation along the flow length for each one of these cases. For Case 0, their thermal resistance curve is similar to the curve observed in Figure 3.4. They indicate that this difference is due to bias in the experimental study since the rest of the cases present a much better agreement with the experimental results. Table 3.2 presents a comparison of the thermal resistance at x=0.9 for the five cases. Based on these results it is possible to conclude that the numerical model discussed above presents good thermal results and, thus, the models to be solved with this model are going to present good thermal accuracy.

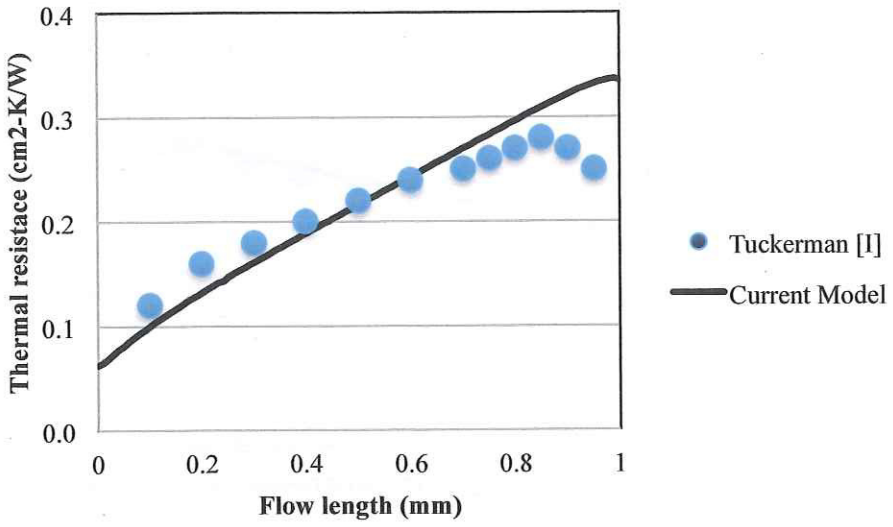

Figure 3.4 Thermal model validation. Comparison of the local thermal resistance in the Case 0 studied experimentally by Tuckerman [I] and the current numerical model.

Table 3.2 Comparison of thermal resistance at x=0.9.

Case	*q"* *(W/cm²)*	*Q* *(cm³/s)*	*R(cm²K/W)* *Tuckerman [I]*	*Toh et al. [43]*	*Current model*
0	34.6	1.277	0.277	0.331	0.321
1	34.6	1.860	0.280	0.253	0.247
2	181	4.700	0.110	0.157	0.151
3	277	6.500	0.113	0.128	0.126
4	790	8.600	0.090	0.105	0.100

On the other hand, and knowing that the numerical results reported by Toh *et al.* [43] present good accuracy, the hydrodynamic validation is done considering the local *fRe* factor along the channel length in the Case 1 proposed by Tuckerman [I] and studied numerically by Toh *et al.* [43]. The friction factor is given by Equation (3.4). Figure 3.5 presents some values reported by [43] along the

flow length as well as the local *fRe* factor computed with the present numerical model. A good agreement is observed between both numerical results, except in the range of $0.2 \leq x \leq 0.4$ where a slight variation is observed. According to these results, it is concluded that the present model generates good hydrodynamic accuracy, and, therefore, a good agreement is going to be obtained in the numerical simulations of the thermal enhancement technique models.

$$f = \frac{-2(dp/dx)D_h}{\rho u_{ave}^2} \tag{3.4}$$

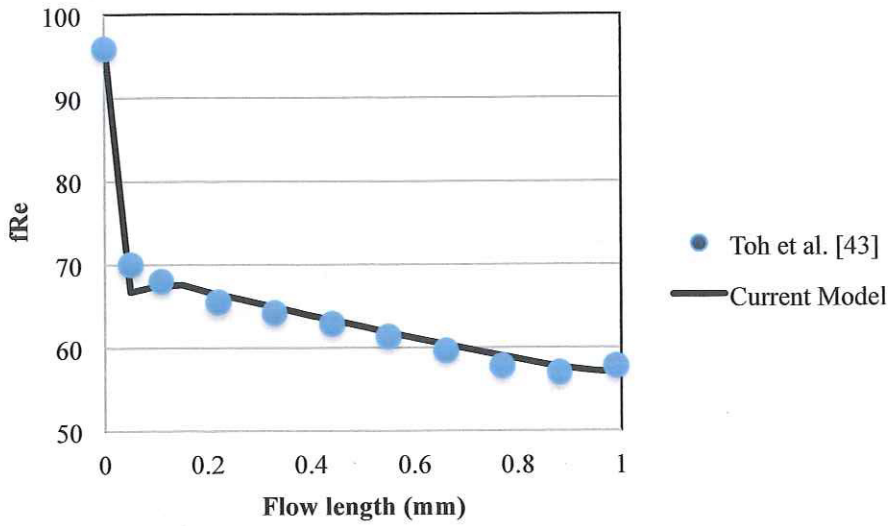

Figure 3.5 Hydrodynamic model validation. Comparison of the local fRe factor fore Case 1 proposed by Tuckerman and studied numerically by Toh et al. [43], and the current numerical model.

Chapter IV
Evaluation of Enhancement Thermal Techniques – Results

COMPUTING Nu_0 AND f_0 FROM NUMERICAL RESULTS

Chapter II showed the six different thermal enhancement techniques proposed in this work. Numerical analyses are developed in order to observe their overall performance given by the ratio ϕ. This dimensionless parameter was described in the first section of Chapter II. As it was mentioned, the computing of this parameter requires knowing the local Nusselt number along the flow length in both the straight microchannel and each one of the enhanced micro heat sink. For this purpose, the following methodology is used for determining this heat transfer parameter from the numerical solutions.

Once the model is solved numerically, the temperature, pressure and velocity variations are known. Thereby, the heat transfer through the interface between fluid and solid domain, the channel wall temperature, the bulk temperature, and the pressure drop can be determined using lineal and surface integration. From theory, the Nusselt number at a k-position is given by Equation (3.1), where a direct dependency of this parameter with the local heat transfer coefficient is observed. By energy balance, the energy transferred from the solid to the fluid through the channel walls is given by Equation (3.2).

$$Nu_k = \frac{h_k Dh_k}{k} \tag{3.1}$$

$$q''\big|_{at\ z=k} = h\left(T_s - T_\infty\right)\big|_{at\ z=k} \tag{3.2}$$

$$T_\infty\big|_{at\ z=k} = \left.\frac{\int_{j=1}^{m}\int_{i=1}^{n} T_{i,j}\,dx\,dy}{A_{channel}}\right|_{at\ z=k} \tag{3.3}$$

$$T_s\big|_{at\ z=k} = \left.\frac{\int_{i=1}^{n} T_{i,0}\,dx}{w_c}\right|_{at\ z=k} + \left.\frac{\int_{j=1}^{m} T_{0,j}\,dy}{h_c}\right|_{at\ z=k} \tag{3.4}$$

$$q''|_{at\ z=k} = \alpha \frac{\int_{i=1}^{n} q''_{i,0}\,dx}{w_c}\bigg|_{at\ z=k} + (\alpha - 1)\frac{\int_{j=1}^{m} q''_{0,j}\,dy}{h_c}\bigg|_{at\ z=k} \tag{3.5}$$

Thus, the heat transfer coefficient can be determined from computing the bulk temperature (surface integration), as well as the wall temperature and the heat flux flowing through the channel walls (lineal integration). The bulk temperature is given by Equation (3.3). The wall temperature and the heat flux are computed by Equations (3.4) and (3.5). In most of the cases, the channel walls have not the same length (i.e. *hc>wc*). Thus, the channel aspect ratio α_c is used in order to indicate the proportion of the total thermal energy that is flowing through each channel wall.

Moreover, the friction factor is computed in a similar way. This parameter is affected by the pressure drop generated until a *k*-position as well as the mean velocity of the fluid at the same point (Equation 3.4). Thus, numerical integrations are required. Furthermore, the variation of the fluid viscosity has an important effect in the computing of this parameter [64]. Equations (3.7) and (3.8) are used for computing numerically the pressure drop and the mean velocity of the fluid at a specific position.

$$f\,\mathrm{Re}|_{at\ z=k} = \frac{\Delta P D_h^2}{2\mu(T) v_{mean} Lz^*}\bigg|_{at\ z=k} \tag{3.6}$$

$$\Delta P|_{at\ z=k} = \frac{\int_{j=1}^{m}\int_{i=1}^{n} P_{i,j}\,dx\,dy}{A_{channel}}\bigg|_{at\ z=k} - \frac{\int_{j=1}^{m}\int_{i=1}^{n} P_{i,j}\,dx\,dy}{A_{channel}}\bigg|_{at\ z=0} \tag{3.7}$$

$$v_{mean}|_{at\ z=k} = \frac{\int_{j=1}^{m}\int_{i=1}^{n} v_{i,j}\,dx\,dy}{A_{channel}}\bigg|_{at\ z=k} \tag{3.8}$$

In order to validate this methodology, the Nu_0 and f_0Re at $z^*=0.9$ are computed from a straight channel with channel aspect ratio of 0.5, a channel hydraulic diameter of 133.33 μm, length of 10 mm, and a fluid inlet velocity of 1 m/s. Table 4.1 presents a comparison between the theoretical results determined by the regressions exposed in Chapter II and the numerical results generated from this methodology. As it is observed, the values computed using the above methodology match with the results exposed in the technical literature (error is lesser than 2%). Thus, this methodology is appropriate for using in the computing of the different Nu_i and f_i values.

Table 4.1 Comparison of Nu_0 and f_0Re generated from Equations (2.8) and (2.9), and numerically at $z^*=0.9$

	Theoretically	*Numerically*	*Error*
Nu_0	4.75	4.67	1.7%
f_0Re	16.08	16.29	1.3%

OVERALL PERFORMANCE OF THE ETM-1

In Chapter II, Table 2.1 shows the matrix of cases which were solved numerically for the enhancement thermal technique based on the variation of the channel cross section (ETM-1). Figure 4.1 presents the variation of the ϕ overall parameter along the dimensionless flow length for these five different enhanced configurations. The curves show that ϕ is 1.0 at z*= 0 since the channel hydraulic diameter is the same that the straight microchannel exposed previously (Section 2.2) at the inlet section. This condition is kept in all the cases. Since the inlet Reynolds number is keeping constant in these cases, the fluid inlet velocity, inlet temperature and fluid properties are the same. Then, the ϕparameter goes down due to the fluid starts developing, as well as its temperature rises, causing an important decrease of the fluid viscosity and affecting its momentum. Taking into account that the straight microchannel correlations are based on the assumption of a constant fluid viscosity value, the overall performance is directly affected by this fluid property at the developing section (entrance region), causing this decrease in the system performance. A minimal value is observed at z^*=0.1. After this point, the increase in the heat dissipation caused by the decrease of the channel cross section becomes important and the ϕ parameter starts rising with different slops depending of the dimensionless parameters $\gamma_{ETM\text{-}1}$ (Equation (2.11)) and $\beta_{ETM\text{-}1}$ (Equation (2.12)).

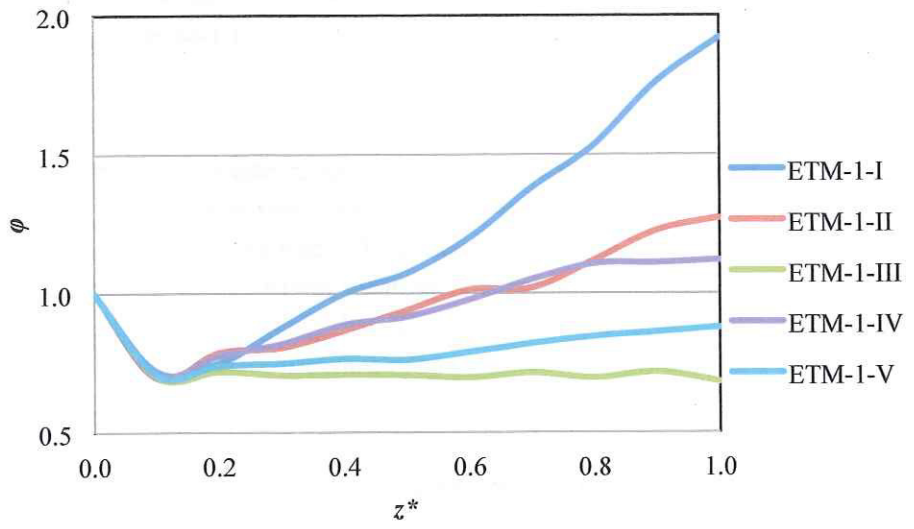

Figure 4.1 Variation of ϕ along the channel length for the five different configurations mentioned in Table 2.1.

The figure shows that the overall performance is increased when the dimensionless parameter $\gamma_{ETM\text{-}1}$ (Equation (2.11)) is reduced keeping $\beta_{ETM\text{-}1}$ as constant. This behavior is observed when the curves of ETM-1-I ($\gamma_{ETM\text{-}1}$ = 0.25), ETM-1-II ($\gamma_{ETM\text{-}1}$ = 0.5) and ETM-1-III ($\gamma_{ETM\text{-}1}$ = 1.0) at $\beta_{ETM\text{-}1}$= 0.5 are compered. Furthermore, this behavior is observed comparing the curves corresponding to ETM-1-IV ($\gamma_{ETM\text{-}1}$ = 0.25) and ETM-1-V ($\gamma_{ETM\text{-}1}$ = 0.5) at $\beta_{ETM\text{-}1}$= 1.0. Thus, performance improvements are obtained when the channel height at the outlet end is reduced strongly. This means that the pressure drop penalty associated with this decrease is compensated with a large increase in the heat dissipation.

Moreover, the ϕ parameter is increased when β_{ETM-1} is reduced at constant values of γ_{ETM-1}. This conclusion is observed when the curves for ETM-1-1 (β_{ETM-1}= 0.5) and ETM-1-IV (β_{ETM-1}= 1.0) at γ_{ETM-1} = 0.25, as well as ETM-1-II (β_{ETM-1}= 0.5) and ETM-1-V (β_{ETM-1}= 1.0) at γ_{ETM-1} = 0.5 are compared. Thus, an increase in the performance is obtained when the channel width at the outlet is reduced up to 50 μm.

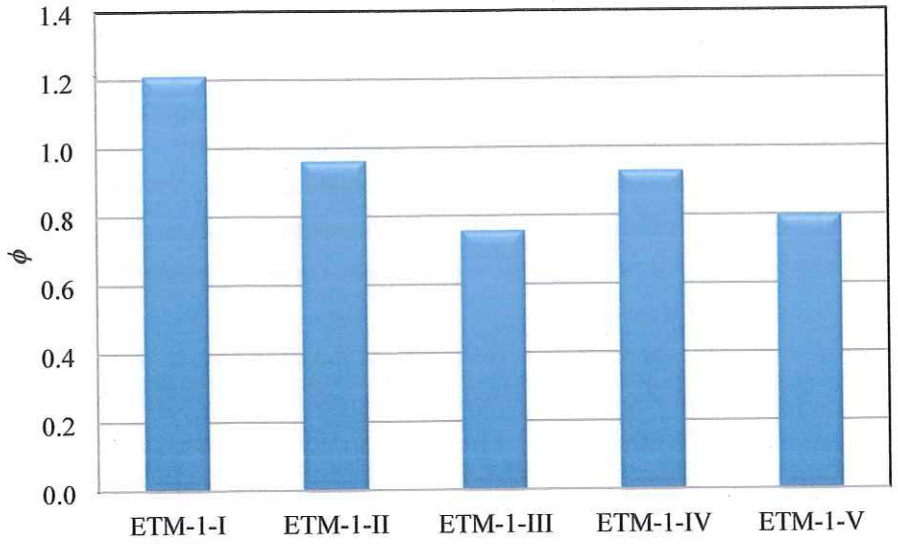

Figure 4.2 Integrated ϕ values for configurations mentioned in Table 2.1.

Figure 4.2 presents the integration of the local ϕ parameter in order to determine the average overall performance of these heat sink configurations based on this thermal enhancement technique. A numerical integration based on trapezoidal method is used. As it was mentioned in Chapter II, this work is aimed to generate enhancement techniques capable to generate thermal performance near or larger than 1.0 because this indicates that the systems has a better heat dissipation than straight microchannels with an appropriate pressure drop penalty. Moving back to Figure 4.2, it is observed that only the configuration ETM-1-I (β_{ETM-1}= 0.5, γ_{ETM-1} = 0.25) is larger than the expected value of ϕ, and, moreover, the configurations ETM-1-II (β_{ETM-1}= 0.5, γ_{ETM-1} = 0.5) and ETM-1-IV (β_{ETM-1}= 1, γ_{ETM-1} = 0.25) are near to the unit. However, the effects of enhancing the performance in the heat sink using this technique become important after the 40% of the channel length (z*=0.4) for the configuration ETM-1-1, achieving performance value near 2.0 at the end of the channel. Thus, although the configuration ETM-1-1 presents the most outstanding performance, it is needed to take into account the behavior observed along the section before z*<0.4.

OVERALL PERFORMANCE OF THE ETM-2

This section presents the results obtained with the matrix of cases for the enhancement thermal technique based on reducing the channel aspect ratio (ETM-2) exposed in Chapter II. Figures 4.3 to 4.5 present the ϕ parameter along the flow length considering the effects of varying the channel width,

channel height and length of each section (i.e. this analysis considers three sections in each configuration). Table 2.3 presents three matrixes of cases corresponding of each variation mentioned above. As well as in the previous thermal enhancement configuration, the channel hydraulic diameter, velocity and temperature of the fluid, and thermal properties at the inlet section are the same for all the cases as well as the straight microchannel heat sink considered in the analysis. Thus, ϕ is 1.0 at this inlet section. Then, the effects of developing the boundary layer as well as the increase of the fluid temperature lead to a reduction in the performance of the heat configuration until the first change of section is located. An increase of ϕ parameter is observed at this position in all the cases and the magnitude of increasing depends of the kind of geometrical variation made in the channel. This enhancement is clearly caused by the destruction of the boundary layers and their subsequent tendencies of developing. After this transition sections, the overall performance tends to go down due to the fluid is reaching fully developed conditions. The length of the section plays an important role in this ϕ tendency. The phenomena are repeated when the channel suffers the second change of section. Then, the overall performance goes down, reaching values as low as 0.4 near the channel end.

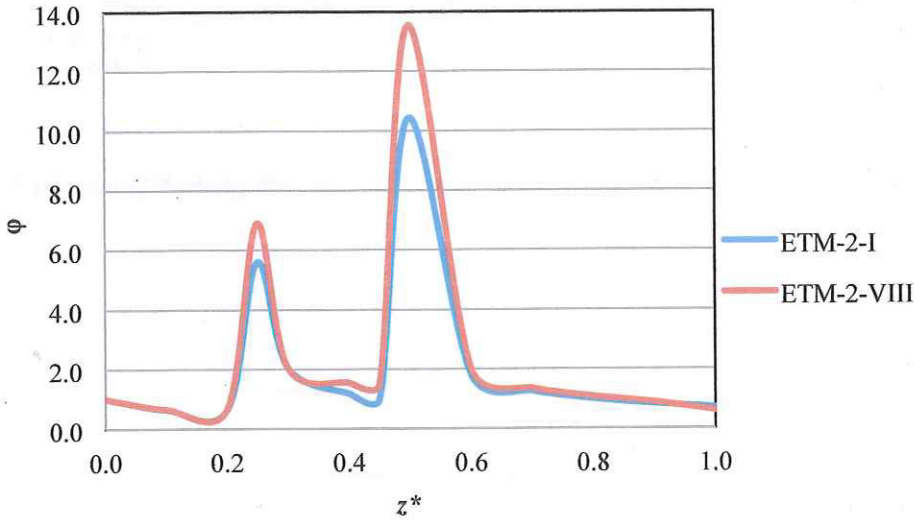

Figure 4.3 Variation of ϕ along the channel length for the cases ETM-2-I and ETM-2-VIII mentioned in Table 2.3.

The effects of varying the channel width per section in this thermal enhancement technique are observed in Figure 4.3. This figure presents the variation of ϕ along the channel length for the cases ETM-2-1 ($\beta_{ETM\text{-}2}$ = 0.5 and $\beta`_{ETM\text{-}2}$ =1.0) and ETM-2-VIII ($\beta_{ETM\text{-}2}$ = 1.0 and $\beta`_{ETM\text{-}2}$ =0.5). Equation (2.13) presents these dimensionless ratios. The channel height is varied from 200 μm to 100 μm at the first section, and from 100 μm to 50 μm at the second section in both cases. According with these results, the reduction of the channel width from 100 μm to 50 μm when the channel height is varied from 200 μm to 100 μm is minimal. This can be observed at z^*=0.25 (first change of section) where ETM-2-I keeps a channel width of 50 μm and ETM-2-VIII changes the channel width into the values mentioned above. The ϕ parameter is 5.6 and 6.9, respectively (around 18% of variation). Moreover, a similar difference between both curves is observed at the second change of section when the channel height is varied from 100 μm to 50 μm. The channel width is kept constant to 50 μm in

the case ETM-2-I, and is varied from 100 μm to 50 μm in the case ETM-2-VIII. The ϕ parameter reaches values of 10.4 and 13.6, respectively. Thereby, a variation of around 30% between both cases is found. Thus, it is observed that the overall performance in this kind of configurations is majorly affected by the variation of the channel height at each change of section.

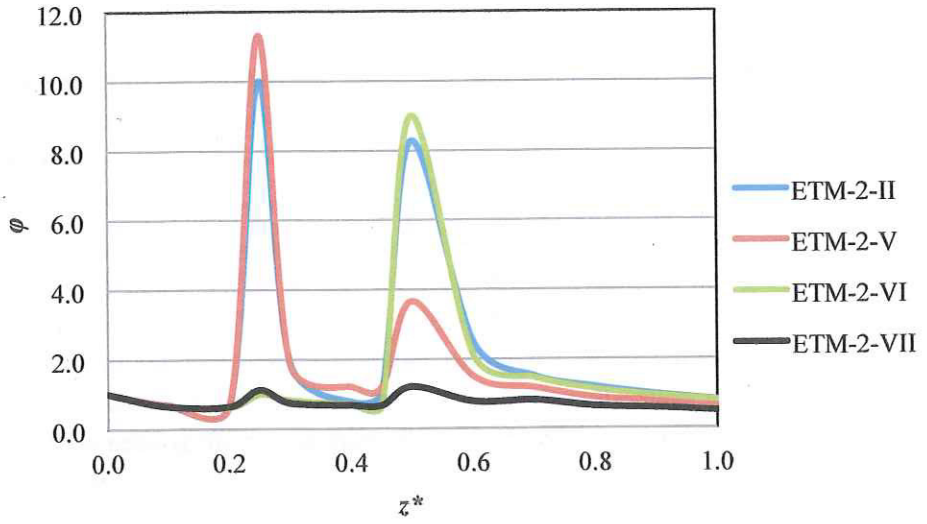

Figure 4.4 Variation of ϕ along the channel length for the cases ETM-2-II, ETM-2-V, ETM-2-VI and ETM-2-VII mentioned in Table 2.3.

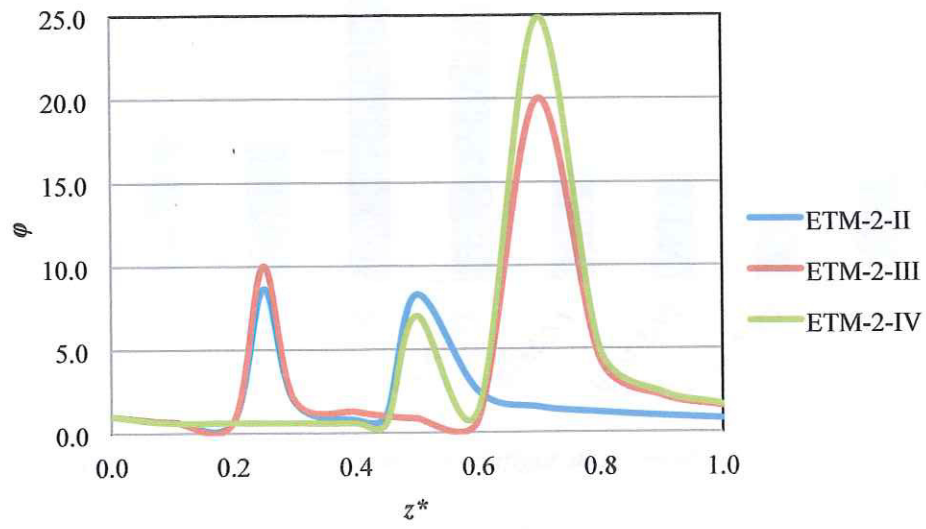

Figure 4.5 Variation of ϕ along the channel length for the cases ETM-2-II, ETM-2-III and ETM-2-IV mentioned in Table 2.3.

Figure 4.4 shows the variation of ϕ along the channel length when the channel height is varied for these four channel configurations, $\beta_{ETM\text{-}2}$ = 0.75, $\beta`_{ETM\text{-}2}$ =0.66, $\xi_{ETM\text{-}2}$ = 0.25, $\xi`_{ETM\text{-}2}$ =0.5. The dimensionless geometrical parameters are defined in Equations (2.13) to (2.15). These results show that the effects of reducing the channel height affect strongly the increase of the overall performance

in the system, majorly at the first change of section. The curves corresponding to ETM-2-II and ETM-2-V (γ_{ETM-2} = 0.5), where the channel height is varied from 200 μm to 100 μm, show an important increase in the ϕ parameter, reaching values larger than 10. This tendency is ratified at the second change of section where the curves corresponding to ETM-II and ETM-VI ($\gamma`_{ETM-2}$ =0.5) reaching ϕ values slightly larger than 8.0. These last two configurations have a variation of the channel height from 100 μm to 50 μm in the first section, and from 200 μm to 100 μm in the second section, The results ratified the fact that thermal dissipation in microchannels is majorly affected by the channel height variation than the channel width variation. Moreover, the effects of keeping a constant value of channel height at each change of section are observed in these curves. Taking into account the chart for the cases ETM-2-VI and ETM-2-VII (γ_{ETM-2} =1.0) at the first change of section, and the cases ETM-2-V and ETM-2-VII ($\gamma`_{ETM-2}$ =1.0) at the second change of section, it is observed a minimal increase in the ϕ parameter, reaching maximum values around 1.1 and 3.5, respectively. Analyzing the curve corresponding to ETM-2-V at this second change of section, this ϕ value of 3.5 is reached, in part, because of the change of section due to the channel width, but furthermore by the fact that an important amount of thermal energy is taken up by the fluid before to flow through this section. Thereby the fluid temperature rises importantly, affecting the fluid viscosity and, thus, the friction factor is reduce, increasing the momentum of the fluid and improving the performance of the heat sink at along this section.

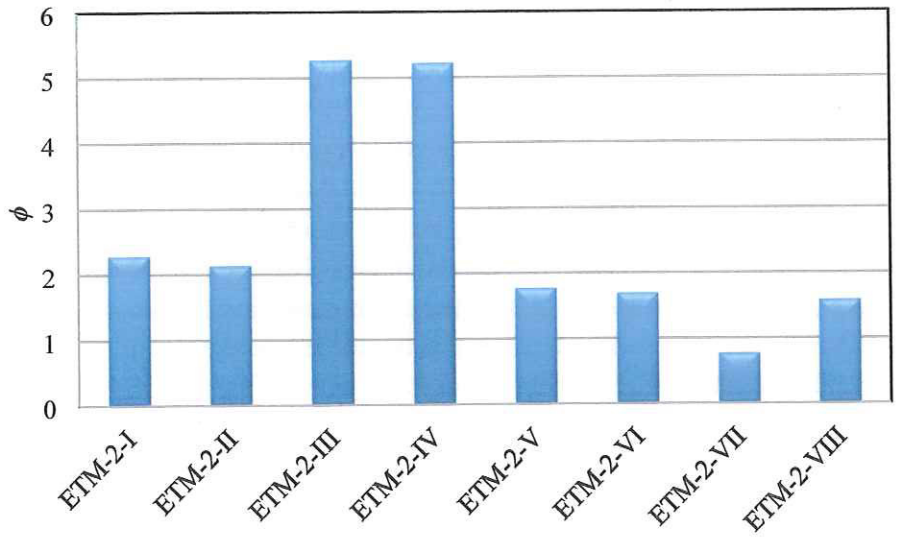

Figure 4.6 Integrated ϕ values for configurations mentioned in Table 2.3.

Figure 4.5 shows the variations of the ϕ parameter along the flow length when the location of each change of section is varied. Three configurations are studied (ETM-2-II, ETM-2-III and ETM-2-IV) when β_{ETM-2} = 0.75, $\beta`_{ETM-2}$ =0.66, $\gamma_{ETM-2}$ = 0.5, $\gamma`_{ETM-2}$ =0.5. The dimensionless parameters are given by the equations mentioned above. As it was indicated previously, same paths are observed at the fluid inlet section as well as the improvement in the overall performance at the change of sections. Moreover, the position of the change of hydraulic diameter affects the magnitude of increasing of the ϕ parameter at the second change of section, reaching values

up to 25 when the second change of section is located at z^*=0.75 (ETM-2-IV). This behavior is caused because the fluid suffers a drastic increase of its temperature (before this point the temperature rise is almost lineal) in just a very small channel length due to the abrupt change of section (first, the boundary layers are destroyed and immediately, the fluid velocity is increased). After this point, the reduction of the overall performance tends to values ranging from 0.8 to 1.7.

Figure 4.6 presents the average ϕ parameter for these configurations based on sectioned channels. The numerical integration indicates that this thermal enhancement technique generates heat sinks with performance much better than straight microchannels (except configuration 2-VII) since their average ϕ value is larger than 1.0. However, the strong increases in the heat dissipation (and the associate friction factor) at the change of sections generate important temperature gradient than would produce important damages in the IC chip. Furthermore, around 80% of the axial length of the heat sink presents a poor thermal performance. Therefore, the reduction of the hydraulic diameter using sectioned channels is not an appropriate alternative for the goals planted in this work.

Overall Performance of the ETM-3

4.4.1 Circle-shaped Micro Pin Fin Heat Sink (ETM-3-C)

The results corresponding to the thermal enhancement technique based on using circle-shaped fins along the flow length are presented in this section for the different geometrical variations. Figure 4.7 presents the variation of this performance parameter along the flow length for three different configurations considering the variation of the $\gamma_{ETM\text{-}3\text{-}C}$ parameter (0.5, 1.0 and 2.0) for constant values of $\beta_{T\text{-}ETM\text{-}3\text{-}C}$ and $\beta_{L\text{-}ETM\text{-}3\text{-}C}$ (1.0 and 2.0, respectively). These results show a clear difference with the results obtained with the first two thermal enhancement techniques mentioned previously (ETM-1 and ETM-2) at the inlet section. The ϕ value at this position is different that 1.0 due to this thermal enhancement technique is not considering an axial channel; these configurations consider a flat plate where the fins are placed on. Then, when the upper wall is placed on the system, a large rectangular channel is formed at the entrance section; this means the channel hydraulic diameter of these configurations is much larger than the straight channel. Moreover, the fluid velocity and temperature as boundary conditions at the inlet where set equal to the previous cases. Thus, although the Reynolds number at the entrance is not the same for both cases, the operating conditions are similar. Due to this geometrical condition, the Nusselt number immediately after z^*=0 is lower than the Nusselt number generated by straight microchannels at the same position, causing this decrease of the thermal performance. After this point, the ϕ parameter increases as the fluid is flowing through the channel along the axial direction. Several peaks are observed along the curves at the positions where the circle-shaped fins are located. Thus, these fast increases of the system performance are caused by the rise of the heat transfer coefficient and the friction factor caused by the increase of the heat transfer area/friction area, destruction of the thermal and hydrodynamic boundary layers, fluid instabilities, etc. However, the results indicate that the increase in the thermal energy dissipation is larger than the increase of the friction factor due majorly to the scale of the system. Moving back to Figure 4.7, it is observed that the system performance is improved when $\gamma_{ETM\text{-}3\text{-}C}$ parameter is increased; this means that the increase of the fin height affects favorably the system performance. This agrees with fins

theory due to the area for transferring heat is increased, causing a better thermal dissipation. However two points emerge from this observation: *i)* the system performance is clearly better when fin height is 200 μm, but *ii)* how much fin height could be used for improving the thermal performance of the system considering the structural limits that the silicon material has (mechanical stresses, weathering, etc.) for this kind of applications at this scale? Studies regards to this thermo-mechanical phenomena are not presented in technical literature for this scale, thus, this could be a future work to develop. The current manufacturing processes at microscale are capable to manufacture structures up to 200 μm deep with relative low cost and appropriate tolerances, keeping the final shape almost similar to the initial design. Thus, this work considers 200 μm as the largest fin height for all the cases based on fin configurations.

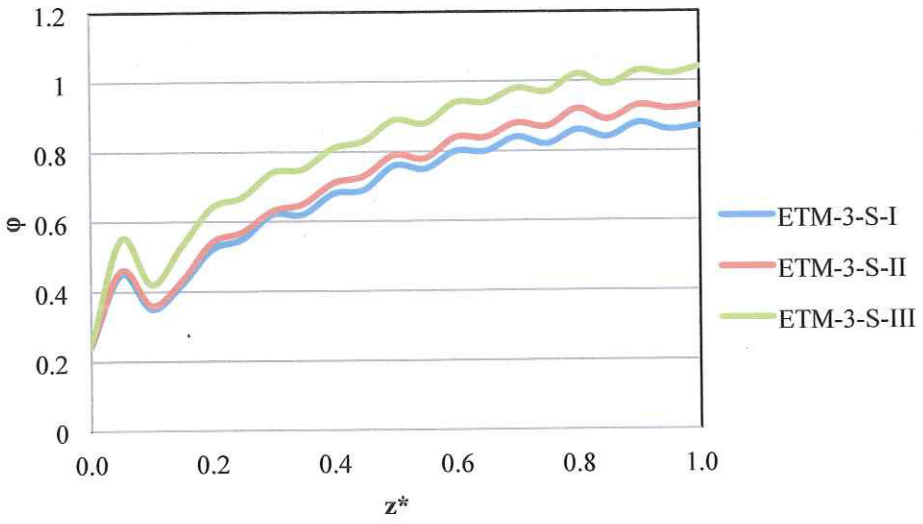

Figure 4.7 Variation of ϕ along the channel length for the cases ETM-3-C-I, ETM-3-C-II and ETM-3-C-III mentioned in Table 2.5.

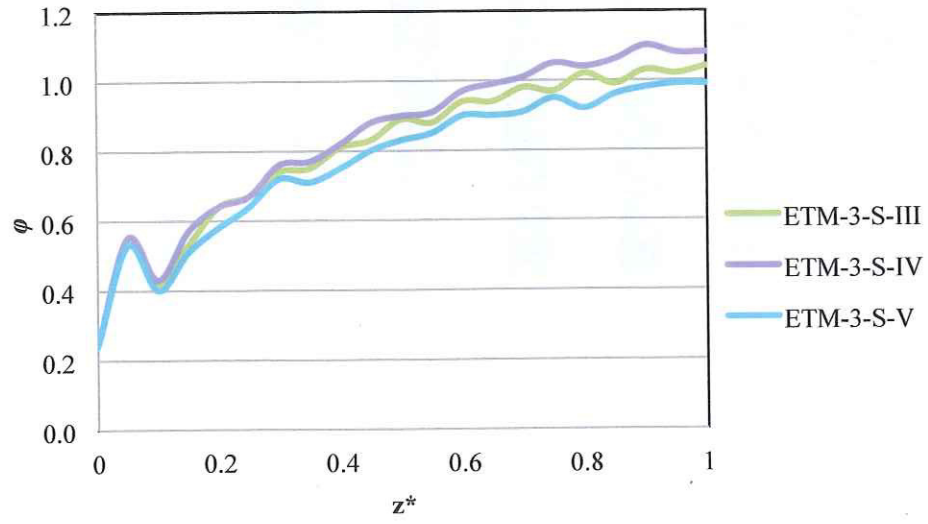

Figure 4.8 Variation of ϕ along the channel length for the cases ETM-3-C-III, ETM-3-C-IV and ETM-3-C-V mentioned in Table 2.5.

Figure 4.8 presents the variation of the ϕ parameter along the flow length considering the variation of the $\beta_{L\text{-}ETM\text{-}3\text{-}C}$ (1.5, 2.0 and 3.0) at constant values of $\gamma_{ETM\text{-}3\text{-}C}$ and $\beta_{T\text{-}ETM\text{-}3\text{-}C}$ (0.5 and 1.0, respectively). The results show that the increase of this longitudinal pitch reduces the system performance. This is an expected result due to the reduction of the heat transfer area as well as the number of times that the boundary layers are destroyed is reduced. Furthermore, the fluid has enough longitudinal space for developing, in an important percentage, its boundary layers between fins. The peaks in the curves are due to the effects described above.

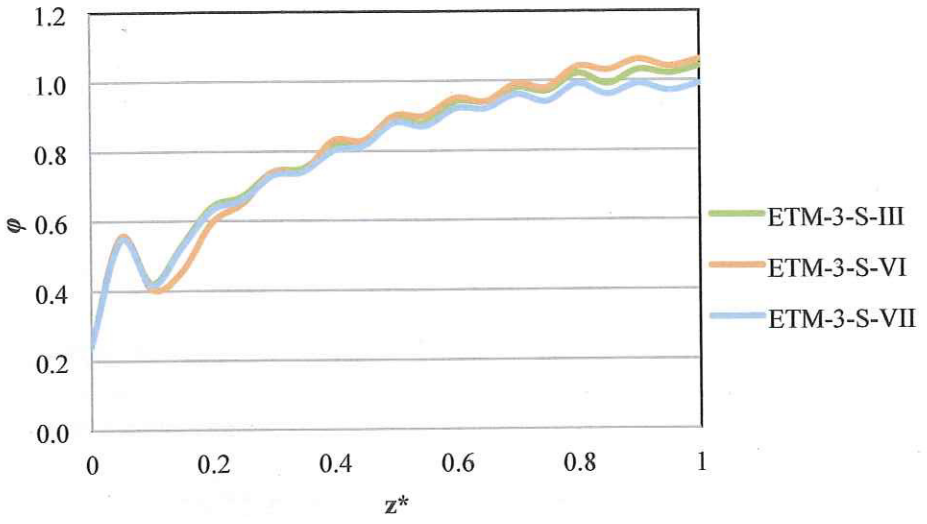

Figure 4.9 Variation of ϕ along the channel length for the cases ETM-3-C-III, ETM-3-C-VI and ETM-3-C-VII mentioned in Table 2.5.

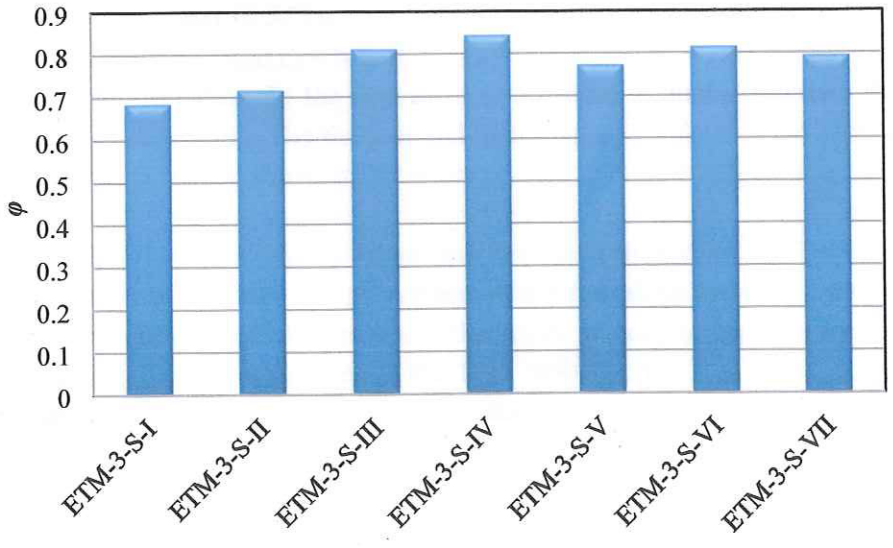

Figure 4.10 Integrated ϕ values for configurations mentioned in Table 2.5.

Figure 4.9 shows the variation of the ϕ parameter along the flow length for different values of $\beta_{T\text{-}ETM\text{-}3\text{-}C}$ (0.5, 1.0 and 1.5) at constant values of $\gamma_{ETM\text{-}3\text{-}C}$ and $\beta_{L\text{-}ETM\text{-}3\text{-}C}$ (0.5 and 2.0, respectively).

Overall, the curves present the same behavior described at the beginning of this subsection. The effects mentioned above cause these behaviors. Moreover, the results show that the system performance is improve when this parameter is reduced, this means that the reduction of the transversal space lead to increase the number of fins at this direction. Thereby, the heat transfer area and the effects of destruction of both boundary layers are increased. Indeed, the gap between fins is reduced, having an increase in the fluid velocity when this is passing through these spaces. Although both heat dissipation and friction factors are increased, the results indicated that the thermal effects have a higher variation. It is important to highlight that the largest variations are observed in the last third part of the system due to the reduction of the temperature difference between the fluid and walls.

Figure 4.10 shows the average overall performance of the seven configurations presented in Table 2.5. As it has been indicated, the goal of this work is to generate configurations capable to generated average ϕ values larger than 1.0. According with this figure, no one configuration was capable to overpass the unit. The most outstanding configurations were the ETM-3-C-IV and ETM-3-C-VI, having ϕ values near 0.9. Although this configuration is below the expectative, two point are important: *i)* the path that the overall performance has along the flow length is growing and achieves values slightly larger than 1.0, and *ii)* there are not constraints in the fins location, this means that these can be placed according with the performance variation that the systems requests (and that is not possible to do with parallel channels).

4.4.2 Square-shaped Micro Pin Fin Heat Sink (ETM-3-S)

The results upon the overall performances of the cooling system using square-shaped fins are presented in this section. Figures 4.11, 4.12 and 4.13 present the variation of the ϕ parameter along the flow length for varying *i)* $\gamma_{ETM\text{-}3\text{-}S}$ parameter (0.5, 1.0 and 2.0), *ii)* $\beta_{L\text{-}ETM\text{-}3\text{-}S}$ parameter (1.5, 2.0 and 3.0), and *iii)* $\beta_{T\text{-}ETM\text{-}3\text{-}S}$ parameter (0.5, 1.0, 1.5), respectively. For each case, the other dimensionless parameters are kept as constant ($\gamma_{ETM\text{-}3\text{-}S} = 0.5$, $\beta_{L\text{-}ETM\text{-}3\text{-}S} = 2.0$, $\beta_{T\text{-}ETM\text{-}3\text{-}S} = 1.0$). Table 2.7 presented the dimensions for each configuration. In the figures, it is observed a similar behavior that the results exposed in the previous subsection. The thermal and hydrodynamic effects at the entrance and at the zones near the fin places described above are therefore present in these configurations.

Moreover, the ϕvalues are slightly larger than the circle-shaped fin configuration. According with theory, when a fluid is flowing through systems where flat plates are placed perpendicularly to the flow direction, the fluid crashes with the wall reducing its velocity to zero and increasing strongly its pressure. Depending of the magnitude of the fluid velocity, this can move forward with the remaining fluid, generate stagnation points, or move back generating waves. Based on the results, the fluid uniquely presents slight stagnation sections at this zone due to the fluid velocity is relatively low. Thermal effects are increased with this stagnation flows due to the thermal boundary layer is destroyed, as well as the heat transfer area which is in direct contact with the fluid (normal direction) is large. Thus, although both the heat transfer coefficient and the friction factor tends to increase, the result show that the increase of the heat transfer coefficient is more dominate in the systems due to there is observed an slight increase of the ϕ parameter along the system length. For some cases, ϕ values larger than 1.0 are obtained at z^* below 0.8. Important local performances are observed for ETM-3-S-III, ETM-3-S-IV and ETM-3-S-VI.

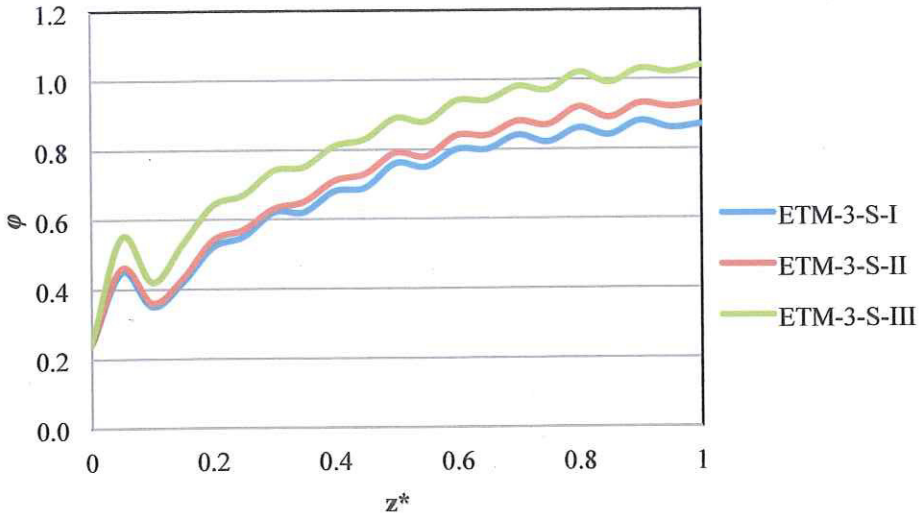

Figure 4.11 Variation of ϕ along the channel length for the cases ETM-3-S-I, ETM-3-S-II and ETM-3-S-III mentioned in Table 2.7.

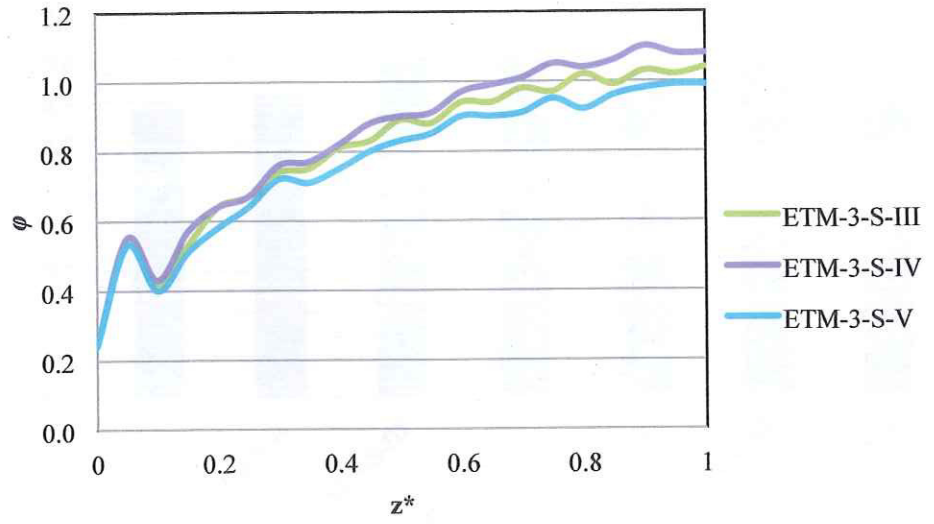

Figure 4.12 Variation of ϕ along the channel length for the cases ETM-3-S-III, ETM-S-C-IV and ETM-3-S-V mentioned in Table 2.7.

Figure 4.14 presents the average ϕvalue for each configuration exposed in the matrix of cases of Table 2.7. The results show that all the systems have an average performance below the expected value of 1.0 due majorly to the low ϕ values observed at the entrance sections. The most outstanding configurations have a performance value slightly larger than 0.8. These configurations are the same that the configurations which presented the best local performance with ϕ values larger than 1.0 after z*=0.8.

Although these square-shaped configurations do not show the expected overall performance, it is important to reconsider the comments mentioned at the end of the previous subsection. The advantage that these configurations do have is that the fin locations are not constrained, and there are not fixed parallel channels that limit the system.

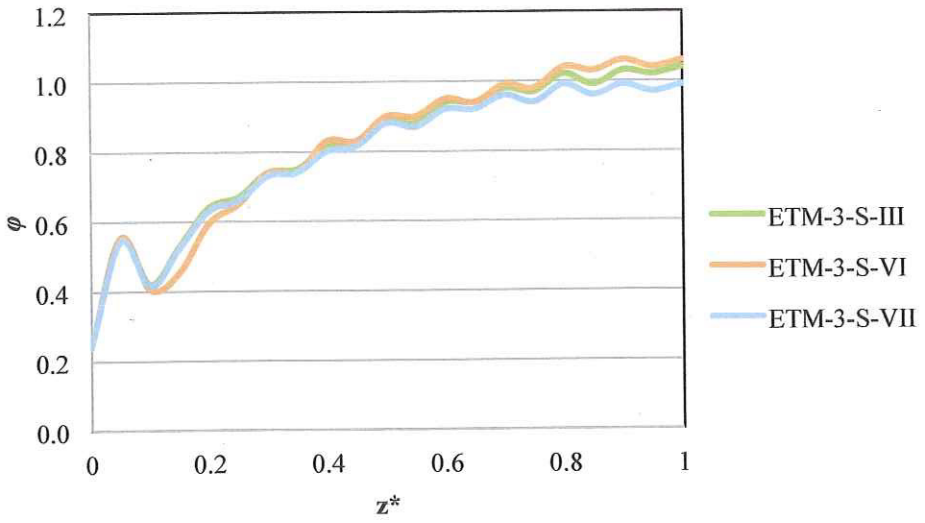

Figure 4.13 Variation of ϕ along the channel length for the cases ETM-3-S-III, ETM-3-S-VI and ETM-3-S-VII mentioned in Table 2.7.

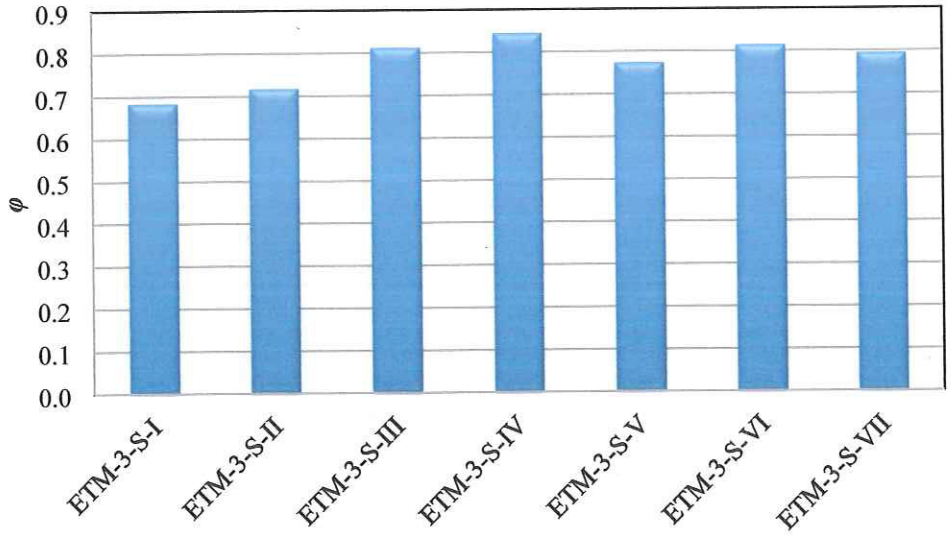

Figure 4.14 Integrated ϕ values for configurations mentioned in Table 2.7.

4.4.3 Ellipse-shaped Micro Pin Fin Heat Sink (ETM-3-E)

This section presents the behavior of the overall performance in the microcooling system using ellipse-shaped pin fins for improving the thermal performance. Figures 4.15, 4.16 and 4.17 presents the local variation of the ϕ parameter along the flow length when the dimensionless parameters are varied: *i)* $\gamma_{ETM\text{-}3\text{-}C}$ parameter (0.5, 1.0 and 2.0), *ii)* $\beta_{L\text{-}ETM\text{-}3\text{-}C}$ parameter (1.5, 2.0 and 3.0), and *iii)* $\beta_{T\text{-}ETM\text{-}3\text{-}C}$ parameter (0.5, 1.0, 1.5), respectively. For each case, the other dimensionless parameters are kept as constant ($\gamma_{ETM\text{-}3\text{-}C}$ = 0.5, $\beta_{L\text{-}ETM\text{-}3\text{-}C}$ = 2.0, $\beta_{T\text{-}ETM\text{-}3\text{-}C}$ = 1.0). Overall, the cooling system based on these fin configurations presents a similar behavior that the previous cases mentioned above, such as at the inlet section as the behavior along the flow length. The thermal and hydrodynamic effects described previously are observed in these curves. Observing the results, the

peaks in the ϕ curves are slightly large compared with the square-shaped configurations due to the shape of the fin leads to reduce the friction factor in the system at these fin locations due to the flow does not reduce its velocity strongly, this slides smoothly around the fin. The parametric results ratify the observations found in the previous cases. The increase of the fin height increases the overall performance due majorly to the rise of the heat transfer area (Figure 4.15). The reductions of the longitudinal and transversal pitches affect positively the overall performance of the system (Figures 4.16 and 4.17, respectively.)

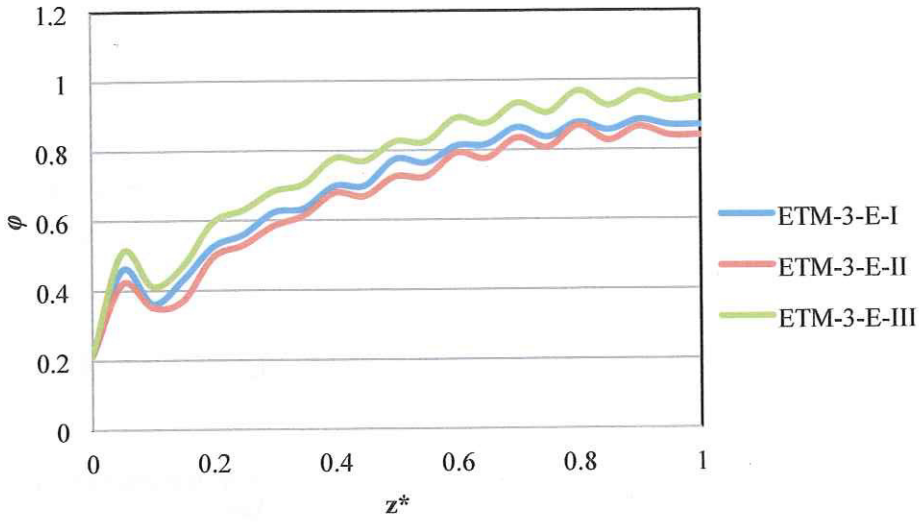

Figure 4.15 Variation of ϕ along the channel length for the cases ETM-3-E-I, ETM-3-E-II and ETM-3-E-III mentioned in Table 2.9.

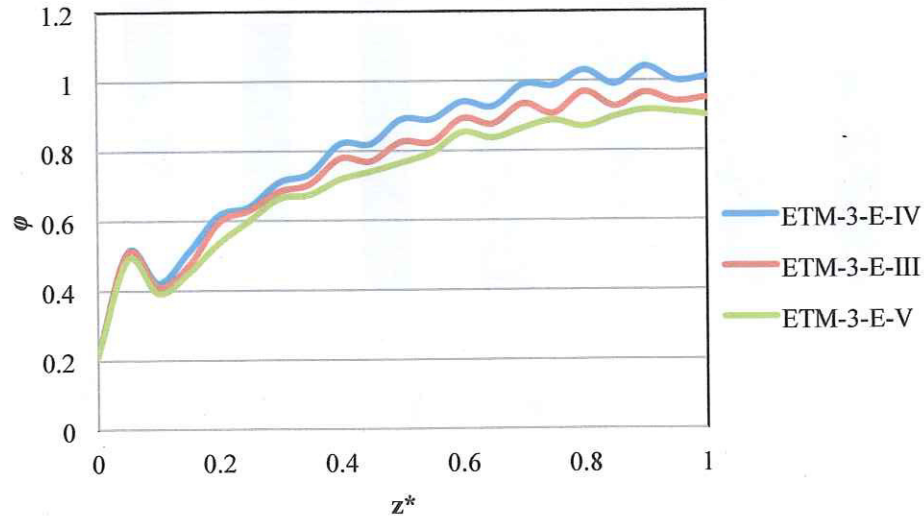

Figure 4.16 Variation of ϕ along the channel length for the cases ETM-3-E-III, ETM-3-E-IV and ETM-3-E-V mentioned in Table 2.9.

Figure 4.18 shows the average value of ϕ performance that each configuration exposed in Table 2.9 has in the cooling system. A numerical trapezoidal integration process is carried out for this purpose as it was mentioned in the previous cases. The results show that the expected value of ϕ=1.0

is not achieved with these configurations. Furthermore, the maximum average overall performance is presented by configuration ETM-3-E-IV and ETM-3-E-VI. These ϕ values are slightly larger than 0.8 and correspond to the cases which consider the smaller longitudinal and transversal pitches. Thus, it is highly recommended to consider these small pitches in the design of these fin configurations.

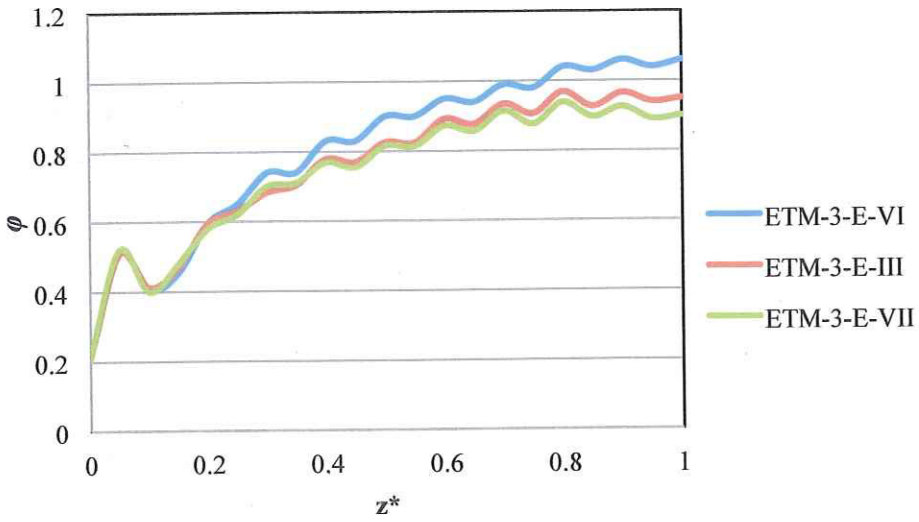

Figure 4.17 Variation of ϕ along the channel length for the cases ETM-3-E-III, ETM-3-E-VI and ETM-3-E-VII mentioned in Table 2.9.

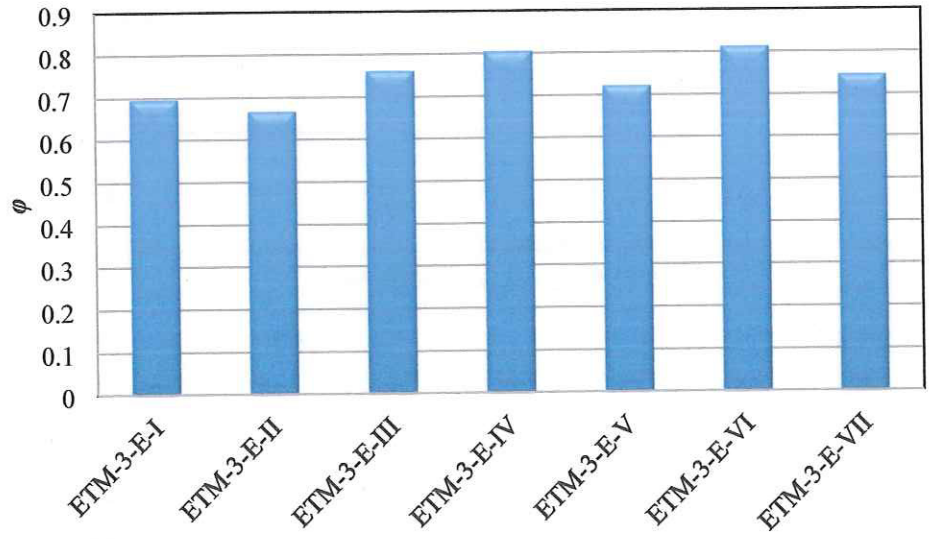

Figure 4.18 Integrated ϕ values for configurations mentioned in Table 2.9.

Although the average ϕ results are not the expected, it is important to mention again that the advantage of this configurations is the fact that these fin configurations are not constraint in the position and, thus, alternative arrangements can be proposed and studied. In particular, this ellipse-shape configuration presented a lower behavior that the square-shaped configuration and almost similar that the circle-shaped. Although the effects of friction factor are reduced, the fluid capacity to transfer heat is reduced as well (a lower Nusselt number).

4.4.4 Flat-shaped with redounded sides Micro Pin Fin Heat Sink (ETM-3-F)

This section presents the results obtained when flat-shaped with redounded sides fins are considered for enhancing the overall performance of a micro heat sink. Similar to the previous three cases mentioned above, the results presented here show the ϕ performance that the system has when the fin height, and transversal and longitudinal pitches are varied: *i)* $\gamma_{ETM\text{-}3\text{-}C}$ parameter (0.5, 1.0 and 2.0), *ii)* $\beta_{L\text{-}ETM\text{-}3\text{-}C}$ parameter (1.5, 2.0 and 3.0), and *iii)* $\beta_{T\text{-}ETM\text{-}3\text{-}C}$ parameter (0.5, 1.0, 1.5), respectively. For each case, the other dimensionless parameters are kept as constant ($\gamma_{ETM\text{-}3\text{-}C} = 0.5$, $\beta_{L\text{-}ETM\text{-}3\text{-}C} = 2.0$, $\beta_{T\text{-}ETM\text{-}3\text{-}C} = 1.0$). Furthermore, the effects of varying the radius of curvature of the redounded side are studied. For this purposes, the dimensionless parameter $\xi_{ETM\text{-}3\text{-}F}$ is proposed (Equation 2.25). Three variation of this parameter are considered (0.25, 0.5 and 0.75). Figures 4.19 to 4.22 present the behavior of the local ϕ parameter along the flow length for each of these geometrical variations, respectively. Overall, the curves present similar behavior that the paths observed in the previous fin enhancement techniques. The ϕ performance increases as fluid is passing through the system. The peaks observed in the curves are caused by the rise of the heat transfer at the zones where the fins are located due to the destruction of the thermal boundary layer as well as the increase of the heat transfer area. Although the friction factor is also increased, the results indicate that the convective coefficient rises more drastically. The curves ratifies that the increase of the fin height improves the overall performance of the system due to the increase of the heat transfer area as well as the gap between fins works as small microchannel. Thereby, the increase of the apparent channel height improves the heat dissipation. It is important to highlight that the curve corresponding to the configuration ETM-3-F-I does not have peaks due to it was only considered 10 points along the flow length and, therefore, the effects between fins is not clearly observed. Since this case corresponds to the shorted fin height, the results are appropriated for this study due to the previous results showed that the enhancement of considering 50-μm fin height are minimal compared with another configurations.

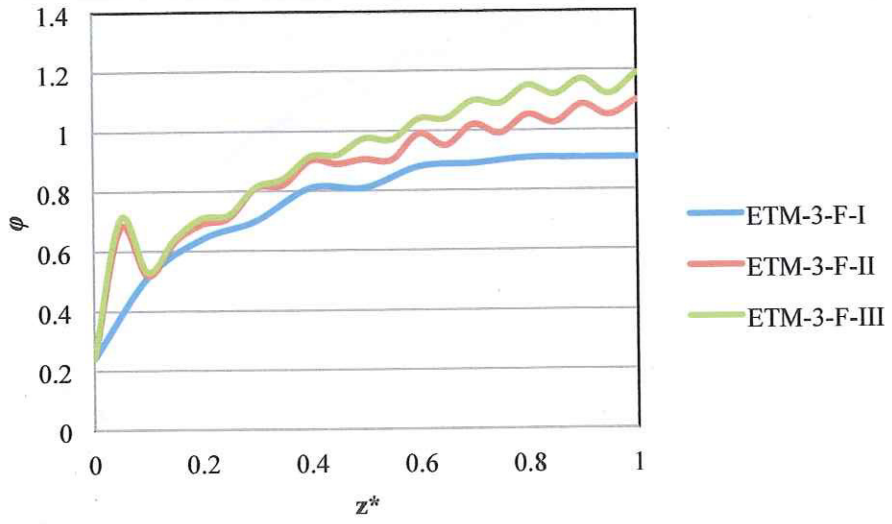

Figure 4.19 Variation of ϕ along the channel length for the cases ETM-3-F-I, ETM-3-F-II and ETM-3-F-III mentioned in Table 2.11.

Moreover, the reduction of the transversal and longitudinal pitches improves the overall performance of the system. This is observed in Figures 4.20 and 4.21 where the configurations that

consider a small pitch presents an important increase of the ϕparameter along the flow length. As it was previously mentioned, the increase of the heat transfer coefficient caused by the reduction of the gap between channels is the major generator of this improvement. Furthermore, the reduction of pith along the flow length reduce the space for developing the thermal boundary layer and thus, a large amount of this energy is transferred to the fluid due to its instability. These effects are more notorious at the second middle of the system.

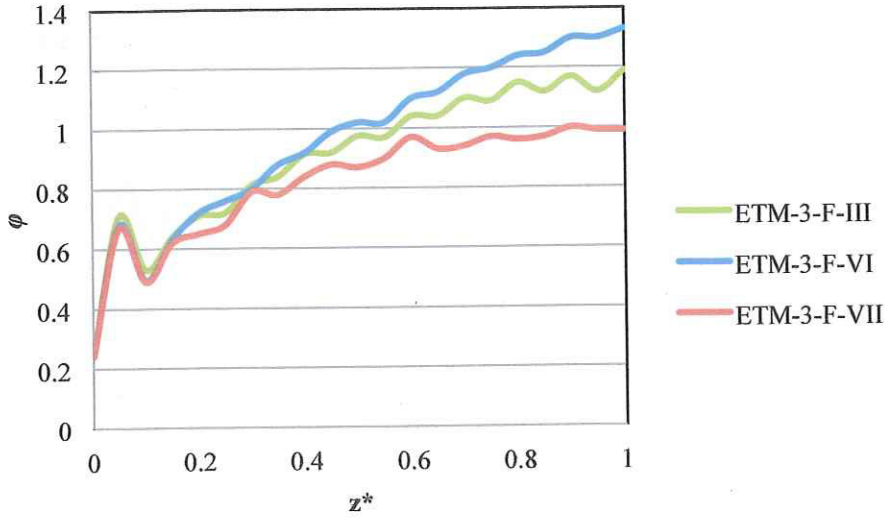

Figure 4.20 Variation of ϕ along the channel length for the cases ETM-3-F-III, ETM-3-F-VI and ETM-3-F-VII mentioned in Table 2.11.

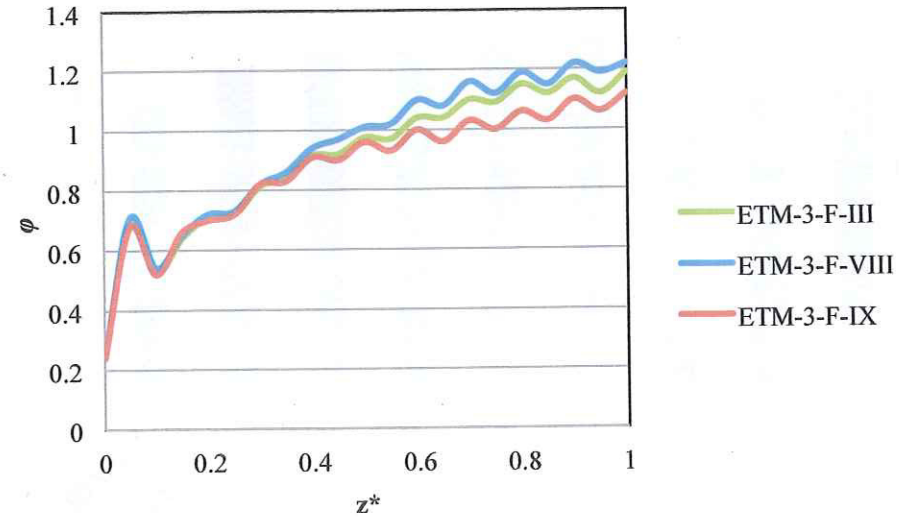

Figure 4.21 Variation of ϕ along the channel length for the cases ETM-3-F-III, ETM-3-F-VIII and ETM-3-F-IX mentioned in Table 2.11.

For this configuration, one additional geometrical variation is studied. The effects that the radius of curvature of the redounded sides does have on the performance of the heat sink are analyzed considering three variations ($\xi_{ETM\text{-}3\text{-}F}$ of 0.25, 0.5 and 0.75). Figure 4.22 presents the results of these variations. Although the increase of the radius of curvature reduces the friction factor due to the fluid

FATURA DE BIBLIOTECAS
CAMPUS IRAPUATO-SALAMANCA

moves more smoothly on the fin surface, the reduction in the heat transfer is notorious since the curves along the flow length present the same path and also there is not observe a large variation of the ϕ parameter with this geometrical variations. Thus, for this purposes of computing the overall performance considering such the thermal as the hydrodynamic effects, the variation of the radius of curvature might be assumed as negligible.

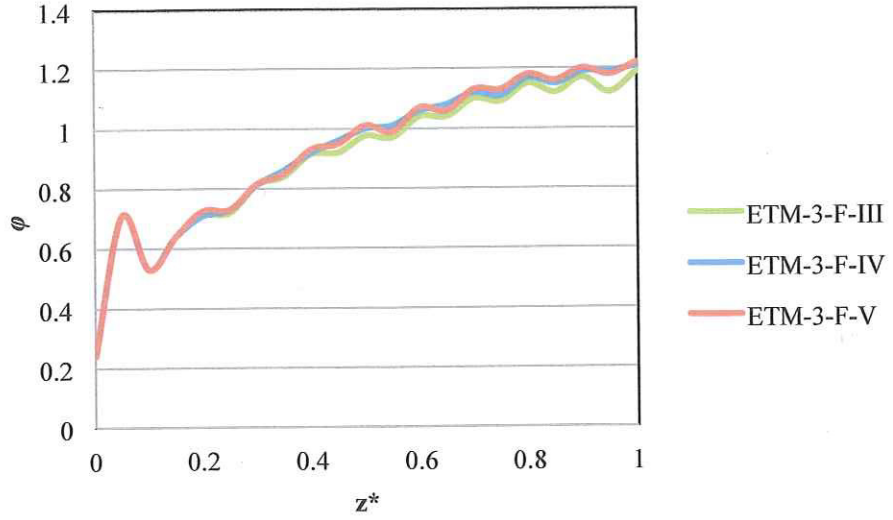

Figure 4.22 Variation of ϕ along the channel length for the cases ETM-3-F-III, ETM-3-F-IV and ETM-3-F-V mentioned in Table 2.11.

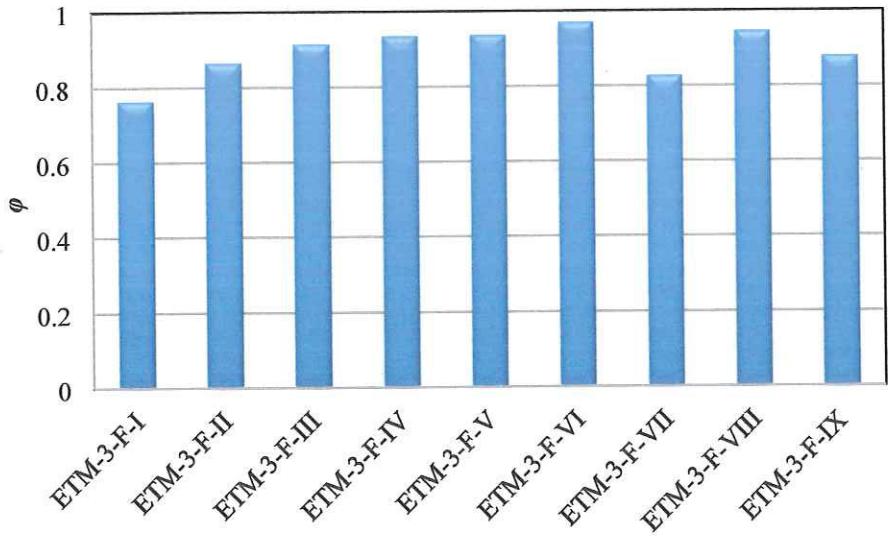

Figure 4.23 Integrated ϕ values for configurations mentioned in Table 2.11.

Moreover, Figure 4.23 presents the average ϕ parameter for the nine configurations based on flat-shaped with redounded sides used in this analysis. The results show that this average parameter is below the expected value of 1.0. However, this thermal enhancement technique presents a better performance that the other configurations based on using fins. The best performance is observed in the configuration ETM-3-F-VI (ϕ=0.96). Furthermore, it is important to mention again the final comment

exposed in the previous subsections. The most important advantage of this kind of fin configurations is the feasibility to move the fins according with the thermal necessities that the IC chip might require. Based on this and upon the results exposed for these configurations, it is possible to observe that the use of flat-shaped fins could be an appropriate alternative for the goals pursued in this work.

OVERALL PERFORMANCE OF THE ETM-4

The overall performance presented by the thermal enhancement techniques based on wavy walls is presented in this section. Figure 4.24 shows the ϕ parameter along the flow length for this proposed enhancement technique considering the variation of γ_{ETM-4} parameter (0.05, 0.1, 0.2), and considering β_{ETM-4} of 0.25. Tables 2.13 and 2.14 present the matrix of cases and the amplitude and length of the wavy for these configurations. At the inlet section, this performance parameter is 1.0 due to the channel inlet and the operating parameters are the same that straight microchannels. Once the fluid starts passing through the channel, there is observed a decrease of ϕ parameter due majorly to the development of the boundary layers and the increase in the friction factor because of the change of direction that the fluid suffers. Values lower than 1.0 are achieved and remained along the flow length. There are not observer outstanding sections in this thermal enhancement technique. Furthermore, the variation of β_{ETM-4} parameter does not affect importantly the overall performance of this thermal enhancement technique. Figure 4.25 presents the average ϕ parameter for all the configurations exposed in the matrix of cases studied for this thermal enhancement technique. This figure shows the minimal enhancement performance obtained with this kind of configurations. This poor improvement is majorly caused by the increase that the friction factor presents due to the change of direction as well as the minimal increase in the heat dissipation that the channel configuration causes in the fluid. Thus, this thermal enhancement technique is not a good candidate for increasing the overall performance of the heat sink.

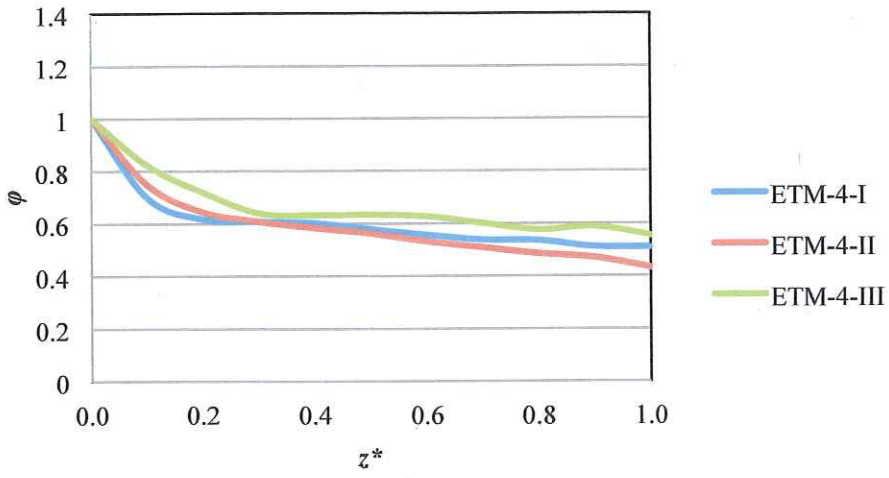

Figure 4.24 Variation of ϕ along the channel length for the cases ETM-4-I, ETM-4-II and ETM-4-III mentioned in Table 2.13.

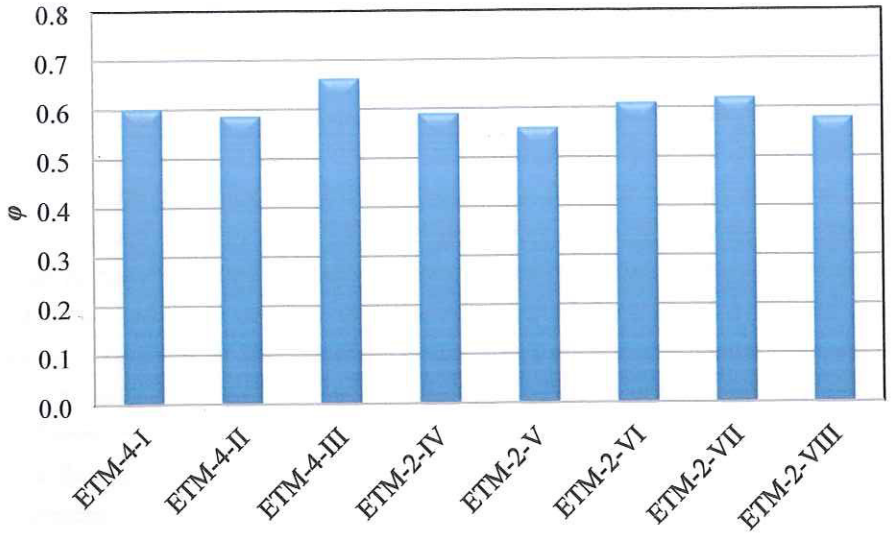

Figure 4.25 Integrated ϕ values for configurations mentioned in Table 2.13.

OVERALL PERFORMANCE OF THE ETM-5

The overall performance parameter generate with the use of channels with dimpled surfaces are presented in this section. The results are based on the geometrical variations of the dimensionless parameters α_{ETM-5}, β_{ETM-5}, γ_{ETM-5} and ξ_{ETM-5} exposed in Equations (2.28) to (2.31). Three variations are considered for each parameter (0.75, 1.0 and 1.5 for α_{ETM-5}; 0.025, 0.05 and 0.1 for β_{ETM-5}; 0.7, 0.85 and 1.0 for γ_{ETM-5}; and 0.125, 0.25 and 0.5 for ξ_{ETM-5}). For each variation, the remaining parameter as fixed as constant values (Table 2.15).

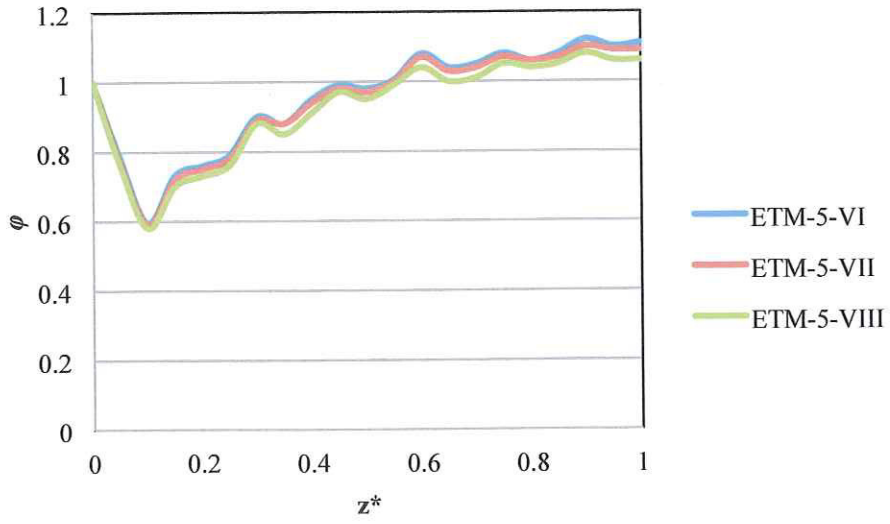

Figure 4.26 Variation of ϕ along the channel length for the cases ETM-5-VI, ETM-5-VII and ETM-5-VIII mentioned in Table 2.15.

The results show that the ϕ parameter is 1.0 at the entrance due to same channel geometries and boundary conditions that the straight microchannel are considered at this section. Then, this performance parameter goes down to the effects that the development of the hydrodynamic boundary layer has in the system, reaching a minimum. After this point, the performance starts increasing due to the reduction of the friction effects coupled to the development of the thermal boundary layers plays a more important role in the phenomenon. Interesting results starts to emerge once the fluid reaches the deeps since there is observed an increase of the ϕ parameter at the zones where the deeps are located. This improvement is caused by the partial deformation of the boundary layer, however, the friction factor is not drastically affected causing that the relationship between this and the Nusselt number increases. Peaks are observed at the position where the dimples are located caused by the effects mentioned above. Similar results were observed when the thermal enhancement techniques based on fins were used. However, the most outstanding observation is the fact that the ϕ parameter goes up as coolant is flowing through the system. According with the phenomena, this enhancement is caused by the fact that the system is formed by two systems: a straight channel that has the features mentioned in Chapter II, and the dimpled surface at the bottom wall of the channel that contributes to increase the heat transfer at this section. Thus, the improvement comes from the channel aspect ratio (majorly the channel height) and the partial destruction of the boundaries layers at the bottom wall of the channel. Figure 4.26 presents the effects that the variation of the dimpled deep has in the system performance. According with the results, it is observed that the increase of this deep reduces slightly the ϕ parameter. Thus, it is possible to assume that the increase of the friction factor is larger that the improvement in the thermal performance as the dimpled deep is increased. Thus, it is recommended to use small deeps for these configurations.

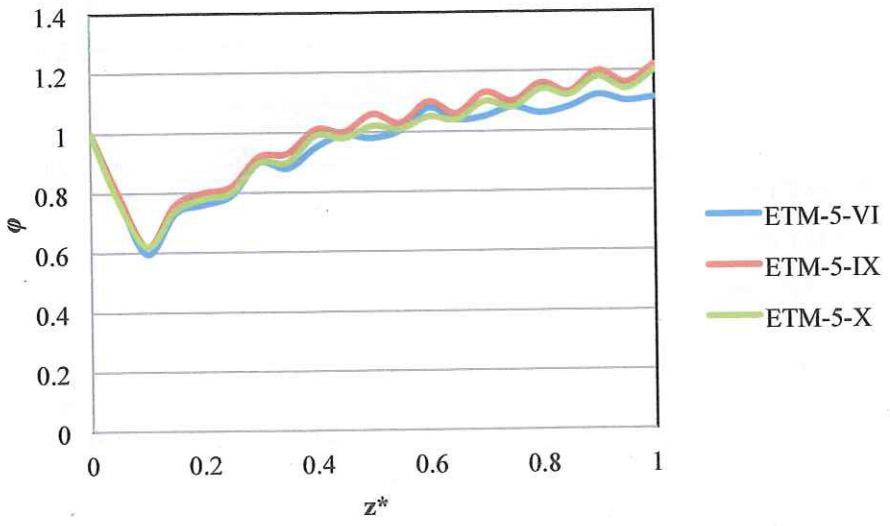

Figure 4.27 Variation of ϕ along the channel length for the cases ETM-5-VI, ETM-5-IX and ETM-5-X mentioned in Table 2.15.

In order to understand the results exposed in Figure 4.27, it is important to remember that the dimple has an ellipse-shape where the *a* dimension is parallel to the flow length and the *b* dimension is perpendicular to the flow direction. Thereby, these results show that the reduction of the large side of

the ellipse increases the ϕ performance in the system. Furthermore, there is observed that the transition to the ellipse-shape with the largest side parallel to the flow length to a circle-shape does a larger improvement in the system than the opposed transition. Thus, it is recommended to use circle-shaped dimples along the channel length.

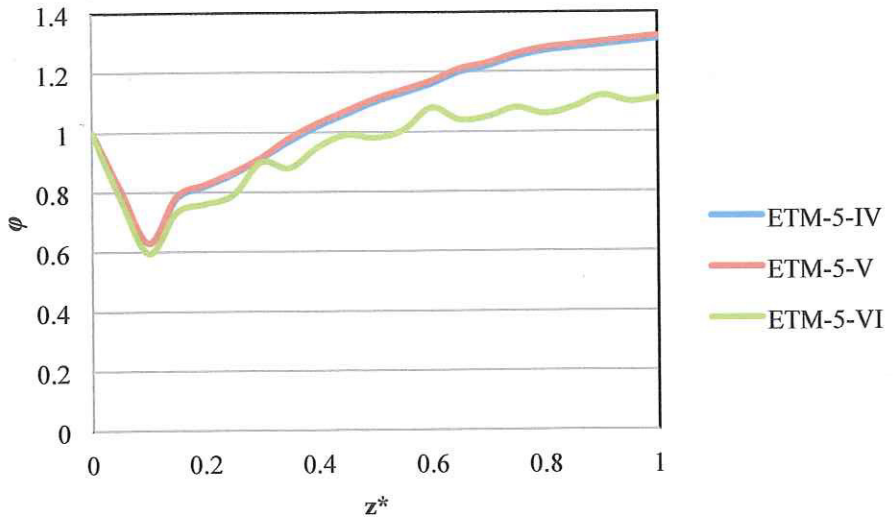

Figure 4.28 Variation of ϕ along the channel length for the cases ETM-5-IV, ETM-5-V and ETM-5-VI mentioned in Table 2.15.

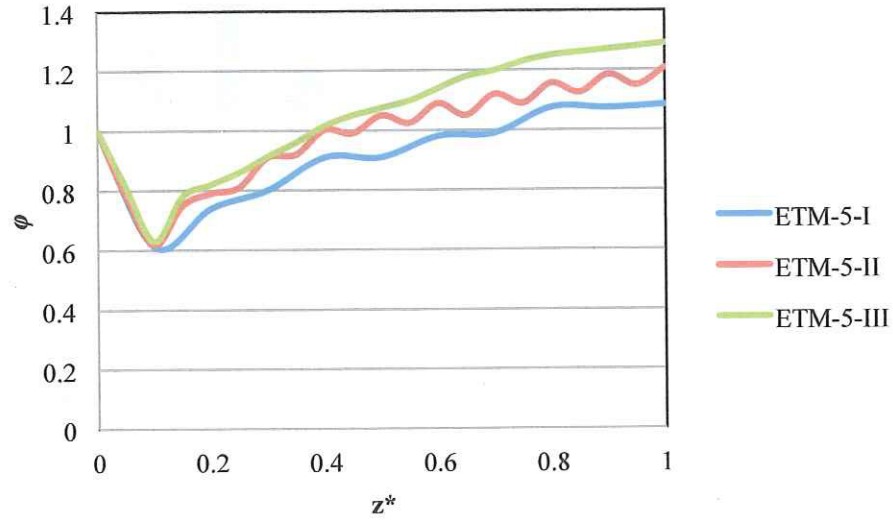

Figure 4.29 Variation of ϕ along the channel length for the cases ETM-5-I, ETM-5-II and ETM-5-III mentioned in Table 2.15.

Moreover, the increase of the *b* dimension of the deep reduces the overall performance of the system as it is observed in Figure 4.28. It is important to highlight that the curves corresponding to the configurations ETM-5-V and ETM-5-VI do not show peaks due to the transversal cuts done on the model in the post-processing stage do not match with the dimples positions due to the

parameterization done and exposed in Chapter II. However, the results show that the increase of the dimple width reduces the overall performance of the systems and, again, the transition from ellipse-shape to circle-shape is useful for enhancing the performance of the system. Figure 4.29 shows the effect that the variation of the pitch between dimples has in the overall performance of the system. The results show that the reduction of space between deeps helps to improve the ϕ parameter. This is an expected results due to the effects of destroying partially the boundary layer are more recurrent when the dimples are close. Figure 4.30 shows the average ϕ parameter for all the configurations exposed in the matrix of cases corresponding to Table 2.15. These results are interesting due to three configurations have values larger than 1.0, and a couple more are very close to this target value. Thus, cooling systems with small dimple deep and dimple pitch, as well as a circle-shape dimple generate the largest improvement in the system performance. Thus, this thermal enhancement technique is a good alternative for enhancing the performance of the cooling system. However, it is needed to considered that gradient of temperature on the IC chip are going to be present due to the path of the ϕ parameter is not uniform.

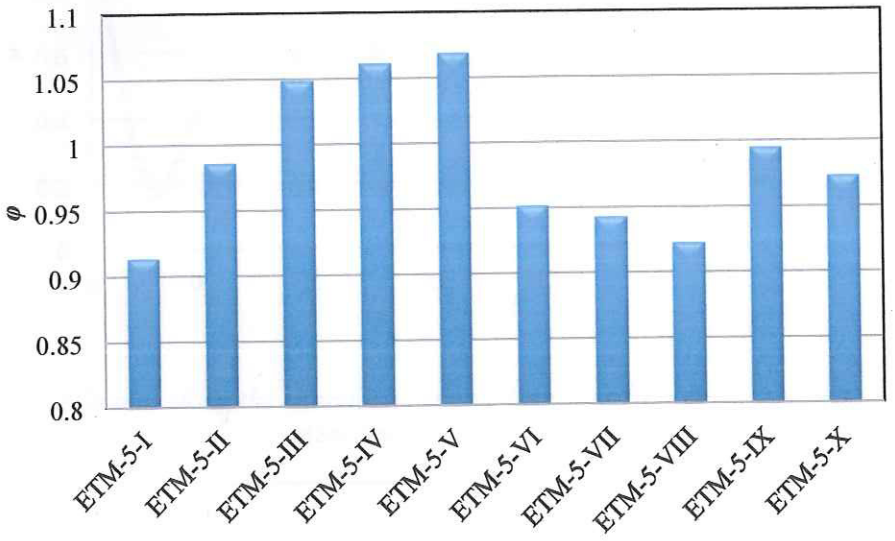

Figure 4.30 Integrated ϕ values for configurations mentioned in Table 2.15.

OVERALL PERFORMANCE OF THE ETM-6

This section presents the behavior that the cooling system has when the thermal enhancement technique based on channels with reentrant triangular cavities are considered. The results are based on the geometrical variations according with the dimensionless parameter $\alpha_{ETM\text{-}6}$, $\beta_{ETM\text{-}6}$, $\gamma_{ETM\text{-}6}$ and $\xi_{ETM\text{-}6}$ given by Equations (2.32) to (2.36). Three variations are considered for each parameter (0.25, 0.5 and 1.0 for $\alpha_{ETM\text{-}5}$; 0.25, 0.5 and 0.75 for $\beta_{ETM\text{-}5}$; 1.0, 1.5 and 2.0 for $\gamma_{ETM\text{-}5}$; and 1.5, 2.0 and 4.0 for $\xi_{ETM\text{-}5}$). For each variation, the remaining parameter as fixed as constant values (Table 2.17). Figures 4.31 to 4.34 presents the variations of the local ϕparameter along the flow length for each geometrical variation. The results show that the performance of the system is 1.0 at the entrance section due to the geometrical and operational conditions are the same that the straight microchannel considered for

comparison. Then, the performance goes down until achieve a minimal due to the friction factor effects and development of the hydrodynamic boundary layer have a large impact in the phenomenon. After this minimum point the local performance starts increasing, indicating that the heat dissipation is increased. The curves show slight increases at the zones where the channel has the reentrant triangular cavities. This improvement is majorly caused by the partial destruction of the thermal boundary layer as well as the slight increase of the heat transfer surface. Furthermore, it is possible to understand that the reduction of the fluid velocity when the fluid found the channel wall affects the thermal performance. According with the results, the increase of the friction effects is important in these configurations. The last comment is ratified when the results generated for this configuration are compared with the previous thermal enhancement technique. Clearly it is observed that the ϕ parameter is not highly increased along the flow length (i.e. the maximum ϕ values are around 0.8.

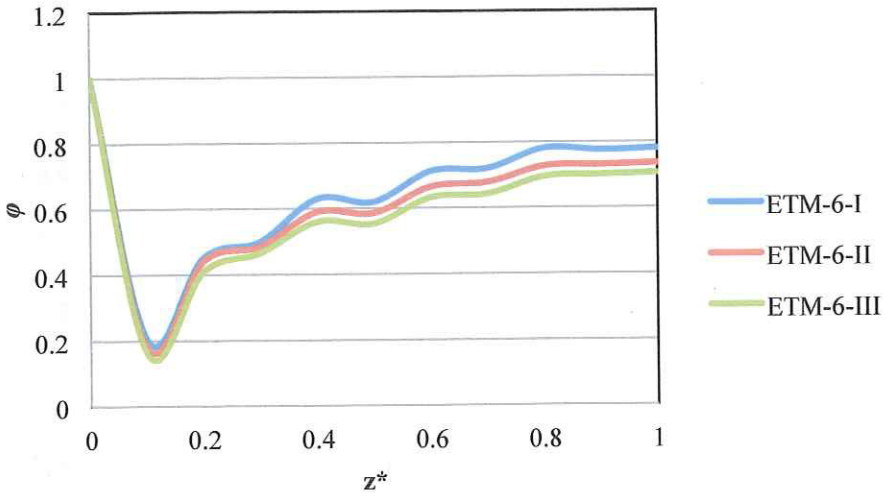

Figure 4.31 Variation of ϕ along the channel length for the cases ETM-6-I, ETM-6-II and ETM-6-III mentioned in Table 2.17.

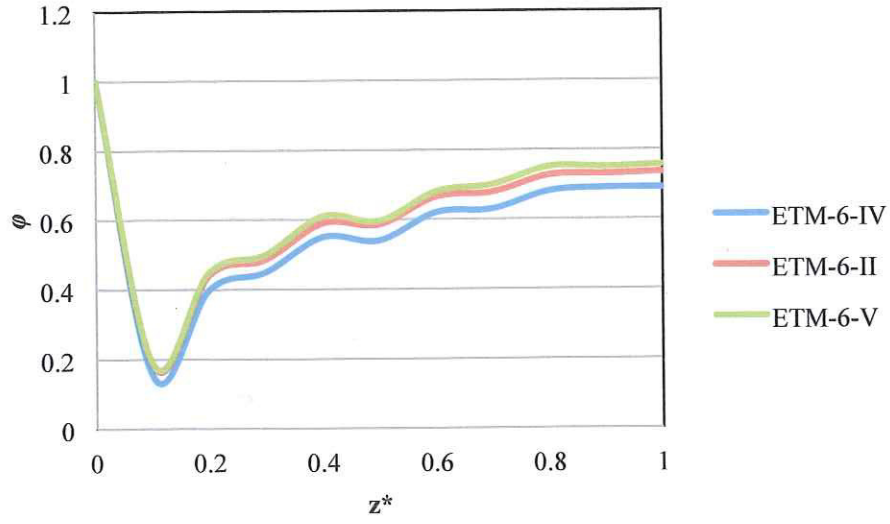

Figure 4.32 Variation of ϕ along the channel length for the cases ETM-6-IV, ETM-6-II and ETM-6-V mentioned in Table 2.17.

Figure 4.31 presents the effects that the variation of the channel aspect ratio has in the cooling system. As it was expected according with the performance of conventional microchannels, the increase of the channel width reduce the performance of the systems due mainly to the reduction of the heat transfer coefficient. Moreover, Figure 4.32 presents the effects that the variation of the cavity width (maximum channel width) has on the ϕ performance. The results show that the increase of this width reduces the performance of the system. When the cavity width is increased, the fluid suffers stagnation within the cavity due to the relative fluid velocity. Thus, this stagnated fluid works as an insolated wall between the channel walls and the fluid reducing the heat dissipation.

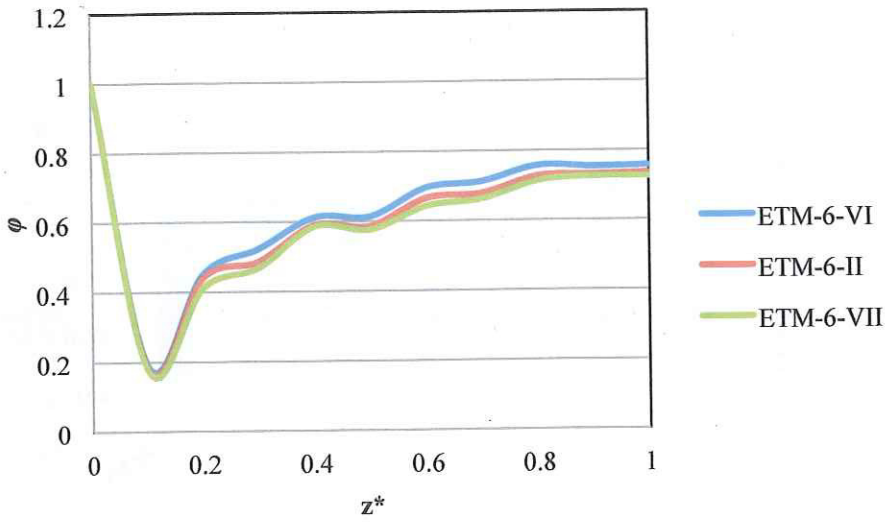

Figure 4.33 Variation of ϕ along the channel length for the cases ETM-6-VI, ETM-6-II and ETM-6-VII mentioned in Table 2.17.

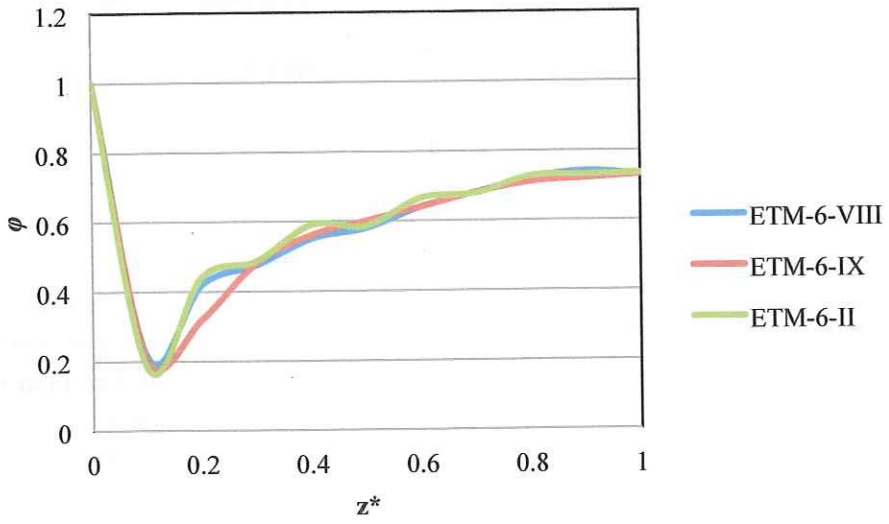

Figure 4.34 Variation of ϕ along the channel length for the cases ETM-6-VIII, ETM-6-IX and ETM-6-II mentioned in Table 2.17.

Figure 4.33 shows the effects of varying the cavity length out (large side of the triangle) in the system. According with the results, the increase of this length reduces the ϕparameter because the stagnated fluid within the cavities is increased, affecting negatively the heat dissipation. Furthermore, the partial destructions of the boundary layers are reduced. Moreover, the variation of the cavity entrance length (short side of the triangle) in the system is minimal. Figure 4.34 presents the ϕ performance along the flow length subject to this geometrical variation. It is observed that the curves do not have important variations, which might indicate important effects of this dimensionless parameter in the performance of the system.

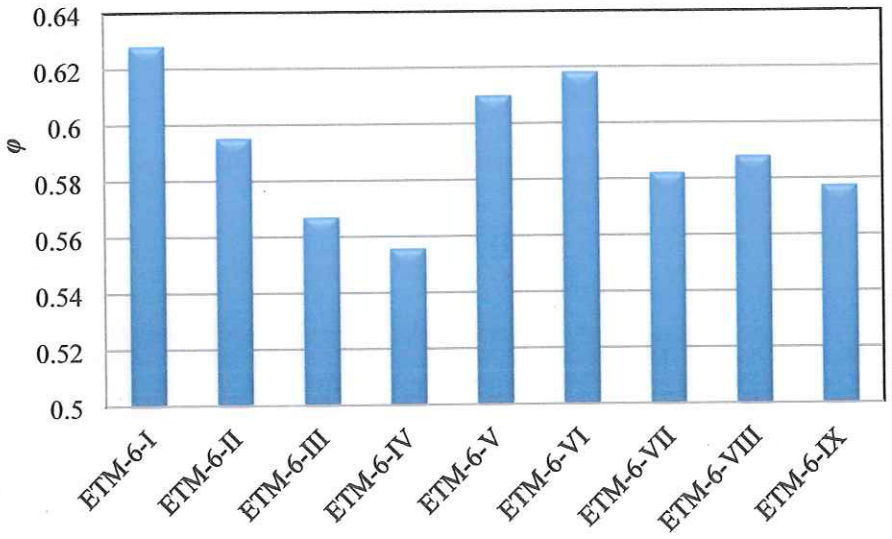

Figure 4.35 Integrated ϕ values for configurations mentioned in Table 2.17.

Figure 4.35 presents the average ϕ value for the configuration exposed in Table 2.17. The results show that these thermal enhancement techniques do not generate the expected value of 1.0. The best configurations have values near to 0.64. Thus, it is possible to conclude that this thermal enhancement technique is not a good candidate for the goal of this work.

REMARKABLE OBSERVATIONS

Six thermal enhancement techniques were evaluated in order to observe their local and average overall performance considering the improvement of the thermal dissipation with the associated penalty in the friction losses. The cooling system based on straight channel with variable channel aspect ratio and the channel with dimpled surface presented important local enhancement at the second half of the channel length. However, it is important to remember that the temperature on the IC chip is directly affected by this performance, and thus, important temperature gradients might be generated with these configurations. The enhancement thermal technique based on the variation of the channel hydraulic diameter presented very large average ϕ values, however, the local performance was very poor due to the large increases generated in the section when the channel hydraulic diameter is varied. Moreover, the use of fin as technique for enhancing the performance of the system generates average ϕvalues lower that the expected value of 1.0. The local performance is important at the

second half of the channel length. However, the most important advantage of these configurations is the fact that the fins can be placed according with the requirement of the IC chip. Thus, these configurations are appropriate for obtaining the objective planted for this work. The remained thermal enhancement technique configurations present a very poor enhancement performance and, thereby, they are unconsidered in this work. The next chapters present the study of a cooling system based on the results that the fin configurations presented, considering the thermal requirements of the IC chip and taking into account the advantage of varying their position.

Chapter V
Micro Pin-Fin Heat Sink with Variable Fin Density

WHY USE VARIABLE FIN DENSITY

In Chapter I it was mentioned that one of the main goals of this work is to generate a micro cooling system capable, among another things, of reducing the temperature gradients on the IC chip to be cooled, that are commonly generated when a coolant is moved through the ducts (internal flow). The technical literature has shown that these temperature gradients are strongly large depending on the amount of heat to be dissipated as well as on the fluid velocities along the system. It has also been reported in the technical literature that the heat transfer coefficient increases if *i)* the channel hydraulic diameter is decreased, or *ii)* the channel aspect ratio decreases. Although these options improve the heat dissipation in this kind of cooling systems, the pressure drop goes up in an inverse cubic proportion as the hydraulic diameter decreases. According to the results presented in the previous chapter for the overall performance of these heat sink configurations, it is observed that the first channel variation generates a gradual increase after a specific position, and that the second channel variation generates important improvements.

Thus, the use of pin fins could be a good alternative for the new generation of cooling systems due to their good thermal performance with appropriate heat dissipation. Also, this kind of configurations has the feasibility to place fins according to the requirements of heat dissipation from the IC chip. Thus, variable densities of pin-fins can be used in order to homogenize the temperature at the bottom wall of the heat sink and, therefore, the thermal damages on the chip due to the generation of hotspots are reduced. At the microscale level, only a few works have been carried out considering pin fin configurations [100,111] but with constant fin density. The next section presents the design of the fin arrangements for the novel heat sink proposed in this work with variable fin density.

UNIFORM TEMPERATURE DISTRIBUTION CONCEPT

A large part of the current conventional liquid cooling technologies is based on forced convection mechanism in internal flow. According to the theory, the temperature difference between the coolant and channel walls remains constant along the flow length when fully developed conditions and constant properties are assumed under constant heat flux boundary condition. The coolant temperature rises along the flow length ($T_{fluid}=T_{fluid}(z)$) and, therefore, the channel wall temperature increases accordingly. Assuming that the temperature difference between the heat sink and the junction wall remains constant, the junction temperature will then vary in a similar manner as the fluid

temperature along the flow direction ($T_{IC}=T_{IC}(z)$). Based on the conservation of thermal energy, the temperature difference between the coolant and the channel wall is determined by the heat flux and the convective thermal resistance (see Figure 5.1). Thus, if the thermal resistance is constant, a temperature variation is observed, similar to the path shown in Figure 5.1. Equation (5.1) expresses this thermal resistance.

$$T_{bottom}(z)-T_{fluid}(z)=q''R_{total} \tag{5.1}$$

According to Equation (5.1), and considering a constant heat flux, a constant junction temperature is achieved when the thermal resistance is reduced as the coolant is passing through the system, this means that $R_{total}=R_{total}(z)$. Figure 5.2 shows this behavior. Since the thermal resistance varies inversely with the product of the heat transfer coefficient, h, and the heat transfer area, A_s, this product should be gradually increased along the flow direction in order to achieve the uniform temperature.

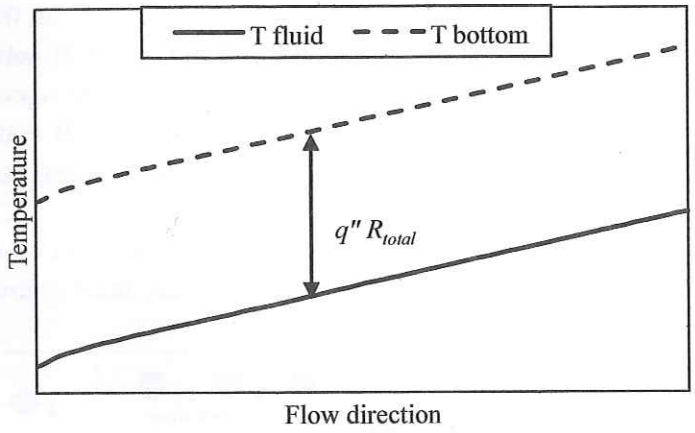

Figure 5.1 Sketch of temperature variation in internal flow systems subject to constant heat flux and thermal resistance.

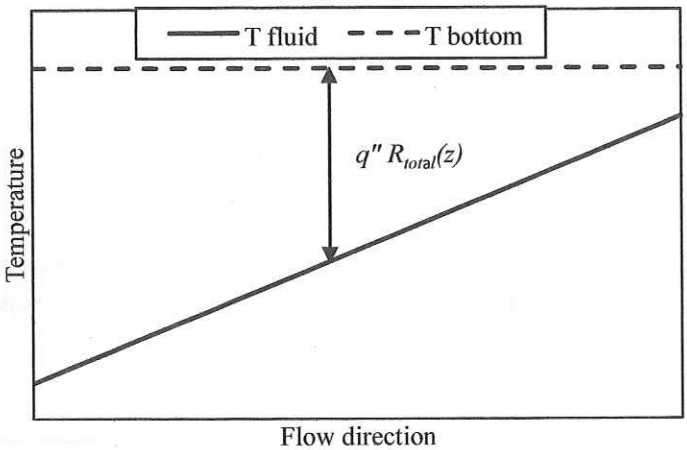

Figure 5.2 Sketch of temperature variation in internal flow systems subject to constant heat flux, uniform wall temperature and variable total thermal resistance.

MICRO PIN-FIN HEAT SINK WITH VARIABLE FIN DENSITY – MODEL DEFINITION

Based upon the previous sections, the model definition of a micro pin fin heat sink with variable fin density is presented here. A 10 mm x 10 mm IC chip surface is considered as the base for designing and building the novel micro pin fin heat sink with variable fin density. This cooling system is going to be formed by a specific number of fins placed on a 200 μm thickness silicon substrate. In order to generate the variable fin density, the silicon plate is "divided" in a specific number of sections (*SI*, *SII*, … *SN*) along the flow direction. Figure 5.3 shows a sketch of these sections. A number of transversal and longitudinal rows separated by S_T and S_L, respectively, are marked on each section. Then, one pin fin is placed at each crossing line. Four overall configurations are developed for study (*i*, *ii*, *iii*, and *iv*). The dimensions of these configurations are presented in Table 5.1.

i. *Configuration I*: micro pin fin heat sink formed by 990 fins placed on 4 sections in an on-line arrangement. The fin height is 200 μm. Circle, square, ellipse, and flat with rounded sides cross section (Figure 2.8) are considered in the analysis. Three fin lengths are used (74 μm, 100 μm and 150 μm).

ii. *Configuration II*: micro pin fin heat sink formed by 3996 fins placed on 4 sections in an on-line arrangement. The fin height is varied (100 μm, 200 μm and 300 μm).

iii. *Configuration III*: micro pin fin heat sink formed by 4748 fins placed on 3 sections in an on-line arrangement. The fin height is set to 200 μm. Flat-shaped fins are considered (see Figure 5.4 *a)*).

iv. *Configuration IV*: micro pin fin heat sink with the same features of *Configuration III* but in an offset arrangement (see Figure 5.4 *b)*).

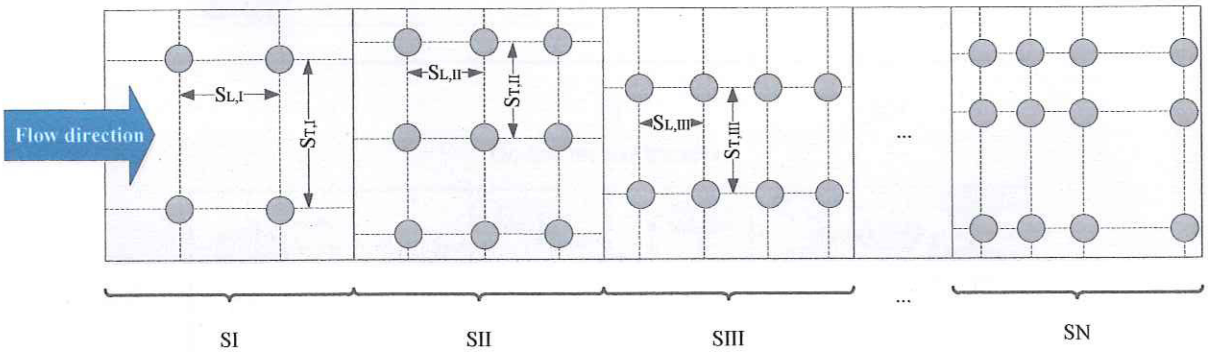

Figure 5.3 Sketch of sections marked on the square heat sink. The transversal and longitudinal rows, S_T and S_L dimensions, and fin places are shown.

Table 5.1 Description of the four configurations of micro pin fin heat sink arrangements.

Parameter	***Section I***	***Section II***	***Section III***	***Section IV***
		Configuration I		
Length (mm)	1.4	2.8	4.2	1.6
No. pin fins	0	231	462	297
No. longitudinal rows	0	7	7	3
No. transversal rows	0	33	66	99
S_L (μm)	0	400	600	600

S_T (μm)	0	300	150	100
$\rho_{pin\ fin}$ (# pin fins/mm^3)	0	41.66	55.55	93.75
Configuration II				
Length (mm)	1.0	3.0	4.2	1.8
No. pin fins	0	660	1848	1188
No. longitudinal rows	0	20	28	12
No. transversal rows	0	33	66	99
S_L (μm)	0	150	150	150
S_T (μm)	0	300	150	100
$\rho_{pin\ fin}$ (# pin fins/mm^3)	0	111.11	222.22	333.33
Configuration III				
Length (mm)	1.5	5.2	3.3	--
No. pin fins	330	2240	2178	--
No. longitudinal rows	10	34	22	--
No. transversal rows	33	66	99	--
S_L (μm)	150	150	150	--
S_T (μm)	300	150	100	--
$\rho_{pin\ fin}$ (# pin fins/mm^3)	111.11	217.94	333.33	--

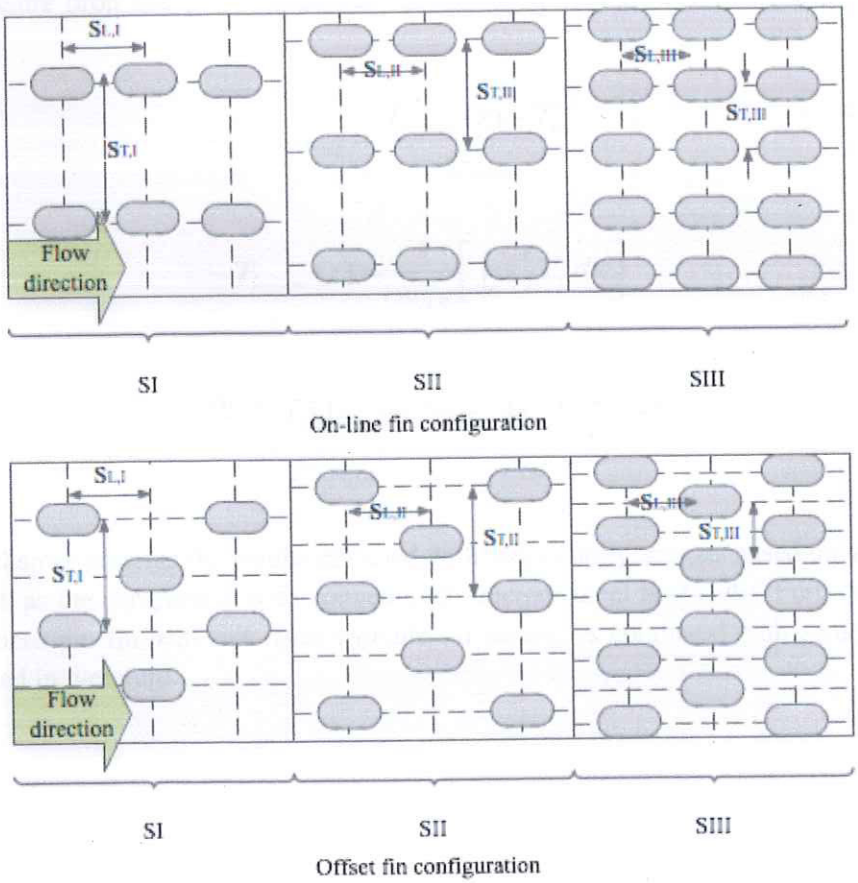

Figure 5.4 Sketch of micro pin fin heat sink with variable fin density using flat-shaped fins and placed on a) on-line, and b) offset fin configurations.

Furthermore, a couple of cooling devices are added to the analysis matrix for comparison purposes:

1. Microchannel heat sink: system formed by 33 rectangular channels with 200 μm height, channel aspect ratio of 1.0, and space between channels of 100 μm.
2. Non-pin fin heat sink: heat sink formed by a single large channel of 200 μm height and 9.9 mm width.

The thickness of the silicon substrate under the channels for all models is 200 μm. Due to the symmetries that the heat sinks present, only 1/66 part of the whole system was solved.

In order to solve these configurations, the assumptions, the governing equations and boundary conditions expressed in Chapter II, Sections 4.1, 4.2 and 4.3, respectively, are applied. The numerical solution follows the same process describe in Chapter III for solving the thermal enhancement models described previously. In order to observe and compare the thermal and hydrodynamic performance of these configurations, the variation of temperature at the bottom wall of the heat sink (junction wall) and the fluid pressure variation along the flow length are computed. Furthermore, the overall thermal resistance, pressure drop and pumping power are calculated using Equations (5.2), (5.3) and (5.4), respectively.

$$R_{total} = \frac{T_{bottom}(z) - T_{in}}{Q_{total}} \tag{5.2}$$

where

$$T_{bottom}(z) = \frac{1}{w_{cell}}\left[\int_0^{w_{cell}} T_x \, dx\right]$$

$$\Delta P = \frac{1}{A_c}\left[\int_{A_c} P_{x,y} dA_c\Big|_{out} - \int_{A_c} P_{x,y} dA_c\Big|_{in}\right] \tag{5.3}$$

$$Pumping\ Power = \Delta P \dot{\forall} \tag{5.4}$$

Next chapter presents the results obtained with these configurations based on varying their fin density, as well as the comparison with conventional microchannel heat sinks. Furthermore, the most outstanding micro pin fin heat sink with variable fin density is compared with some micro cooling systems exposed in literature.

Chapter VI
Results and Comparisons of Micro Pin-Fin Heat Sink with Variable Fin Density

EFFECTS OF PIN-FIN SHAPES

This chapter presents the effects on the bottom wall temperature variation and the increase in the pressure that the novel micro pin fin heat sinks with variable fin density described in the previous chapter have. Figure 6.1 shows the junction wall temperature variation of the micro pin fin heat sink based on Configuration I with different fin shapes along the dimensionless flow direction ($z^*=z/L$). The operating conditions are: flow rate of 1 mL/s and a heat flux of 100 W/cm^2. For simplification, the heat sinks are called as M*A*-50x***LLL*x*HHH*-*NN*** *(please refers to Figure 2.8)*, where:

- ***A*** indicates the fin shape (C-circle, S-square, E-ellipse, F-flat),
- ***LLL*** indicates the fin length (μm),
- ***HHH*** indicates the fin height (μm), and
- ***NN*** indicates the number of longitudinal rows that forms the arrangement.

The temperature variations for the conventional microchannel heat sink and non-pin fin heat sink, which were described in the previous chapter as well, are shown in Figure 6.1 for comparison purposes. Although these last two models have different temperature magnitudes caused mainly by the increase of the heat transfer coefficient when microchannels are used, the paths are similar. The lowest temperature is found at the fluid inlet section and the curve increases almost linearly. The largest temperature is found at $z^*=1.0$. The bottom wall temperature difference is ~41 K and ~68 K for microchannel and non-pin fin heat sinks, respectively. Moreover, the temperature profiles generated by the proposed micro pin fin heat sinks at this bottom wall look more homogeneous. This is clearly caused by using variable fin density configurations. These temperature curves show four slight peaks/valleys near the transition zones among fin sections. These variations are caused by the increase of the heat transfer area from one section to the next one, as well as by the increase of the heat transfer coefficient when the gap between fins is reduced.

In the temperature curves it is observed that the circle-shaped fin presents the largest junction temperature as well as the largest temperature difference between maximum and minimum points. Moreover the flat-shaped fin improves the heat dissipation since it has the lowest junction temperature as well as the lowest temperature difference. The overall performance of these configurations is shown in Table 6.1. The heat transfer area-fluid volume ratio, γ, is considered as a parameter for comparison. The results show that the heat dissipation is improved when γ is slightly increased (e.g. the γ increase

between circle- and flat-shaped fin configurations is ~1.1% and the overall temperature is reduced 6.6 K). The square- and ellipse-shaped fin configurations present similar temperature results with minimal differences at the inlet section. One important observation is that the fin shape does not affect the heat dissipation since it is possible to achieve a similar temperature profile with square- or ellipse-shaped fin configurations because γ is almost the same in both cases.

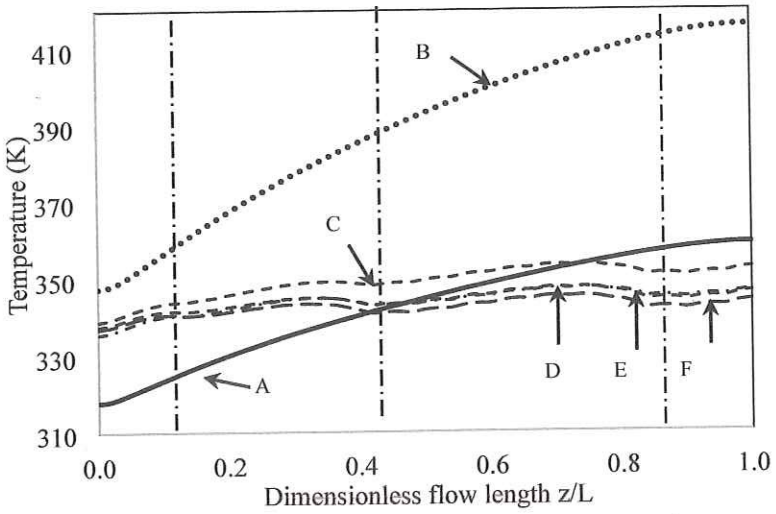

Figure 6.1 Variation of the junction temperature along the dimensionless flow length for the microchannel heat sink, non-pin fin heat sink and micro pin fin heat sinks based on Configuration I with different fin shapes (Table 6.1). q"=100 W/cm^2 and flow rate of 1 mL/s.

Table 6.1 Overall performances of microchannel, non-pin fin and micro pin fin heat sink based on Configuration I with different fin shapes.

Heat Sink	$T_{bottom,avg}$ (K)	ΔT_{bottom} (K)	ΔP (kPa)	R (K/W)	γ (mm^2/mm^3)
A) Microchannel	342.75	41.31	5.80	0.498	15.00
B) Non-pin fins	389.16	68.28	1.61	0.962	5.20
C) MC-50x50x200-17	349.06	14.72	4.63	0.561	6.91
D) MS-50x50x200-17	344.02	12.06	5.76	0.510	7.40
E) ME-50x75x200-17	344.30	10.06	5.01	0.513	7.42
F) MF-50x75x200-17	342.46	8.47	5.61	0.495	7.47

Figure 6.2 shows the pressure drop variation of micro pin fin heat sink configurations with 17-rows and different fin shapes. Microchannel and non-pin fin heat sinks pressure drop variations along the flow direction are shown as well. For these last two cases, the pressure drop variation is linear with a slight curvature at the fluid inlet section due to the hydrodynamic development effects. There is a difference of ~4 kPa between both heat sinks due to the decrease of the channel hydraulic diameter when microchannels are used. Moreover, the pressure curves of pin fin heat sink models show several waves along the flow length. The increase/decrease of the fluid velocity across the fin arrangement and the stagnation points near the fin walls cause these paths. Overall, the results show that the pressure drop increases when the transversal pitch is reduced, remaining the longitudinal pitch in the section. Also, it is observed that the fin shape plays a very important role in the energy lost by friction

effects. Analyzing the results shown in Table 6.2 for these four configurations, it is observed that the lowest pressure drop is generated when circle-shaped fins are used (4.6 kPa). Moreover, the largest pressure drop is found in square- and flat-shaped fin configurations (~5.7 kPa) although there is a 50% difference of fin length between both models. Thus, it is possible to highlight that the friction losses are strongly reduced when the fin walls perpendicular to the flow direction are redounded, and rise slightly when the fin length increases. These effects are more notorious when ellipse- and flat-shaped fins are compared. Although they have the same fin length, the pressure drop is lower in the first configuration (~12% lower) because it has a larger wall curvature than the second one. According to these results, using ellipse- and flat-shaped fins arrangements formed by 17-rows produce reliable heat sinks. However, the thermal resistance is larger than the value required by the 2016's IC chips.

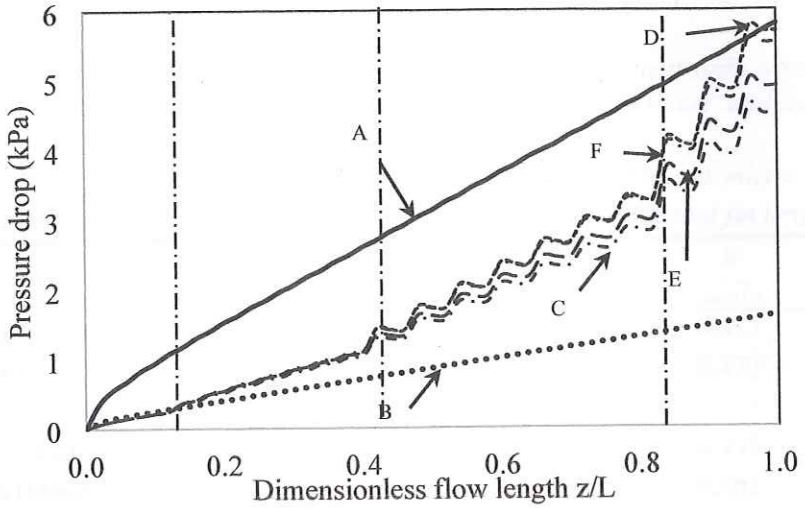

Figure 6.2 Variation of the pressure drop along the dimensionless flow length for the microchannel heat sink, non-pin fin heat sink and micro pin fin heat sinks based on Configuration I with different fin shapes (Table 6.1). q"=100 W/cm^2 and flow rate of 1 mL/s.

EFFECTS OF FIN LENGTH

Figure 6.3 shows the junction temperature and pressure drop of the heat sink with ellipse- and flat-shaped fins for three different fin lengths (75, 100 and 150 μm). The heat dissipation is improved when the fin length is increased because of γ increase (Table 6.2). The average bottom temperature is reduced 2.5% and 2.1% for ellipse- and flat-shaped fins, respectively, when the fin length is varied from 75 μm to 150 μm. Moreover, the pressure drop is larger when flat-shaped fins are used due to the increase of the surface walls parallel to the flow direction. The results indicate that, although the ellipse-shaped fin heat sink has the largest improvement in the heat dissipation with the increase of the fin length, the lowest IC chip temperature is achieved using flat-shaped fins. Thus, it is highly recommended to use this fin shape in this kind of micro heat sink. Furthermore, reliable heat sinks are obtained if a 100 μm fin length is used.

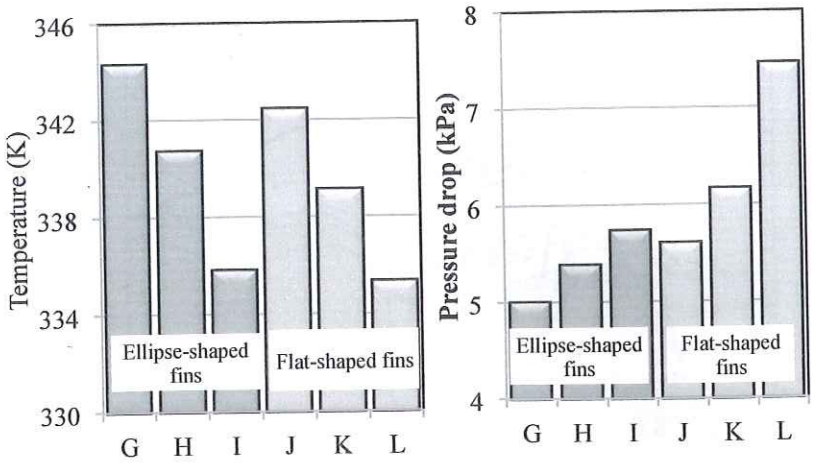

Figure 6.3 Overall junction temperature and pressure drop for pin fin heat sinks with ellipse- and flat-shaped fins based on Configuration I and different fin lengths. q"=100 W/cm^2 and flow rate of 1 mL/s.

Table 6.2 Overall performances of microchannel, non-pin fin and micro pin fin heat sink based on Configuration I with ellipse- and flat-shaped fins subject to different fin lengths.

Heat Sink	$T_{bottom,avg}$ *(K)*	ΔT_{bottom} *(K)*	ΔP *(kPa)*	R *(K/W)*	γ *(mm^2/mm^3)*
G) ME-50x75x200-17	344.30	10.06	5.01	0.513	7.42
H) ME-50x100x200-17	340.73	8.50	5.39	0.477	8.00
I) ME-50x150x200-17	335.83	4.31	5.74	0.428	9.26
J) MF-50x75x200-17	342.46	8.47	5.61	0.495	7.47
K) MF-50x100x200-17	339.13	4.19	6.17	0.461	8.14
L) MF-50x150x200-17	335.33	5.15	7.46	0.423	9.96

Effects of Fin Height and Flow Rate

Figure 6.4 shows the junction temperature variation along the flow length for micro heat sink based on *Configuration II* with different fin heights and flow rates. Clearly, the heat dissipation is improved when the amount of coolant increases; however, the junction temperature variation loses uniformity. Two different effects at two different heat sink sections cause this uniformity loss. First, the heat sink works as a single channel at the first section (*SI*) whereby the heat dissipation is improved when the fin height (channel height) decreases and vice versa (e.g. the bottom temperature at z^*=0.1 is 321.5 K and 331.46 K when the fin height is 100 μm and 300 μm respectively). Second, the increase of the fin height improves the heat dissipation at the subsequent sections (*SII-SIV*) because of the increase of the heat transfer area (e.g. the bottom temperature at z^*=0.8 is 328.06 K and 324.2 K when the fin height is 100 μm and 300 μm respectively). As it is possible to observe, the variation of the fin height affects positively the heat dissipation of the system at one section and negatively at another sections at the same time, affecting seriously the temperature uniformity. Thus, it is recommended to avoid sections without fins in this kind of micro heat sink.

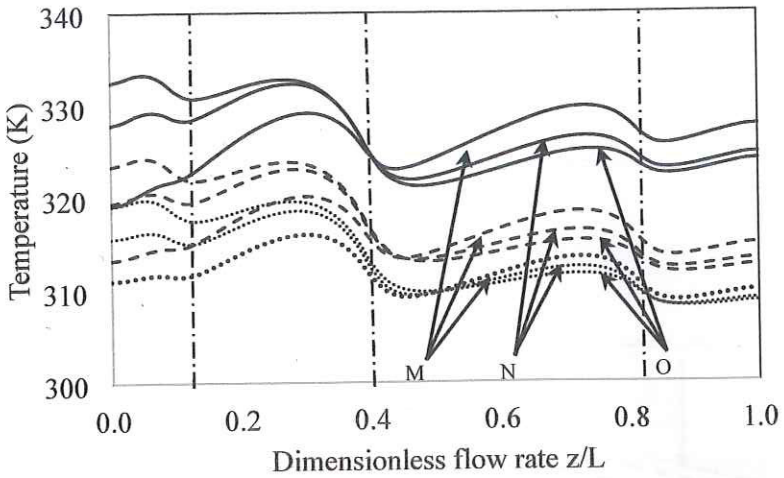

Figure 6.4 Variation of the junction temperature along the flow length in the heat sinks based on Configuration II with different fin heights and flow rates. q"=100 W/cm^2.

Figure 6.5 presents the overall thermal resistance variation in the heat sinks based on *Configuration II* for different flow rates and fin heights. The thermal resistance is almost the same for the three fin height cases when the flow rate is below 1.5 mL/s. For flow rates larger than 1.5 mL/s, the effects of increasing the heat transfer area become more important in the heat dissipation. These results show that the 60-rows heat sink configuration requires an important amount of water for getting thermal resistance values around 0.1 K/W since this curve decreases slightly after 2 mL/s.

Figure 6.6 shows the pressure drop variation when the fin height is varied for different flow rates. The pressure drop rises when the flow rate increases; however, the friction losses are larger for fin heights smaller than 200 µm. The effects of the single channel at *SI* and the decrease of the gap between fins ("apparent channels") at the subsequent sections cause this large pressure drop. The fin height effects are minimal after this point for fin heights larger than 250 µm.

Table 6.3 Overall performances of micro pin fin heat sinks based on Configuration II with different fin heights and flow rates.

Mass flow rate (mL /s)	$T_{bottom,avg}$ *(K)*	ΔT_{bottom} *(K)*	ΔP *(kPa)*	R *(K/W)*
M) MF-50x100x100-60				
1	326.09	10.68	44.13	0.339
2	316.15	6.32	98.80	0.232
3	311.88	7.72	163.04	0.189
N) MF-50x100x200-60				
1	326.47	10.30	13.87	0.335
2	316.92	10.50	30.04	0.239
3	312.78	9.01	49.50	0.198
O) MF-50x100x300-60				
1	326.55	11.90	7.99	0.336
2	317.24	12.32	17.30	0.242
3	313.41	11.57	27.68	0.204

Table 6.3 presents the overall performance of *Configuration II* subject to different fin heights and flow rates. These results show that using fins with a 200 μm height generates reliable results. The heat sink can achieve thermal resistance values around 0.2 K/W.

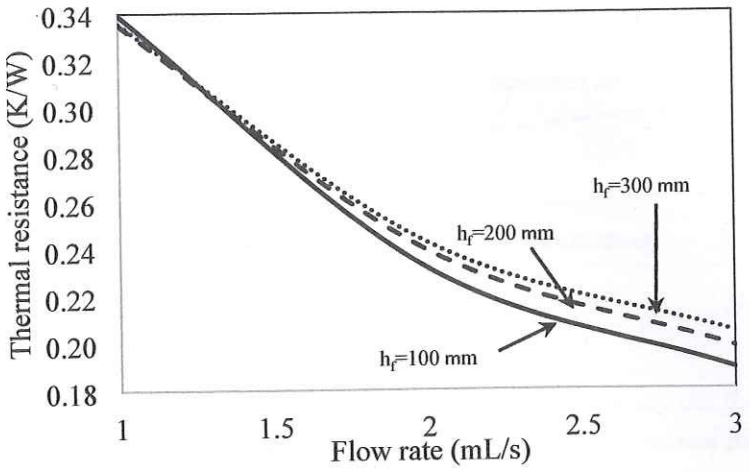

Figure 6.5 Thermal resistance variations for different flow rates and fin heights (h_c) based on Configuration II. q"=100 W/cm^2.

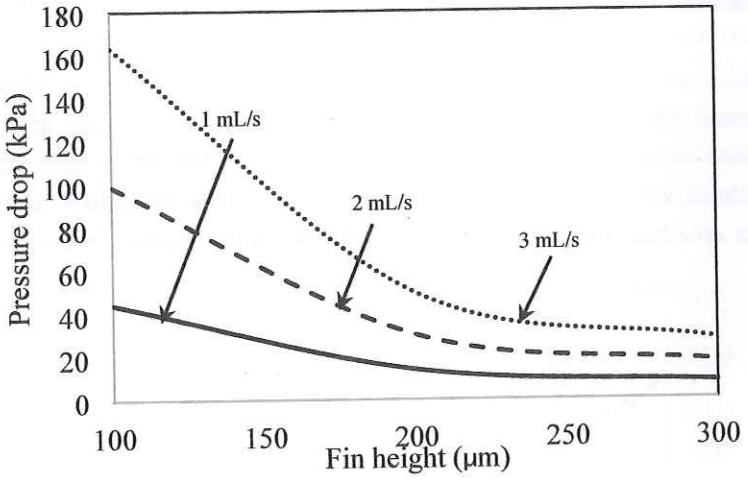

Figure 6.6 Pressure drop variation for different flow rates and fin height based on Configuration II. q"=100 W/cm^2.

PERFORMANCE OF MF-50X100X200-66 HEAT SINK

Figure 6.7 shows the junction temperature profile of the micro pin fin heat sink based on *Configuration III*. The temperature profiles generated with microchannel heat sink and non-pin fin heat sink models are added in the figure for comparison. The figure shows that this proposed heat sink reaches adequate average bottom temperature with a uniform temperature profile ($T_{bot,ave}$=39.9°C, ΔT=5.7°C) compared to microchannels heat sink ($T_{bot,ave}$=57°C, ΔT=38°C) and non-pin fin heat sink ($T_{bot,ave}$>100°C, ΔT=68°C).

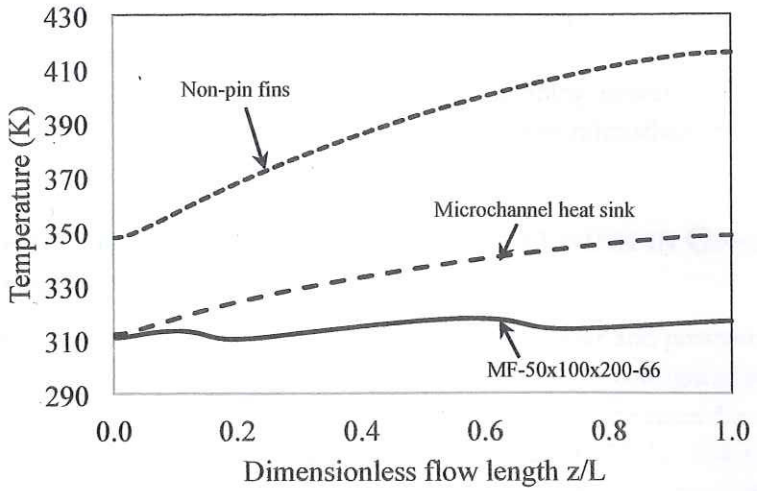

Figure 6.7 Variation of fluid temperature and junction temperature along the flow direction for i) conventional microchannel heat sink, ii) non-pin fin heat sink, iii) conventional pin fin heat sink with constant fin density based on Configuration III.

In this work the temperature gradient along the flow length is used as a parameter of comparison. Thus, according with the temperature difference shown above, the microchannel heat sink, the non-pin fin heat sink and the MF-50x100x200-66 heat sink have temperature gradients of 6.83°C/mm, 3.75°C/mm and only 1.63°C/mm, respectively. Clearly, the proposed heat sink shows an important improvement in the lifetime of the IC chips. Moreover, two drastic zones are found in the temperature curve of the MF-50x100x200-66 heat sink at the positions where changes of section take place. Considering the maximum and minimum points at the vicinity of these zones, the temperature gradient is ~2.7°C/mm. Although this value is larger than the overall temperature gradient of the device, it remains below the gradient values found for the microchannel heat sink and non-pin fin heat sink.

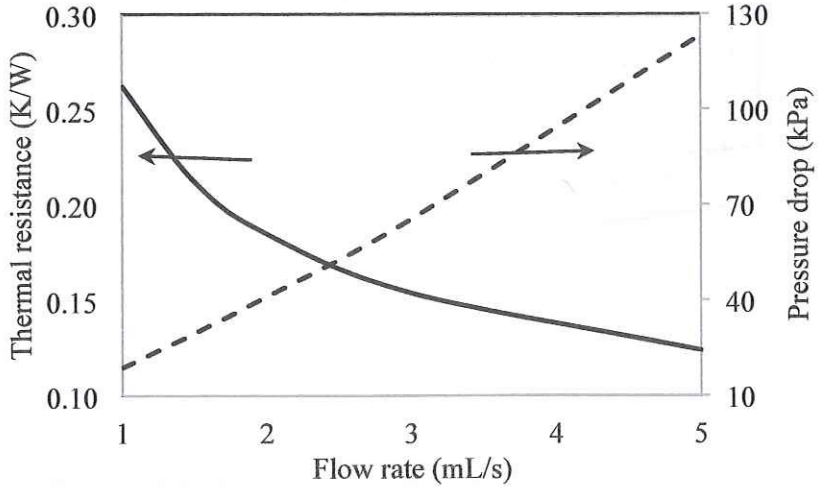

Figure 6.8 Thermal resistance and pressure drop variation for different flow rates for the MF-50x100x200-66 heat sink.

Figure 6.8 shows the thermal resistance and pressure drop variation of the MF-50x100x200-66 heat sink for different flow rates. These results shows that this proposed heat sink is reliable since it is capable to achieve the thermal resistance requested by the 2016's IC chips [6] (0.14 – 0.25 °C/W) with an adequate pressure drop penalty (28-90 kPa). Also, the pumping power required in the systems is ranging from 0.02 to 0.34 W, which is at least 10 times lower than microchannel heat sinks.

PERFORMANCE OF THE MF-50x100x200-66 HEAT SINK IN ON-LINE AND OFFSET FIN CONFIGURATION

This last section presents the comparison on the heat transfer and pressure drop performances for the MF-50x100x200-66 heat sink using an on-line and offset fin configuration. Figure 6.9 shows the temperature profile along the dimensionless flow length for the three cases for 1 mL/s of water and heat flux of 100 W/cm^2. The average temperature values are 334.39 K, 314.15 K and 309.63 K, respectively. Clearly, the offset micro pin-fin heat sink improves the heat dissipation and reduces the IC chip surface temperature (~7.5% compared to microchannel heat sink and 1.5% compared to on-line micro pin fin heat sink). As it was mentioned by [106], the constant developing of the thermal boundary layer enhances the heat transfer coefficient and reduces the overall thermal resistance. In the figure it is observed that the offset fin configuration produces a more uniform temperature profile and reduces the peaks/valleys caused by the change-of-section (*SI-SII* and *SII-SIII*). The uniformity of the bottom temperature impacts directly the temperature gradients along the flow length. The average gradient values for the on-line and offset fin configurations are 1.63°C/mm and 1.19°C/mm, respectively. In the results reported by [112] for the on-line fin configuration, the average temperature gradient at the vicinity of the change-of-sections (*SI-SII* and *SII-SIII*) was 2.7°C/mm. The offset micro pin fin heat sink shows an important reduction of these local temperature gradients, mainly in the second zone. Temperature gradient values of 2.29°C/mm and 0.9°C/mm are generated, respectively. These results impact directly the performance and lifetime of the IC chip.

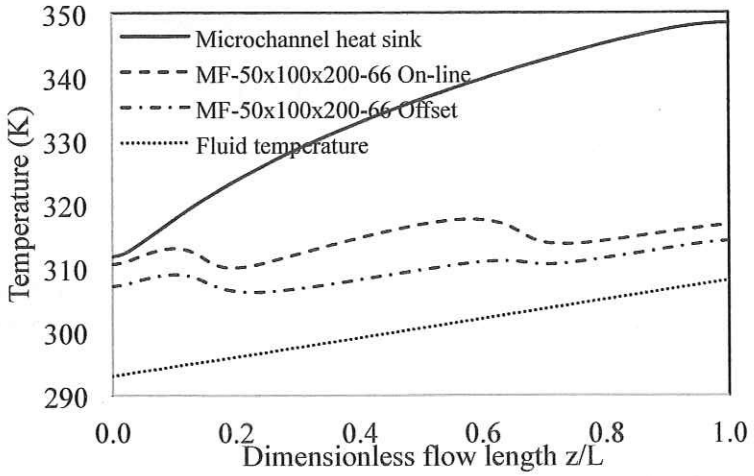

Figure 6.9 Temperature profile at the bottom wall of the heat sink along the dimensionless flow length for microchannel heat sink and micro pin-fin heat sinks with variable fin density for both on-line and offset fin configurations. q"=100 W/cm^2 and flow rate of 1 mL/s.

Figure 6.10 shows the thermal resistance and pressure drop variations of the MF-50x100x200-66 micro pin-fin heat sinks for on-line (solid line) and offset (dotted line) configurations subject to different flow rates. Overall, the flow rate reduces the thermal resistance of the systems; however, the curves show a large negative slope when the flow rate is less than 2 mL/s; and a smaller decrease after this point. In the figure the offset micro pin fin heat sink presents almost 1.3 times less thermal resistance than the on-line micro pin fin heat sink at the same operating conditions. This is a clear manifestation of the passive thermal enhancement caused by the offset arrangement.

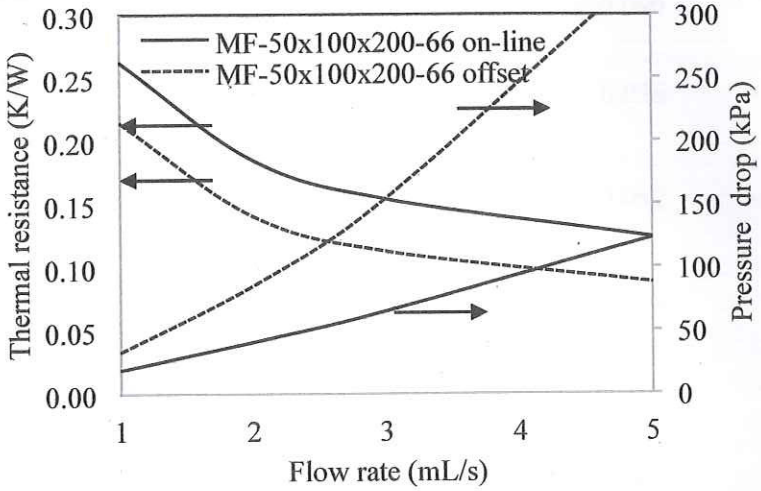

Figure 6.10 Thermal resistance and pressure drop variation with different flow rates for micro pin fin heat sinks with variable fin density and both on-line and offset fin configurations. q"=100 W/cm^2.

Otherwise, the pressure drops in both fin configurations show an almost constant rise with the increase of the flow rate; however, this energy lost is larger for the offset micro pin fin heat sink. The decrease of the "apparent hydraulic diameter" that this fin configuration has (the cross section area is reduced in half at each section) causes this pressure drop penalty. Overall, the offset micro pin fin heat sink generates almost 2.5 times larger pressure drop than the on-line microcooling system.

According to these results, both micro pin-fin heat sinks are capable of cooling the 2016's IC chips since their overall thermal resistances lie in the range required by *ITRS* (0.14 to 0.25 K/W). However, the operating conditions required by these systems are different. The MF-50x100x200-66 on-line requires up to 3.8 mL/s of water for obtaining the lower value of thermal resistance (0.14 K/W) whereas the offset fin configuration needs only 2 mL/s of coolant to get the same thermal resistance condition. Moreover, the pressure drops are similar in both systems (~90 kPa) for this thermal performance. Considering the pumping power that the system requires to work as a parameter of comparison, the offset fin configuration presents a better performance since it only requires 0.18 W of pumping energy to get a thermal resistance of 0.14 K/W. The on-line fin configuration requires almost 2 times more pumping energy (0.35 W) to obtain a similar thermal performance. In summary, the offset micro pin-fin heat sink is more reliable for near future applications because:

- it generates more uniform temperature profiles on the IC chip (overall temperature gradient of 1.2 °C/W) and,

- the maximum heat expected by 2016's IC chip (288W) can be dissipated appropriately with only 0.18 W of energy to be supplied into the system.

Table 6.4 Performance of micro heat sinks using overall performances of micro pin fin heat sinks based on Configuration II with different fin heights and flow rates.

Author	*Description*	*ΔP [kPa]*	*R [K/W]*	*Pump. power [W]*	*q''_{max}* [W/cm^2]*
Tuckerman and Pease (1981) [13]	Rectangular microchannel heat sink	207	0.090	2.3	>650
Knight *et al.* (1992) [22]	Rectangular microchannel heat sink using turbulent flow	207	0.056	>10.0	>1000
Gillot *et al.* (2000) [37]	Rectangular microchannel heat sink for multichips modules	180	0.092	~47.0	>650
Peles *et al.* (2005) [100]	Micro heat sink with circular staggered pin fins	203	0.039	--	>1500
Colgan *et al.* (2007) [102]	Micro heat sink with "semi-elliptical" staggered pin fins	<35	0.105	<0.9	>500
Husain and Kim (2008) [64]	Optimized microchannel heat sink	--	0.081	--	>700
Daguenet-Frick *et al.* (2010) [87]	Radial heat sink with boiling fluid	--	0.080	0.05	750
Escher *et al.* (2010) [104]	Heat sink formed by manifold channels	<10	0.087	~0.15	>680
Current work (2012)	MF-50x100x200-66 on-line	90	0.140	0.34	430
	MF-50x100x200-66 offset	86	0.140	0.18	430

*Considering 1cm x 1cm IC chip with maximum design temperature of 85°C and ambient temperature of 25°C.

Table 6.4 shows a comparison between different cooling devices found in the literature. The on-line and offset micro pin fin heat sinks working with the appropriate operating conditions to get a thermal resistance of 0.14 are added in this comparative table. The water flow rate for each configuration is 3.8 mL/s and 2.0 mL/s, respectively. Clearly, these configurations dissipate appropriately the heat generation expected by the 2016's IC chips. The offset fin configuration requires a lower amount of energy than the on-line arrangements, and also than the other heat sinks shown in this table (e.g. conventional microchannel heat sink and Colgan *et al.*'s heat sink). In this line, the micro pin fin heat sinks are only topped by cooling systems based on boiling cooling [87].

Moreover, large part of the research is aimed to generate cooling systems with thermal resistances lower than 0.1 K/W. Considering this thermal performance in both micro pin fin heat sinks, an important increase of the pressure drop is clearly observed (Figure 6.10), mainly in the offset

fin configuration. However, when the requirements of pumping power are compared, interesting results are observed. In order to get an overall comparison, Figure 6.11 presents the pumping power required by a conventional microchannel heat sink [3], a robust micro cooling system [18], and both on-line and offset micro pin-fin heat sink with variable fin density. All these cooling systems are operating at specific conditions in order to obtain a thermal resistance of 0.1 K/W. A very important reduction in the input energy is clearly observed with these last three cooling systems compared to conventional microchannel heat sinks (~100 %). Also, the robust cooling system and the offset micro pin-fin configuration present similar values of pumping power (~0.9 W). Therefore, the claim that offset micro pin-fin heat sinks are pretty good alternatives for cooling near future IC chips is ratified. Furthermore, this cooling system presents an easy integration in 2D and 3D IC chip packagings.

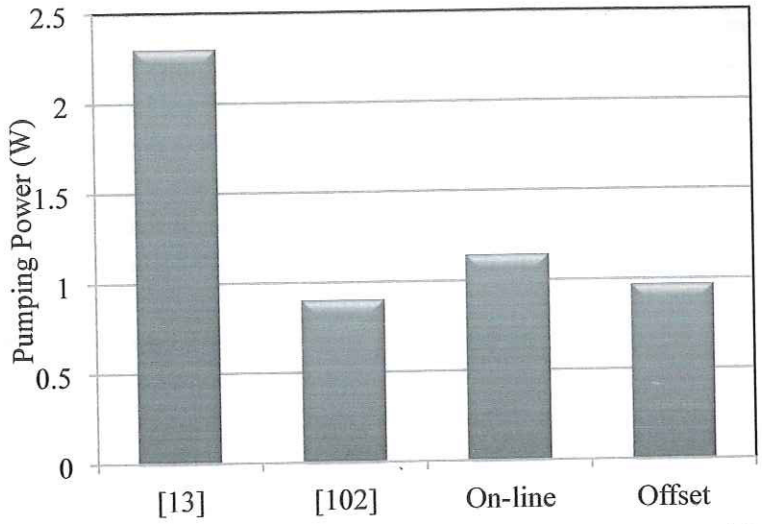

Figure 6.11 Comparison of the pumping power required by the Tuckerman and Pease's microchannel heat sink [13], Colgan et al.'s cooling device [102], and MF-50x100x200-66 on-line and offset heat sinks.

Following this comparison of pumping power, the offset micro pin-fin heat sink presents a better performance when the flow rate is less than 5 mL/s (thermal resistance around 0.1 K/W and pumping power less than 0.45 W) than the on-line fin configuration. After this thermal resistance value, both configurations have almost similar overall pumping power requirements. Thus, novel and reliable micro cooling systems capable to generate uniform junction temperature should be studied aiming to attain thermal resistances smaller than 0.1 K/W.

Conclusions

The present work was aimed to evaluate some thermal enhancement techniques in order to enhance the performance of current micro cooling systems, such as microchannel heat sinks for IC chip applications. Some of these techniques had been exposed in the technical literature. The goal of this first stage was to increase the overall performance (heat transfer coefficient) of the cooling system with the lowest pressure drop penalty due to this improvement affects directly the amount of energy to be supplied into the system (pumping power). In a second stage, this work analyzed some non-conventional configurations of micro cooling systems in order to reduce the temperature gradients and hot spot that are commonly generated on the IC chip when microchannel heat sinks based on straight channels are used. Thus, micro pin fin heat sink with variable fin density were proposed and analyzed. Their results showed an extraordinary performance for the goal of keeping uniform temperature on the IC chip. An overall comparison of these systems with alternative cooling systems exposed in technique literature was carried out. The results showed that these novel configurations are capable to fulfill the requirements expected for the next generation of IC chip cooling systems. The major conclusions of this work are mentioned below.

An overall performance parameter, ϕ, was considered in order to evaluate different thermal enhancement techniques. This parameter considers the variation of the local Nusselt number and friction factor along the flow length and then is compared with the dimensionless Nu and f values generated by a straight microchannel. The results showed that this parameter generates a good point of comparison.

Six thermal enhancement techniques were considered in the study. The effects that their geometrical variations have on the overall performance of the heat sink were studied. The results show that some techniques such as considering channels with variable channel aspect ratio or with dimpled surface have important improvements on the overall performance of the cooling system. However, the improvement was observed at least passing the middle of the channel length. This reduces the improvement at the entrance section, causing increases in the temperature variation on the chip. Other configurations presented a poor performance (channels with wave walls or with triangular reentrant cavities). Moreover, the use of micro fin configurations in the cooling system presented relative low performance than the ϕ value expected of 1.0. However, the major advantage of these configurations is the fact that they can be positioned according with the requirements of thermal dissipation. Overall, the flat-shaped and ellipse-shaped configurations presented the best performance due to the increase of the heat transfer is appropriated considering the relative low increase in the friction factor. The square-shaped configuration presented a good thermal performance but with an important friction factor increase. The poor performance was obtained with the circle-shaped configurations. Furthermore, the results show that the increase of the fin height up to 200 μm, and the reduction of the transversal and

longitudinal pitches affect favorably the overall performance of the system. The variation of the radius of curvature in the flat-shaped configurations has minimal effects in the performance. The average ϕ value for these configurations was slightly below the expected value. Thereby, the thermal enhancement technique based on fin configurations was considered for the second stage of this work

As it was mentioned above, the second stage of this work was aimed to analyze numerically some micro pin fin heat sinks with variable fin density in order to dissipate high heat fluxes with the lowest pressure drop and uniform junction temperature. The results show that the fin shape plays an important role in the pressure drops rather than the heat dissipation, which is mainly affected by the heat transfer area-fluid volume, ration, γ. The best performance is obtained when flat-shaped fins are used. The 100 μm fin length makes the system more reliable (good heat dissipation with a reasonable pressure drop). Moreover, the results generated with the fin height variation are interesting since two different effects were found. According with these observations, it is recommended to avoid the usage of sections without fins in this kind of microcooling systems.

MF-50x100x200-66 heat sink presents an appropriate performance compared on previous microcooling devices exposed in the technical literature. This proposed device can dissipate the heat flux expected by 2016's IC chips with a pressure drop around 20 kPa and a pumping power as low as 0.04 W. Furthermore, the system keeps a uniform junction temperature with a difference below 6°C. Considering the temperature gradient as a parameter of comparison, this cooling system has an overall value of 1.63°C/mm which is 4 times lower than the temperature gradient generated in rectangular microchannel heat sinks subject to similar sizes and operating conditions.

An offset micro pin-fin heat sink configuration with variable fin density was studied numerically. This heat sink is based on *Configuration III* exposed by [22]. The results show that this offset fin configuration improves the heat dissipation and reduce at less 1.3 times the system thermal resistance. This represents 1.5% and 7.5% reduction in the overall bottom wall temperature compared to the on-line micro pin-fin heat sink and microchannel heat sink, respectively. Furthermore, the offset fin configuration improves the temperature uniformity since the peaks/valleys that the on-line fin arrangement presents at the change-of-section zones are clearly smoothed. This has an important impact in the overall temperature gradient which is reduced down to 1.19 °C/W.

Hydraulically, the pressure drop rises importantly when the offset fin configuration is used in the micro pin-fin heat sink. However, the amount of coolant that this offset fin system requires to obtain a specific thermal resistance is lower than the required by the on-line fin configuration due to the heat transfer enhancement. The pumping power is a very good parameter for comparison. According to this parameter, these micro pin-fin heat sinks have an almost similar overall performance that Colgan *et al.*'s cooling device with a thermal resistance of 0.1 K/W.

The results show that the offset micro pin-fin heat sink is highly reliable for cooling systems with thermal resistances larger than 0.1 K/W since the pumping power is less than the pumping energy required by the on-line fin configurations. For cooling systems that require thermal resistances much lower than 0.1 K/W, this micro pin-fin configuration with variable fin density are not recommended due to their large increase of the pressure drop.

References

Literatures

A. W. C. O'Mara, R. B. Herring, L. P. Hunt, *Handbook of Semiconductor Silicon Technology*, Noyes Publications, 1990, ISBN 0-8155-1237-6.

B. F. Incropera, *Liquid Cooling of Electronic Devices by Single-Phase Convection*, Wiley, 1999, ISBN 978-0471159865.

C. S. G. Kandlikar, S. Garimella, D. Li, S. Colin, M. R., King, *Heat Transfer and Fluid Flow in Minichannels and Microchannels*, 1st Edition, 2006, Elserver Publishers, ISBN 0-08-044527-6.

D. L. Zhang, K.E. Goodson, T.W. Kenny, *Silicon Microchannel Heat Sinks, Theories and Phenomena*, 1st Edition, 2004, Springer Publishers, ISBN 3-540-4081-4

E. *Intel® Core® i7-900 Desktop Processor Extreme Edition Series and Intel® Core® i7-900 Desktop Processor Series and LGA1366 Socket - Thermal and Mechanical Design Guide*, Intel Corporation, Document 320837-004, March 2010.

F. P. Lall, M.G. Pecht, E.B. Hakin, *Influence of Temperature on Microelectronic and Reliability*, CRC Press, West Palm Beach, FL, USA, 1997.

G. R.K. Shah, A.L. London, *Laminar Flow Forced Convection in Ducts*, Academic Press, New York, 1978.

H. A. Bejan, *Shape and Structure, from Engineering to Nature*, Cambridge University Press, Cambridge, UK, 2000, ISBN 0-5217-9388-2.

I. D.B. Tuckerman, Heat Transfer Microstructures for Integrated Circuits, Ph.D. Thesis, Stanford University, 1984.

Papers

[1] D. A. Hodges, H. G. Jackson, R. Saleh, *Analysis and Design of Digital Integrated Circuits*, Mc.Graw-Hill, 1st Edition, 2003.

[2] J. M. Rabaey, A. Chandrakasan, B. Nikolic, *Digital Integrated Circuits*, Mc Graw-Hill, 2nd Edition, 2003.

[3] Intel Corporation, Moore's Law in Perspective, Intel Information Sheet 306971-001US, 2005.

[4] International Technology Roadmap for Semiconductors, 2010.

[5] International Technology Roadmap for Semiconductors, 2006.

[6] S.P. Gurrum, S.K. Suman, Y.K. Joshi, A.G. Federov, *Thermal Issues in Next-generation Integrated Circuits*, IEEE Trans. Dev. Mater. Reliab. 4 (4) (2004) 709–714.

[7] S.G. Kandlikar, W.J. Grande, *Evolution of Microchannel Flow Passages-Thermohydraulic Performance and Fabrication Technology*, Heat Transfer Eng., 24 (1) 2003 3-17.

[8] S.G. Kandlikar, W.J. Grande, *Evaluation of Single Phase Flow in Microchannels for High Flux Chip Cooling – Thermohydraulic Performance Enhancement and Fabrication Technology*, Heat Transfer Eng. 25(8) 2004 5-16.

[9] S.G. Kandlikar, H.R. Upadhye, *Extending the Heat Flux Limit with Enhanced Microchannels in Direct Single-Phase Cooling of Computer Chips*, Invited Paper, 21st Annual IEEE Semiconductor Thermal Measurement and Management Symosium, March 15–17, 2005, 8–15.

[10] M.E. Steinke, S.G. Kandlikar, *Single-Phase Liquid Heat Transfer in Plain and Enhanced Microchannels*, 4th Int. Conf. Nanochannels, Microchannels and Minichannels, ICNMM2006, June 19-21, 2006, 943-951S.G. Kandlikar, A. Bapat, *Evaluation of Jet Impingement, Spray and Microchannel Chip Cooling Options for High Heat Flux Removal*, Heat Transfer Eng. 28 (11) 2007 911-923.

[11] D. Cooke, S.G. Kandlikar, *Pool Boiling Heat Transfer and Bubble Dynamics Over Plain and Enhanced Microchannels*, ASME J. Heat Transfer, 133 (2011) 052902-9.

[12] S.G. Kandlikar, *History, Advances and Challenges in Liquid Flow and Flow Boiling Heat Transfer in Microchannels: A Critical Review*, Keynote Paper presented at the ASME J. Heat Transfer, 2011.

[13] D.B. Tuckerman, R.F.W. Pease, *High-Performance Heat Sinking for VLSI*, IEEE Electron. Dev. Letter EDL-2 (1981) 126–129.

[14] M.T. Bohr, Interconnecting Scaling the Real Limiter to High Performance ULSI, IEEE Proc. Int. Electron. Dev. Meeting, Dec 1995, pp. 241-244.

[15] G.O. Workman, J.G. Fossum, S. Krishnan, M.M. Pelella, Physical Modeling of Temperature Dependences of SOI CMOS Devices and Circuits including Self-heating", IEEE Trnas. Electron Dev., vol. 45, no. 4, pp. 125-133, Jan 1998.

[16] R.J. Phillips, *Micro-channel Heat Sinks, in: A. Bar-Cohen, A.D. Kraus (Eds.)*, Advances in Thermal Modeling of Electronic Components, vol. 2, ASME Press, New York, 1990, pp. 109–184.A.

[17] R.W. Knight, J.S. Goodling, D.J. Hall, *Optimal Thermal Design of Forced Convection Heat Sinks – Analytical*, ASME J. Electron. Packag. 113 (3) (1991) 313–321.

[18] J. Pfahler, J. Harley, H. Bau, J. Zemel, *Liquid Transport in Micron and Submicron Channels*, Sensors Actuat. A21–A23 (1991) 431–434.

[19] J. Pfahler, J. Harley, H. Bau, J. Zemel, *Gas and Liquid Flow in Small Channels*, Micromechanical Sensors, Actuators and Systems 32 (1991) 49–60.

[20] S.B. Choi, R.F. Barron, R.O. Warrington, *Fluid Flow and Heat Transfer in Microtubes*, Micromechanical Sensors, Actuators and Systems, vol. 32, ASME DSC, Atlanta, GA, 1991, pp. 123–134.

[21] A. Weisberg, H.H. Bau, J.N. Zemel, *Analysis of Microchannels for Integrated Cooling*, Int. J. Heat Mass Transfer 35 (1992) 2465–2474.

[22] R.W. Knight, D.J. Hall, J.S. Goodling, R.C. Jaeger, *Heat Sink Optimization with Application to Microchannels*, IEEE Trans. Compon. Hybrids Manufact. Technol. 15 (5) (1992) 832–842.

[23] Bejan, A.M. Morega, *Optimal Arrays of Pin Fins and Plate Fins in Laminar Forced Convection*, ASME J. Heat Transfer 115 (1993) 75–81.

[24] X.F. Peng, G.P. Peterson, B.X. Wang, *Frictional Flow Characteristics of Water Flowing through Rectangular Microchannels*, Exper. Heat Transfer 7 (1994) 249–264.

[25] X.F. Peng, G.P. Peterson, B.X. Wang, *Heat Transfer Characteristics of Water Flowing through Microchannels*, Exper. Heat Transfer 7 (1994) 265–283.

[26] X.F. Peng, G.P. Peterson, *Convective Heat Transfer and Flow Friction for Water Flow in Microchannel Structures*, Int. J. Heat Mass Transfer 39 (1996) 2599–2608.

[27] X.F. Peng, G.P. Peterson, *Forced Convection Heat Transfer on Single-phase Binary Mixtures through Microchannels*, Exp. Thermal and Fluid Science 12 (1996) 98-104.

[28] Y.S. Muzychka, M.M. Yovanovich, *Solution of Poisson Equation within Singly and Doubly Connected Prismatic Domains*, Paper No. AIAA97-3880, In: Proceedings of National Heat Transfer Conference, Baltimore, MD, August 10–12, 1997.

[29] H.H. Bau, *Optimization of Conduits' Shape in Micro Heat Exchangers*, Int. J. Heat Mass Transfer 41 (1998) 2717–2723.

[30] M. Gad-el-Hak, *The Fluid Mechanics of Microdevices – The Freeman Scholar Lecture*, J. Fluids Engineering, Vol. 121 (1999) 5-33.

[31] G.M. Mala, D. Li, *Flow Characteristics of Water in Microtubes*, Int. J. Heat Fluid Flow 20 (1999) 142–148.

[32] D.Y. Lee, K. Vafai, *Comparative Analysis of Jet Impingement and Microchannel Cooling for High Heat Flux Applications*, Int. J. Heat Mass Transfer 42 (1999) 1555–1568.

[33] S.J. Kim, D. Kim, *Forced Convection in Microstructures for Electronic Equipment Cooling*, J. Heat Transfer 121 (1999) 639–645.

[34] T.M. Harms, M.J. Kazmierczak, F.M. Gerner, *Developing Convective Heat Transfer in Deep Rectangular Microchannels*, Int. J. Heat Mass Transfer 20 (1999) 149–167.

[35] A.G. Federov, R. Viskanta, *Three-dimensional Conjugate Heat Transfer in the Microchannel Heat Sink for Electronic Packaging*, Int. J. Heat Mass Transfer 43 (2000) 399-415.

[36] C. Perret, J. Boussey, C. Schaeffer, M. Coyaud, *Analytical Modeling, Optimization, and Realization of Cooling Devices in Silicon Technology*, IEEE Trans. Compon. Packag. Technol. 23 (4) (2000) 665–672.

[37] C. Gillot, C. Schacffer, A. Bricard, *Integrated Micro Heat sink for Power Multichip Module*, IEEE Trans. Industr. Appl., 36(2000) 217-221.

[38] D. Pfund, D. Rector, A. Shekarriz, A. Popescu, J. Welty, *Pressure Drop Measurements in a Microchannel*, AICHE J. 46 (8) (2000) 1496–1507.

[39] G. Hetsroni, A. Mosyak, Z. Segal, *Nonuniform Temperature Distribution in Electronic Devices Cooled by Flow in Parallel Microchannels*, IEEE Trans. Components Packag. Technol. 24 (2001) 16–23.

[40] C.B. Sobhan, S.V. Garimella, *A Comparative Analysis of Studies on Heat Transfer and Fluid Flow in Microchannels*, Microscale Thermophys. Eng. 5 (2001) 293–311.

[41] J.H. Ryu, D.H. Choi, S.J. Kim, *Numerical Optimization of the Thermal Performance of a Microchannel Heat Sink*, Int. J. Heat Mass Transfer 45 (2002) 2823–2827.

[42] Y.S. Muzychka, M.M. Yovanovich, *Laminar Flow Friction and Heat Transfer in Non-circular Ducts and Channels Part 1: Hydrodynamic Problem*, Compact Heat Exchangers, A Festschrifton the 60th Birthday of Ramesh K. Shah, Grenoble, France, 2002, pp. 123–130.

[43] K.C. Toh, X.Y. Chen, J.C. Chai, *Numerical Computation of Fluid Flow and Heat Transfer in Microchannels*, Int. J. Heat Mass Transfer 45 (2002) 5133–5141.

[44] J. Judy, D. Maynes, B.W. Webb, *Characterization of Frictional Pressure Drop for Liquid Flows through Microchannels*, Int. J. of Heat Mass Transfer 45 (2002) 3477–3489.

[45] W. Qu, I. Mudawar, *Analysis of Three-Dimensional Heat Transfer in Micro-Channel Heat Sinks*, Int. J. Heat and Mass Transfer 45 (2002) 2973-2985.

[46] C.Y. Zhao, T.J. Lu, *Analysis of Microchannel Heat Sinks for Electronics Cooling*, Int. J. Heat and Mass Transfer, 45(2002) 4857-4869.

[47] H.E. Hegab, A. Bari, T. Ameel, *Friction and Convection Studies of R-134a in Microchannels within the Transition and Turbulent Flow Regimes*, Exper. Heat Transfer 15 (2002) 245–259.

[48] H.Y. Wu, P. Cheng, *Friction Factors in Smooth Trapezoidal Silicon Microchannels with Different Aspect Ratios*, Int. J. Heat Mass Transfer 46 (2003) 2519–2525.

[49] C. Yang, J. Wu, H. Chien, S. Lu, *Friction Characteristics of Water, R-134a, and Air in Small Tubes*, Microscale Thermophys. Eng. 7 (2003) 335–348.

[50] J. Koo, C. Kleinstreuer, *Liquid Flow in Microchannels: Experimental Observations and Computational Analyses of Microfluidics Effects*, J. Micromech. Microeng. 13 (2003) 568–579.

[51] K.V. Sharp, R.J. Adrian, *Transition from Laminar to Turbulent Flow in Liquid Filled Microtubes*, Exp. Fluids 36 (5) (2004) 741–747.

[52] D. Liu, S. Garimella, *Investigation of Liquid Flow in Microchannels*, J. Thermophysics Heat Transfer, AIAA 18 (1) (2004) 65–72.

[53] C. Kleinstreuer, J. Koo, *Computational Analysis of Wall Roughness Effects for Liquid Flow in Micro-conduits*, J. Fluids Eng. 126 (2004) 1–9.

[54] R. Baviére, F. Ayela, S. Le Person, M. Favre-Marinet, *Experimental Characterization of Water Flow through Smooth Rectangular Microchannels*, Phy. of Fluids 17 (2005) 098105-1-4.

[55] P.S. Lee, S. Garimella, D. Liu, *Investigation of Heat Transfer in Rectangular Microchannels*, Int. J. Heat Mass Transfer 48 (9) (2005).

[56] M.J. Kohl, S.I. Abdel-Khalik, S.M. Jeter, D.L. Sadowski, *An Experimental Investigation of Microchannel Flow with Internal Pressure Measurements*, Int. J. Heat and Mass Transfer 58(2005) 1518-1533.

[57] S.G. Kandlikar, *High Heat Flux Removal with Microchannels – A Roadmap of Challenges and Opportunities*, Heat Trans. Eng., 26(8), 2005.

[58] J. Koo and C. Kleinstreuer, *Analysis of Surface Roughness Effects on Heat Transfer in Micro-Conduits*, Int. J. Heat and Mass Transfer, 48 (2005) 2625-2634.

[59] G. Hetsroni, A. Mosyak, E. Pogrebnyak, L.P. Yarin, *Heat Transfer in Micro-channels: Comparison of Experiments with Theory and Numerical Results*, Int. J. Heat Mass Transfer 48 (2005) 5580–5601.

[60] J. Li, G.P. Peterson, *Geometric Optimization of a Micro Heat Sink with Liquid Flow*, IEEE Trans. Compon. Packag. Technol. 29 (1) (2006) 145–154.

[61] L.A.O. Rocha, S. Lorente, A. Bejan, *Conduction Tree Network with Loops for Cooling a Heat Generating*, Int. J. Heat Mass Trans. Vol. 49 (2006) 2626-2635.

[62] J. Li, G.P. Peterson, *3-Dimensional Numerical Optimization of Silicon-based High Performance Parallel Microchannel Heat Sink with Liquid Flow*, Int. J. Heat Mass Transfer 50 (2007) 2895-2904.

[63] G. Croce, P. D'agaro, C. Nonino, *Three-dimensional Roughness Effect on Microchannel Heat Transfer and Pressure Drop*, Int. J. Heat Mass Transfer 50 (2007) 5249–5259.

[64] A. Husain, K.Y. Kim, Optimization of a Microchannel Heat Sink with Temperature Dependent Fluid Properties, Appl. Therm. Eng., 28(2008) 1101-1107.

[65] O. Mokrani, B. Bourounga, C. Castelain, H. Peerhossaini, *Fluid Flow and Convective Heat Transfer in Flat Microchannels*, Int. J. Heat and Mass Transfer, 52 (2009) 1337-1352.

[66] McHale, S.V. Garimella, *Heat Transfer in Trapezoidal Microchannels of Various Aspect Rations*, Int. J. Heat Mass Transfer, 53(2010) 365-375.

[67] E.S. Cho, J.W. Choi, J.S. Yoon, M.S. Kim, *Experimental Study on Microchannel Heat Sinks Considering Mass Flow Distribution with Non-uniform Heat Flux Conditions*, Int. J. Heat Mass Transfer, 53(2010) 2159-2168.

[68] J. Chu, J. Teng, R. Greif, *Experimental and Numerical Study on the Flow Characteristics in Curved Rectangular Microchannels*, Applied Thermal Engineering, 30(2010) 1558-1566.

[69] E.S. Cho, J.W. Choi, J.S. Yoon, M.S. Kim, *Experimental Study on Microchannel Heat Sinks considering Mass Flow Distribution with Non-uniform Heat Flux Conditions*, Int. J. Heat Mass Transfer, 53(2010) 2159-2168.

[70] E.S. Cho, J.W. Choi, J.S. Yoon, M.S. Kim, *Modeling and Simulation on the Mass Flow Distribution in Microchannel Heat Sinks with Non-uniform Heat Flux Conditions*, Int. J. Heat Mass Transfer, 53(2010) 1341-1348.

[71] V.V. Dharaiya, R.R. Srivastava, S.G. Kandlikar, *Numerical Investigation of Heat Transfer Effects in Microchannels under H2 Boundary Condition*, Proc. Int. Heat Transfer Conference, IHTC-14-23118, 2010.

[72] G. Xia, L. Chai, H. Wang, M. Zhou, Z. Cui, *Optimum Thermal Design of Microchannel Heat Sink with Triangular Reentrant Cavities*, Applied Thermal Engineering, 31(2011) 1208-1219.

[73] M. Reyes, J.R. Arias, A. Velazquez, J.M. Vega, *Experimental Study of Heat Transfer and Pressure Drop in Micro-channel Based Heat Sinks with Tip Clearance*, Applied Thermal Engineering, 31(2011) 887-893.

[74] A. Bejan, *Constructal Tree Networks for Fluid Flow between a Finite Size Volume and One Soured or Sink*, Rev. Gen. Therm., 36(1997) 592-604.

[75] G.B. West, J.H. Brown, B.J. Enquist, *A General Model for the Origin of Allometric Scaling Laws in Biology*, Science, 276(1997) 122-126.

[76] D.V. Pence, *Reduced Pumping Power and Wall Temperature in Microchannel Heat Sinks with Fractal-like Branching Channel Networks*, Microscal Thermophy. Eng., 6(2002) 319-330.

[77] W. Wechsatol, S. Lorente, A. Bejan, *Optimal Tree-shaped Networks for Fluid Flow in a Disk-shaped Body*, Int. J. Heat Mass Transf., 45(2002) 4911-4924.

[78] W. Wechsatol, S. Lorente, A. Bejan, *Dendritic Heat Convection on a Disc*, Int. J. Heat Mass Transfer, 46(2003) 4381-4391.

[79] S. Lorente, W. Wechsatol, A. Bejan, *Tree-shaped Flow Structures Designed by Minimizing Path Lengths*, Int. J. Heat Mass Transfer, 45(2002) 3299-3312.

[80] V.D. Zimparov, A.K. da Silva, A. Bejan, *Thermodynamic Optimization of Tree-shaped Flow Geometries with Constant Wall Temperature*, Int. J. Heat Mass Transfer, 49(2006) 4839-4849.

[81] V.D. Zimparov, A.K. da Silva A. Bejan, *Constructal Tree-shaped Parallel Flow Heat Exchanger*, Int. J. Heat Mass Transfer, 49(2006) 4558-4566.

[82] C. Biserni, L.A.O. Rocha, G. Stanescu, E. Lorenzini, *Constructal H-shaped Cavities According to Bejan's Theory*, Int. J. Heat Mass Transfer, 50(2007) 2132-2138.

[83] W. Wechsatol, S. Lorente, A. Bejan, *Tree-shaped Networks with Loops*, Int. J. Heat Mass Transfer, 48(2005) 573-583.

[84] X.-Q Wang, C. Yap, A.S. Mujumdar, *Laminar Heat Transfer in Constructal Microchannel Networks with Loops*, J. Elec. Pack., 128(2006) 273-280.

[85] K.-M. Wang, S. Lorente, A. Bejan, *The Transient Response of Vascular Composites Cooled with Grids and Radial Channels*, Int. J. Heat Mass Transfer, 52(2009) 4175-4183.

[86] R. Revellin, J.R. Thome, A. Bejan, J. Bonjour, *Constructal Tree-shaped Microchannel Networks for Maximizing the Saturated Critical Heat Flux*, Int. J. Thermal Sci., 48(2009) 342-352.

[87] X. Daguenet-Frick, J. Bonjour, R. Revellin, *Constructal Microchannel Network for Flow Boiling in a Disc-shaped Body*, IEEE Comp. Pack. Tech., March 2010, Vol. 33 (1), 115-126.

[88] D.V. Pence, *Improved Thermal Efficiency and Temperature Uniformity using Fractal-like Branching Channel Networks*, Int. Conf. Heat Transfer Transp. Phen. Micro Scale, Banff, Canada, 2000, 142-148.

[89] Y. Chen, P. Cheng, *Heat Transfer and Pressure Drop in Fractal Tree-like Microchannel Nets*, Int. J. Heat Mass Transfer, 45(2002) 2643-2648.

[90] Y. Chen, P. Cheng, *An Experimental Investigation on the Thermal Efficiency of Fractal Tree-like Microchannel Nets*, Int. Comm. Heat Mass Transfer, 32(2005) 931-938.

[91] X.Q Wang, A.S. Mujumdar, C. Yap, *Numerical Analysis of Blockage and Optimization of Heat Transfer Performance of Fractal-like Microchannel Nets*, J. Electron. Packages, 128(2006) 38-45.

[92] X.Q Wang, A.S. Mujumdar, C. Yap, *Effects of Bifurcation Angle in Tree-shape Microchannel Networks*, J. Appl. Phys., 102(2007) 072530.

[93] X.Q Wang, P. Xu, A.S. Mujumdar, C. Yap, *Flow and Thermal Characteristics of Offset Branching Networks*, Int. J. Thermal Sci., 49(2010) 272-280.

[94] L. Luo, B. Yu, J. Cai, M. Mei, *Symmetry is not Always Prefect*, Int. J. Heat Mass Transfer, 55(2010) 5022-5024.

[95] P. Xu, B. Yu, M. Yun, M. Zou, *Heat Conduction in Fractal Tree-like Branched Networks*, Int. J. Heat Mass Transfer, 49(2006) 3746-3751.

[96] C.D. Murray, *The Physiological Principle of Minumum Work, 1, The Vascular System and the Cost of Blood Volume*, Proc. Natl, Acad. Sci., USA, 12(1926) 207-214.

[97] D. Pence, *The Simplicity of Fractal-like Flow Networks for Effective Heat and Mass Transport*, Exp. Thermal Fluid Sci., 34(2010) 474-486.

[98] J. Zhang, Y.F. Zhang, M. Miao, Y.F. Jin, S.L. Bai, J.Q. Chen, *Simulation of Fluid Flow and Heat Transfer in Microchannel Cooling for LTCC Electronic Packages*, IEEE Int. Conf. Elec. Pack. Tech. High Density Pack. (ICEPT-HDP), 2009, 327-330.

[99] M. Miao, J. Zhang, Y. Qiu, Y. Zhang, Y. Jin, H. Gan, *A LTCC Microsystem Vacuum Package Substrate with Embedded Cooling Microchannel and Pirana Gauge*, Proc. 5th IEEE Int. Conf. Nano/Micro Eng. Molecular Systems, January 20-24, Xiamen, China, 2010.

[100] Y. Peles, A. Koşar, C. Mishra, C.J. Kuo, B. Shneider, Forced Convective Heat Transfer Across a Pin Fin Micro Heat Sink, Int. J. Heat Mass Transfer, 48(2005) 3615-3627.

[101] E.G. Colgan, B. Furman, M. Gaynes, N. LaBianca, J.H. Magerlein, R. Polastre, R. Bezama, K. Marston, R. Schmidt, *High Performance and Subambient Silicon Microchannel Cooling*, J. Heat and Mass Transfer, ASME, August 2007, Vol. 129, 1046-1051.

[102] E.G. Colgan, B. Furman, M. Gaynes, W.S. Graham, N. LaBianca, J.H. Magerlein, R. Polastre, M.B. Rothwell, R.J. Benzema, R.Choudhary, K. C. Marston, H. Toy, J. Walkil, J.A. Zitz, R.R. Schmidt, *A Practical Implementation of Silicon Microchannel Coolers for High Power Chips*, IEEE Comp. Pack. Tech., June 2007, Vol. 30 (2), 218-225.

[103] R. Wälchli, T. Brunschwiler, B. Michel, D. Poulikakos, *Combined Local Microchannel-scale CFD Modeling and Global Chip Scale Network Modeling for Electronic Cooling Designs*, Int. J. Heat Mass Transfer, 53(2010) 1004-1014.

[104] W. Escher, B. Michel, D. Poulikakos, *A Novel High Performance, Ultra Thin Heat Sink for Electronics*, Int. J. Heat Fluid Flow, 31(2010) 586-598.

[105] M.E. Steinke, S.G. Kandlikar, *Single-phase Heat Transfer Enhancement Techniques in Microchannel and Minichannel Flows*, Proc. 2nd Int. Conf. Microchannel and Minichannel, ICMM2004-2328, Rochester, NY, 2004.

[106] M.E. Steinke, S.G. Kandlikar, *Single-phase Liquid Heat Transfer in Plain and Enhanced Microchannels*, Proc. 4th Int. Conf. Nanochannels, Microchannels and Minichannels, ICNMM2006-96227, Limerick, Ireland, 2006.

[107] L. Gong, L. Kota, W. Tao, Y. Joshi, *Thermal Performance of Microchannels with Wavy Walls for Electronics Cooling*, Proc. 12th Int. Conf. Thermal and Thermomechanical Phenomena in Electronic Systems, Las Vegas, NV, 2010.

[108] X.J. Wei, Y.K. Yoshi, P.M. Ligrani, *Numerical Simulation of Laminar Flow and Heat Transfer Inside a Microchannel with One Dimpled Surface*, J. Electronic Packages, 129(2007) 63-70.

[109] G. Xia, L. Chai, H. Wang, M. Zhou, Z. Cui, *Optimum Thermal Design of Microchannel Heat Sink with Triangular Reentrant Cavities*, Applied Thermal Engineering, 31(2011) 1208-1219.

[110] R.J. Phillips, *Forced Convection, Liquid Cooled, Microchannel Heat Sinks*, MS Thesis, Department of Mechanical Engineering, Massachusetts Institute of Technology, Cambridge, MA, 1987.

[111] M.E Steinke, S.G. Kandlikar, J.H. Magerlein, E.G. Colgan, A.D. Raisanen, *Development of an Experimental Facility for Investigating Single-phase Liquid Flow in Microchannels*, Heat Transfer Eng. vol. 27, no. 4, pp. 41-52, 2006.

[112] C.A. Rubio-Jimenez, S.G. Kandlikar, A. Hernandez-Guerrero, "Numerical Analysis of Novel Micro Pin Fin Heat Sink with Variable Fin Density", IEEE Trans. Components and Packaging Technologies, vol. 2(5), pp. 825-833, 2012.